NEW AXIAL REACTIVITY OF TRIMETALLIC COMPOUNDS

by

Yevgeniya Turov

A dissertation submitted in partial fulfillment of

the requirements for the degree of

Doctor of Philosophy

(Chemistry)

at the

UNIVERSITY OF WISCONSIN – MADISON

2012

Date of final oral examination: 08/15/2012

The dissertation is approved by the following members of the Final Oral Committee:

John F. Berry, Assistant Professor, Chemistry
Shannon S. Stahl, Professor, Chemistry
Mahesh K. Mahanthappa, Assistant Professor, Chemistry
Judith N. Burstyn, Professor, Chemistry
Thomas Brunold, Professor, Chemistry

New Axial Reactivity of Trimetallic Compounds

Yevgeniya Turov

Under the supervision of Assistant Professor John F. Berry

University of Wisconsin – Madison

Abstract. Axial ligand substitution reactions of trimetallic complexes stabilized by the 2,2'-dipyridylamine (dpa) of the type $M_2M'(dpa)_4X_2$ are explored. The nature of the axial ligands can dramatically influence the reactivity of these complexes. When the axial ligand is changed from chloride to triflate or thiocyanate, the complexes show a long-range effect of the axial ligands on the properties of the metal atom at the other end of the trimetallic chain. When the axial ligand is changed to azide, there is evidence of thermal N-N bond cleavage and loss of dinitrogen, indicating the possibility of generating a reactive terminal nitrido species, which is unprecedented for compounds of this type.

Other reactive nitrido compounds leading to N-atom transfer reactions are also explored. Mn(N)salen (where salen = N,N′-Bis(salicylidene)ethylenediamine) can transfer a nitrogen atom to Fe and react with substrates such as phosphines to generate new N-P bonds.

DEDICATION

This work is dedicated to my parents, Natalya and Igor Turov, who inspired me to pursue my dreams and to love education; to my grandparents, Tatyana and Michael Karmalyuk, who always support me; to my grandmother Valentina Turova; to the memory of my grandfather, Robert Turov; and to my brother, Vadim Turov. This work is also dedicated to my loving husband, Jason Foht.

ACKNOWLEDGMENTS

I would like to thank my advisor, Professor John F. Berry, for being a great mentor, for pushing me to try new experiments, and for supporting my research and career goals. Though it hasn't always been a smooth path through graduate school, I can't imagine having anyone other than John as my advisor, mentor and teacher.

I would also like to thank members of the Berry group, past and present, for helping me through: Michael, for teaching me the beauty and intricacies of trimetallic synthesis and crystallization; Mandy, for being a great friend, teacher, and waffle buddy; Kasia, for being such a close friend, confidante, and inspiration; Wes, Ryan, Brian, and Amanda, for being hilarious and wonderful colleagues; and all the others who will thrive in this excellent group.

Thanks to my committee members, Shannon Stahl and Mahesh Mahanthappa, who challenged me, made me think critically about science, and helped me grow as a chemist. Thanks also to my thesis committee members Judith Burstyn and Thomas Brunold for fruitful scientific discussions.

Special thanks to Ilia Guzei and Lara Spencer for teaching me X-ray crystallography and putting up with my shenanigans. Thanks to Martha Vestling for help with MALDI-MS. Thanks to Charlie Fry and Monika Ivancic for help with strange paramagnetic NMR spectra. Extra thanks to Bob Shanks for help with the liquid helium cryostat – no EPR spectra would have been possible without his help.

Thanks to my undergraduate mentor, Nathaniel K. Szymczak (currently Assistant Professor at the University of Michigan), who introduced me to the fine art of inorganic

synthesis and showed me the nuances of Schlenk line and glovebox technique, taught me how to eat properly at Taco Bell, and encouraged me to pursue graduate education. Thanks to my undergraduate advisor, Professor David R. Tyler, for allowing me to gain a great deal of experience by making mistakes in his lab and learning from them to become a better scientist and critical thinker.

Thanks to my inorganic division colleagues and friends, who were there through cumes, classes, late-night study sessions, teaching, and learning how to be Ph.D.-level scientists. We were each other's reasons for sticking this out, and I'm so glad we did.

Thanks to my family for listening to grad school drama, putting off their dreams of grandchildren so I could finish my work, and for being so loving and supportive.

A very special thanks to my husband, Jason Foht, who has been by my side through successes and failures (large and small), who has given me the strength and courage to finish grad school and pursue my dreams, and who is my best friend and biggest supporter.

TABLE OF CONTENTS

Appendix 1

Synthesis of a Novel Tripodal Ligand and Attempts to Prepare Metal Complexes of this Ligand

LIST OF TABLES

LIST OF FIGURES

LIST OF SCHEMES

Chapter 1

Wisconsin Initiative for Science Literacy: Introduction for a General Audience

1.1 Inorganic Chemistry

When starting out in any general chemistry class, students are first exposed to inorganic chemistry, often without their knowledge. In its most basic essence, inorganic chemistry may be defined as the study of inorganic compounds, namely, anything not containing a carbon-hydrogen bond. Although most of the building blocks of life, such as amino acids, are organic and contain carbon and carbon-hydrogen bonds, a large majority of the items we use each day to make our lives easier and more enjoyable are composed of inorganic materials.

Although most students and the public in general are more familiar with the popularized -organic compounds that are present in food, medicine, and many other products, it is important to understand inorganic chemistry and exploit it for its many uses. Inorganics comprise most of the periodic table (excluding carbon) and it is these elements that truly have the most interesting properties and reactivity. For example, the lithium batteries in cell phones and other electronics, the steel and other metals used to construct buildings and modes of transportation, and the metal impurities that give color to precious gems, among many other materials, are all inorganic materials. The study of inorganic compounds is highly relevant to the advancement of science and to the lifestyle people enjoy today.

One important and often misunderstood element of inorganic chemistry is that metals do not only exist as the bulk solid, but also as ions in solution, and this is where

most of the exciting reactivity takes place. The properties that people often associate with metals, such as high conductivity, shiny appearance, malleability and ductility, among others, are not always true for metals, especially transition metals that have reacted with other substances to form inorganic complexes.

1.2 Transition Metals

The transition metals are found in the center of the periodic table as shown in Figure 1.1. Among inorganic compounds, arguably the most interesting are those containing transition metals. The transition metals have a range of properties from highly metallic to relatively inert, so selecting the proper metal center for a given type of reaction is an important part of inorganic synthesis.

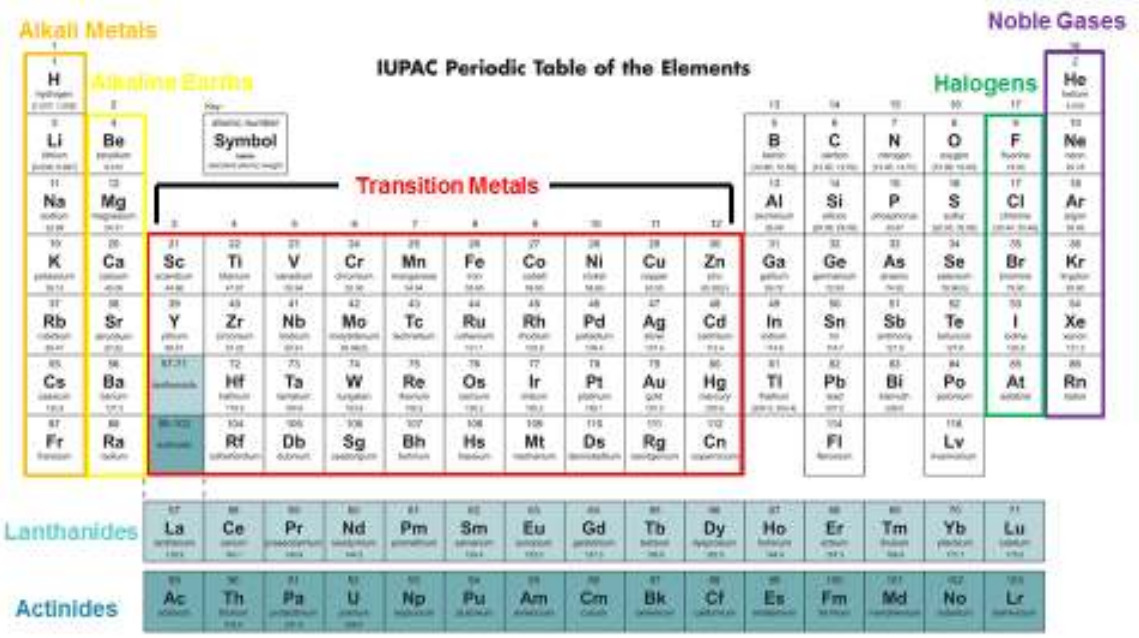

Figure 1.1. The periodic table, with transition metals highlighted in red.[1]

Transition metals are involved in a variety of reactions and processes. In order to fully make use of the capabilities of the transition metals, it is important to study them

extensively and have a fundamental understanding of their reactivity. Although the transition metals encompass all the elements highlighted in Figure 1.1, the discussion in this chapter will mostly focus on what are known as the "*d*-block" elements, or those found in the rectangle formed by Sc, La, Hg, and Zn.

1.3 Metal Oxidation States

The determination of oxidation states of atoms or ions is based on a set of rules that are taught early in general chemistry courses. Often, the property of a transition metal that determines its reactivity is its oxidation state. The oxidation state refers to the charge of the metal center and is counted based on the number of electrons at the metal center. Depending on the atoms bonded to the metal center, electrons can either be added or removed from the electron cloud surrounding the metal center and this will change the oxidation state. There are several different methods for assigning the metal oxidation state experimentally (which will be discussed in more detail later), but chemists can use their intuition and knowledge about the behavior of certain atoms and molecules to "count electrons" and assign the metal oxidation state.

Most transition metals have oxidation states that are more commonly accessible, and for this reason, chemists can predict how certain molecules will react with these metals. For example, chromium (Cr) often exists in the +2 or +3 oxidation state (meaning the metal electron cloud has given up two or three electrons, respectively, to form a bond) and easily forms compounds such as $CrCl_2$ or $CrCl_3$. Although simple compounds of this type are useful, it is of great interest to chemists to test the limits of metal oxidation states

and study how this affects the reactions these metal compounds are capable of carrying out.

1.4 Gaining Fundamental Understanding

The chemistry of a transition metal is dramatically affected by its ligand environment. Ligands are simply ions or molecules that bond to the transition metal. The metal and ligands can form single, double, or triple bonds. When a metal bonds to any number of ligands, the result is known as a coordination complex, and coordination complexes of the same metal often have very different properties, including the observed color of the complex, which is one of the most exciting aspects for students entering the field of inorganic chemistry. Several examples of well-known transition metal complexes and their corresponding colors are given in Figure 1.2.

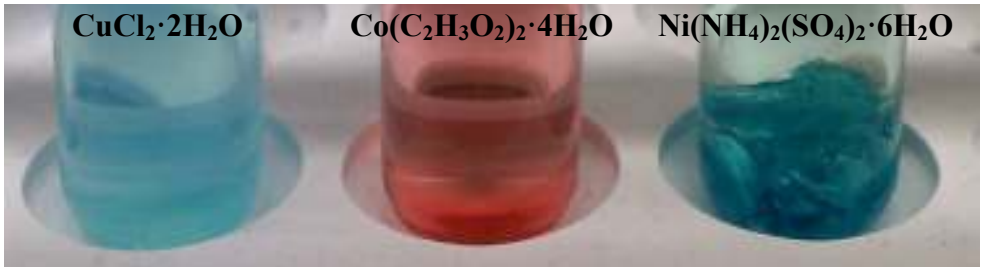

Figure 1.2. Colorful transition metal complexes in water.[2]

The colors of the compounds shown in Figure 1.2 appear because of the structures of the compounds, depending mainly on the identity of the metal center and its ligands. It is important to understand the structure and properties of coordination compounds to predict their behavior and make compounds that will have useful applications, as catalysts, pigments, and therapeutic agents, among others.

1.5 Characterization Methods

There are numerous ways to probe the structure and properties of coordination compounds. One very powerful and diverse tool to study chemical structure is spectroscopy, which is the study of the interaction of matter and radiated energy. The electromagnetic spectrum (Figure 1.3) shows the relationship between the different types of energy in terms of wavelength and frequency, as well as common sources of these types of energies. There are numerous types of spectroscopies, including infrared (IR), absorption (UV/Vis), nuclear magnetic resonance (NMR), electron paramagnetic resonance (EPR), and X-ray crystallography, which are all used extensively in the Berry group to probe coordination compounds. Although the physics behind each technique will not be described here, a brief overview of each method will be given so that the reader will understand how we use these powerful tools.

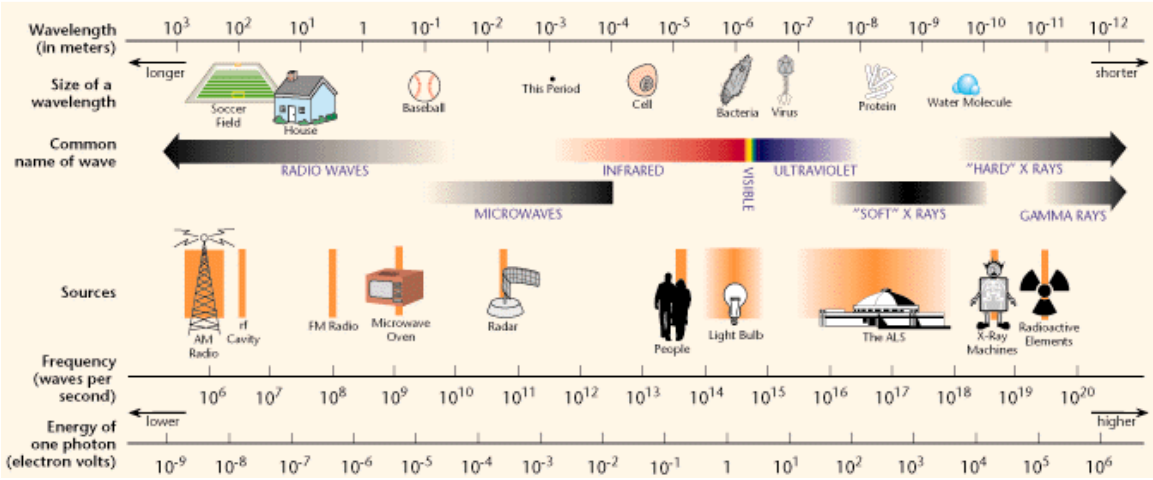

Figure 1.3. The electromagnetic spectrum.[3]

1.5.1 Infrared Spectroscopy

Infrared (IR) spectroscopy relies on the principle that molecules are in constant motion. The types of atoms and bonds in a molecule determine the type of motion that will be present in the molecule, such as stretching and bending, as well as the energy of this motion. IR spectroscopy studies these vibrations of molecules and their energies. Passing infrared light over a small sample allows molecules to absorb this light energy based on the strength of the bonds in the molecule. This information is depicted by peaks of certain shape and size that correspond to the identity of the bonds in the molecule and help to determine a structure.[4] An example of an experimental IR spectrum is shown in Figure 1.4, and the peak at 2051 cm^{-1} is a signature for the presence of an N_3^- group in the molecule. The absence of peaks between 4000 and 2100 cm^{-1} indicates that this compound has no bonds that respond (stretch or bend) to this energy range.

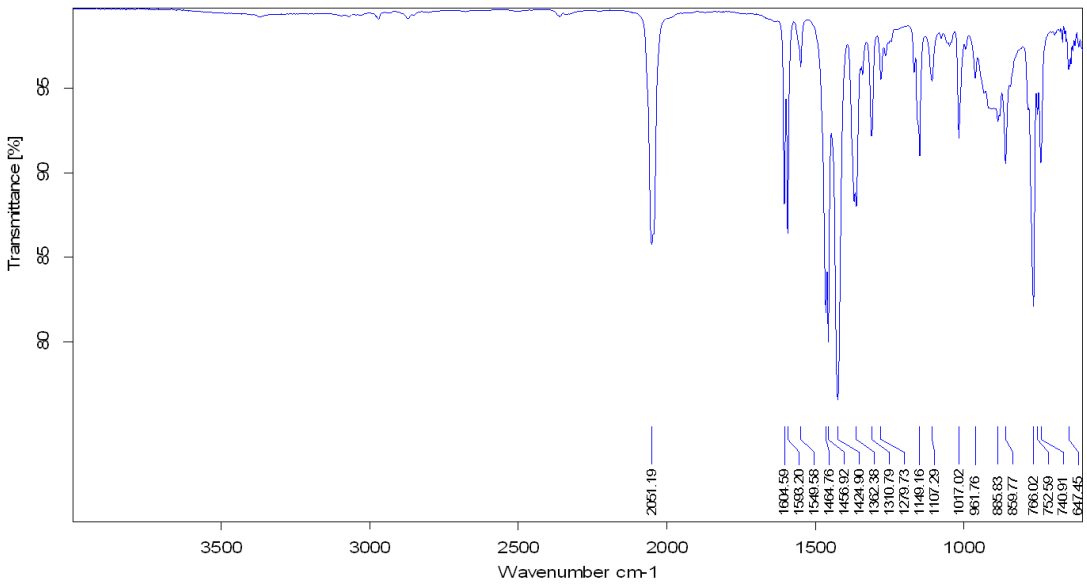

Figure 1.4. IR spectrum of $Cr_2(dpa)_4(N_3)_2$.

1.5.2 UV/Visible Absorption Spectroscopy

UV/Visible (UV/Vis) absorption spectroscopy measures the amount of ultraviolet or visible light that passes through a solution of a compound. This technique is only useful if a solution is colored, as colorless solutions will allow all of the light to pass through and no information will be collected. At certain energies, more or less light will pass through the sample depending on the identity of the compound, and this gives insight into the structure of the compound. This technique works on the premise that ultraviolet and visible light have enough energy to push an electron into a higher energy orbital.[5] The amount of energy needed for this process to occur in a certain molecule gives insight about the energy of the orbitals in the compound, which is very important for understanding chemical reactivity. This method is also useful to monitor a reaction, since the starting material and product will usually have quite different spectra. A sample spectrum is given in Figure 1.5.

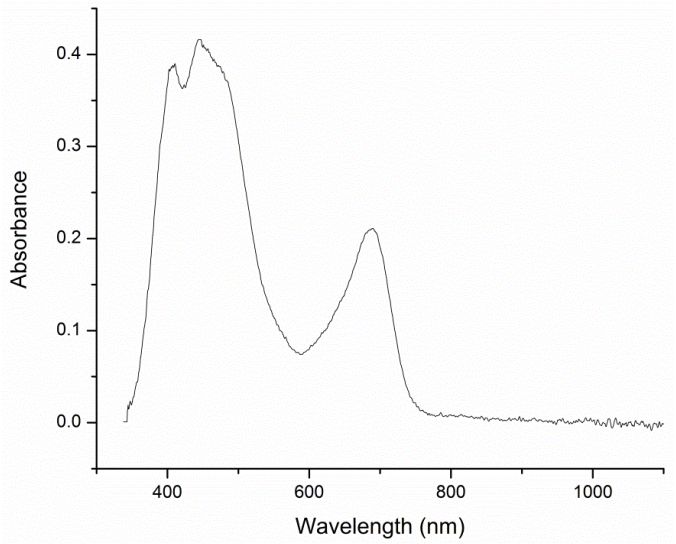

Figure 1.5. UV/Vis spectrum of $Cr_2Fe(dpa)_4(SO_3CF_3)_2$ in acetonitrile.

To analyze a UV/Vis spectrum, it is useful to consider a color wheel (Figure 1.6). The spectrum above shows that the compound absorbs color at around 700 nm (in the red region of the visible light spectrum). This means that the observed color of the solution is actually green. Since the compound also absorbs at 450 nm, we should also observe orange color in the solution, so the resulting color is actually a mixture of both orange and green. Indeed, the color of the solution depicted in Figure 1.4 is dark brown.

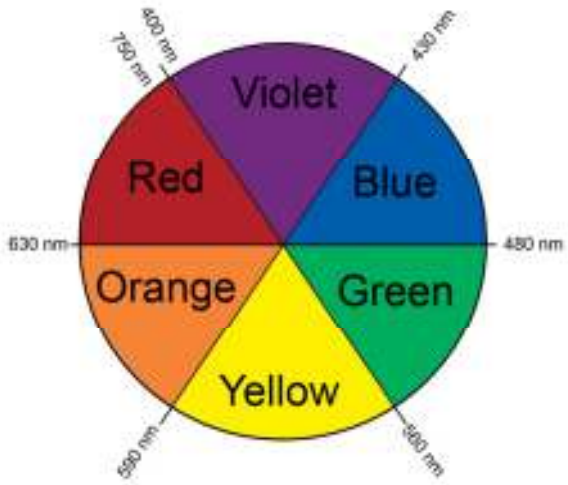

Figure 1.6. Color wheel depicting the relationship between absorbed color and observed color.

1.5.3 Nuclear Magnetic Resonance Spectroscopy

Nuclear magnetic resonance (NMR) spectroscopy is a powerful tool that can often be used exclusively to confirm a structure because it gives information about how different atoms are bonded to one another. In NMR spectroscopy, it is important to know that atomic nuclei can spin around and generate a magnetic field. When atomic nuclei are in solution, they can spin at random; however, when they are placed near a larger magnetic field, they will become aligned either with or against the field. [5] (A helpful analogy is swimming fish: in a lake (absence of magnetic field), they can swim any

which way they please, but if they are placed in a river (a magnetic field), they must either swim with or against the current.) When a magnetic field is applied, all of the nuclei flip to the same orientation, but in the absence of magnetic field, the nuclei can return to either the "with" or "against" state they were originally in. At that point, the nuclei generate a signal related to the difference in energy between the "with" and "against" state. A portion of a sample spectrum is shown in Figure 1.7.

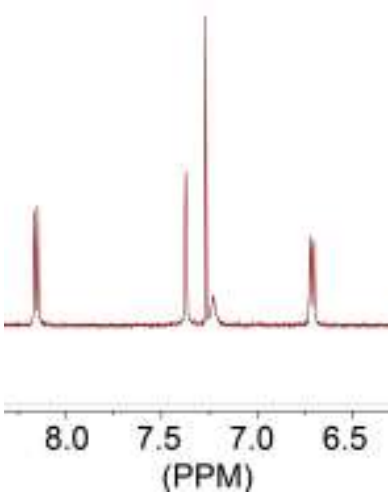

Figure 1.7. Sample NMR spectrum in CD_2Cl_2.

These signals give clear information about the structure of the compound.[5] The shape and location of the peaks indicate the type of bonds and functional groups near a given nucleus. In Figure 1.7, we can look at the peak at 7.3 ppm and see a tall singlet peak. This region tells us that we likely have a phenyl proton. The absence of any divisions in the peak tells us that there are no hydrogen nuclei nearby to interact with this group. Thus, from one peak, we have a great deal of information that we can combine with some knowledge of the reactions we perform to determine the structure of the compounds we make.

1.5.4 Electron Paramagnetic Resonance Spectroscopy

Electron paramagnetic resonance (EPR) spectroscopy is similar to NMR, but is used to study structures that are paramagnetic, i.e. have unpaired electrons, and relies on electron spin rather than nuclear spin. Electrons have two possible spin states, either up or down, and EPR makes use of this property. Microwave radiation has enough energy to flip the spin of an electron in the presence of a magnetic field. The difference between the number of electrons in the up and down spin states generates a signal and the larger the difference, the higher the signal.[6] The magnetic field at which a signal appears gives information about which atom the electron is located on and which orbitals are occupied by these electrons. This technique is especially useful for transition metal compounds, as they often have unpaired electrons, an example of which is given in Figure 1.8.

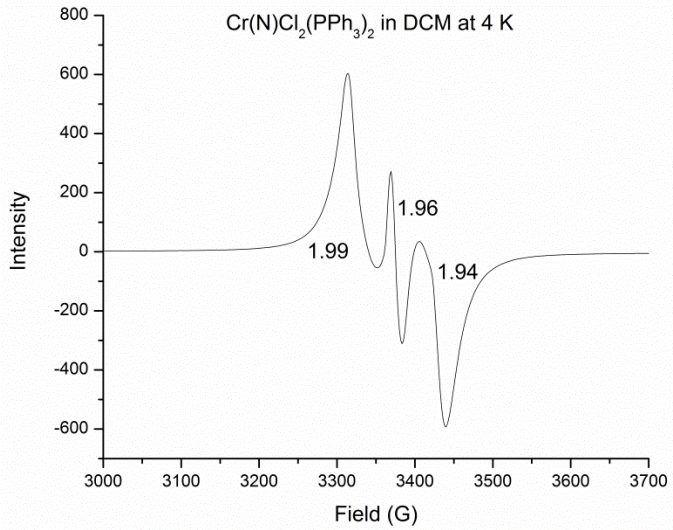

Figure 1.8. EPR spectrum of $Cr(N)(PPh_3)_2Cl_2$ in dichloromethane, including g values that help determine the location of the unpaired electron.

1.5.5 X-Ray Crystallography

X-ray crystallography is the process of determining the structure of a crystalline compound using X-ray diffraction patterns. With some luck, pure compounds crystallize out of solutions and it is possible to obtain a picture of the composition and connectivity of atoms in a molecule. It is important to note that a crystal "consists of atoms arranged in a pattern that repeats periodically in three dimensions"[7] and sometimes compounds appear crystalline but are actually fine powders or are not well-ordered. As a result, it is not typically easy to obtain nice, diffraction-quality crystals, which explains why this technique is usually not a first resource even though it is very powerful. When quality crystals are available, X-ray diffraction is very helpful for solving transition metal coordination structures that are difficult to analyze by other methods (due to paramagnetism or small quantities). A diffractometer is used to analyze the crystals. A source shoots X-rays at a single crystal, and detectors collect the diffraction pattern that results. Based on the composition of a crystal, there will be different angles and strengths with which the X-rays are diffracted. After some complicated computations, it is possible to assign the peaks as molecule and understand how all the atoms are bonded to one another. An example crystal structure is shown in Figure 1.9.

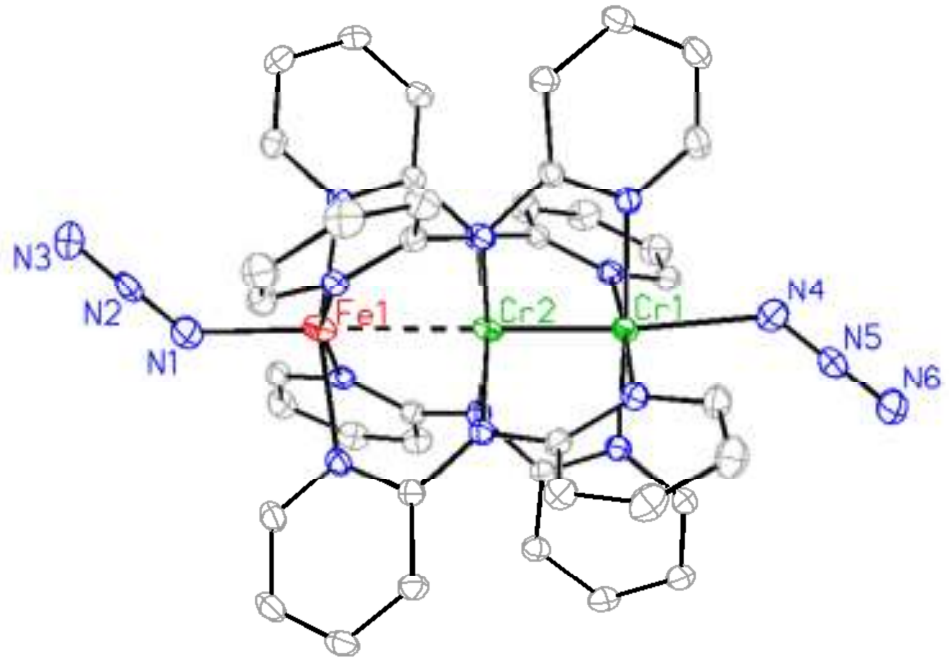

Figure 1.9. X-ray crystal structure of $Cr_2Fe(dpa)_4(N_3)_2$ (blue = nitrogen, gray = carbon and hydrogen atoms are not shown to help visualize the molecule).

1.5.6 Thermogravimetric Analysis and Differential Scanning Calorimetry

In this thesis, we discuss the formation of azide compounds (as shown in Figure 1.9 and described in Section 1.7), which are able to lose dinitrogen when heated or in the presence of light. There are two useful techniques that help quantify the changes occurring in the azide compounds upon heating, which should result in the loss of dinitrogen. One of which is thermogravimetric analysis (TGA), which is essentially just a measurement of the mass of a sample as it is heated. The other useful technique is differential scanning calorimetry (DSC), which measures heat loss from a sealed sample as it is heated. Often, when there is a physical change, such as melting or gas loss, there is a huge spike in the DSC curve, which indicates the energy of the change. Figure 1.10

shows both TGA and DSC plots that indicate the loss of two molecules of dinitrogen from the overall molecule, and the energy of this process.

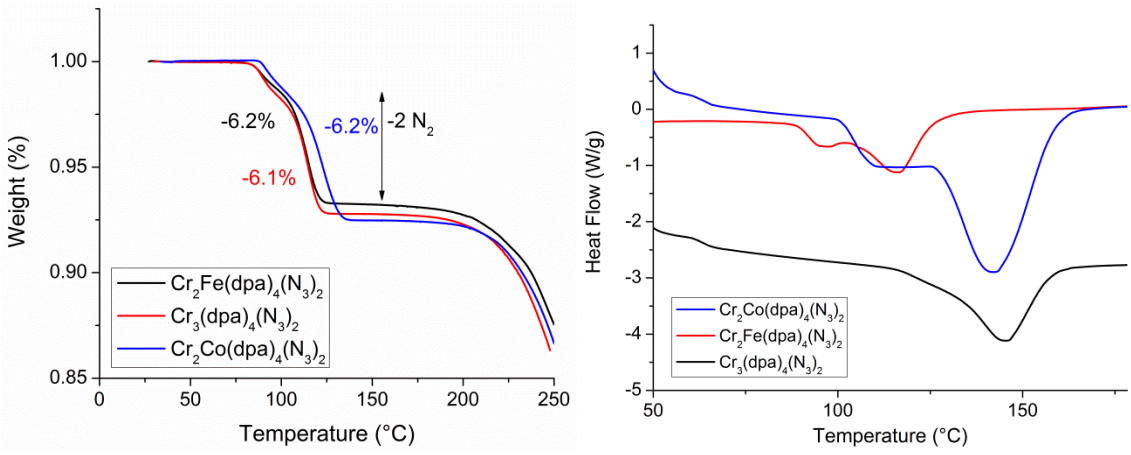

Figure 1.10. TGA data for three trimetallic azide compounds (left), showing a mass loss corresponding to loss of two dinitrogen molecules. DSC data (right), showing that energy is required for the system to lose N_2.

1.6 Metal-Metal and Metal-Ligand Multiple Bonding

In the Berry group, we are very interested in studying reactions of transition metals. We believe that if one metal center has many interesting properties, then a compound containing two or three metal centers has that many times more interesting properties. Bimetallic (complexes with two metal centers) and trimetallic (three metal centers) are those most often studied in our group, especially if two of the metal centers are interacting with each other through a bond. Most transition metals can form compounds wherein there are two of the same metal center bonded to one another, with different bond orders - single bonds, double bonds, triple bonds, quadruple bonds,[8] or even quintuple bonds (though these are quite rare).[9]

Since the early 1960s, metal-metal bonded compounds have been actively studied, especially with the help of X-ray crystallography, which confirmed the (previously unknown) presence of metal-metal bonds.[8] A wealth of compounds has been made since that time, but because the properties of these compounds span such a large range of reactivity (including catalytic properties), there are many more yet to be prepared. One relatively unexplored area in this field is the preparation of complexes with both metal-metal multiple bonds and metal-ligand multiple bonds. There are many compounds that have metal-ligand multiple bonds and these are often useful for transferring atoms or understanding the steps in catalytic cycles. However, there is a scarcity of compounds containing both metal-ligand and metal-metal multiple bonds and we believe these would be of great interest for making reactive metal-ligand multiply bonded species, as well as for understanding the interactions responsible for the proposed enhanced reactivity.

1.7 Exploring New Reactivity

Bimetallic and trimetallic linear compounds have been made by our group and by others for several years, and the methodology is well-established. However, the methods for preparing systems containing both metal-metal and metal-ligand bonds had to be developed. In my research, I sought to expand on this idea by adding a third metal to the mix. Trimetallic compounds of the type shown in Figure 1.11 are well-studied, and usually feature three metals of the same type (homometallic), but can also have different metals (heterometallic), where two of the metals are quadruply bonded and the third metal has some interaction without a formal bond. In these compounds, the metals centers are almost all held in place by bridging ligands. One limitation in these

compounds is the choice for the ligand at the axial (end) site, which are primarily chloride ions or solvent molecules, with little variation.

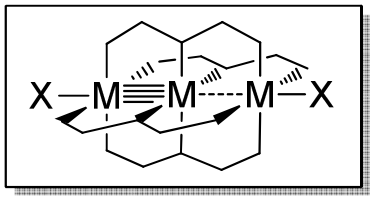

Figure 1.11. A trimetallic complex where X is an axial ligand such as chloride and the ligands surrounding the metal are shaped in paddlewheel formation.

The main goal of this thesis is to prepare trimetallic compounds with more variation at the axial site, with the hope of accessing metal-ligand bonding. The most straightforward way to approach this problem is to isolate a compound with an axial ligand that is able to react in such a way that it forms multiple bonds under some reaction conditions, such as oxidation, heating, or exposure to light. One useful starting point is the azide ligand, N_3^-, which easily loses nitrogen (N_2) upon heating or irradiation (Figure 1.12).

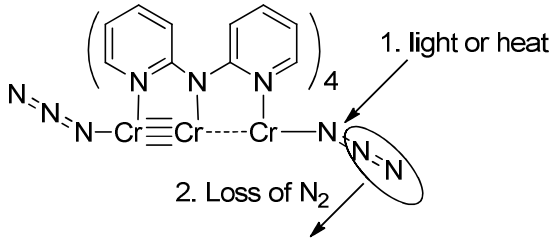

Figure 1.12. Loss of N_2 from azide (may occur on either or both sides of the molecule).

The trimetallic azide compound is very interesting because it could, in principle, lose a dinitrogen molecule from either side of the compound or from both sides, resulting in the formation of a chromium-nitrogen multiple bond. These compounds are also useful because it is easy to prepare analogues containing a different metal, such as manganese,

cobalt, or iron in the third site while the chromium-chromium quadruply bonded unit remains intact. This allows us to study the effect of both changing axial ligands and seeing how the metal choice affects the reactivity of the compound.

We also studied the starting materials and products by a variety of spectroscopic methods, and gained insight into the structure and reactivity of these compounds. Clearly, the use of azide ligands is a very useful way to make trimetallic compounds with new axial ligands.

Another method for making trimetallic compounds with new axial ligands is by simple switching. This thesis describes the use of triflate (an SO_3CF_3 group that is bonded to the metal atom through oxygen), thiocyanate (SCN), or chloride groups in varying arrangements on the trimetallic chain. The preparation of these compounds is straightforward, and usually forms crystals that can be analyzed by X-ray crystallography (see above) to determine their structure. Interestingly, the ligands on one side of the molecule have an impact on the bond lengths and angles on the other side of the molecule. This result was somewhat unexpected because the metal centers are fairly far apart, but it also corroborates the idea that the metal centers are very sensitive to changes in the ligands.

1.8 Conclusions

To conclude, the main goals of this project are three-fold: 1. to determine strategic ways to prepare trimetallic compounds with new axial ligands; 2. to analyze these materials with various spectroscopic techniques to learn about their structures; and 3. to understand how the reactivity of the compounds changes with changes in the structure. I

hope that this chapter has given the reader a glimpse into the logic (and sometimes luck) that goes into preparing new compounds and exploring the depths to which we can push our understanding of fundamental chemical interactions. Thank you for reading!

References

(1) IUPAC, IUPAC Periodic Table of the Elements. http://old.iupac.org/reports/periodic_table/IUPAC_Periodic_Table-1Jun12.pdf, Ed. 2012.

(2) Image taken by the author in the Berry group laboratory.

(3) LBL, The Electromagnetic Spectrum. http://www.lbl.gov/MicroWorlds/ALSTool/EMSpec/EMSpec2.html, Ed. 2012.

(4) Rubinson, K. A.; Rubinson, J. F., *Contemporary Instrumental Analysis*. Prentice-Hall, Inc.: Upper Saddle River, 2000; p 840.

(5) Bruce, P. Y., *Organic Chemistry*. 4th ed.; Pearson Education, Inc. : Upper Saddle River, 2004; p 1228.

(6) Robblee, J. Electron Paramagnetic Resonance (EPR). http://spectroscopy.lbl.gov/EPR-Robblee/EPR-Robblee.pdf (accessed May 24).

(7) Sands, D. E., *Introduction to Crystallography*. Dover Publications, Inc.: New York, 1969; p 165.

(8) Cotton, F. A.; Murillo, C. A.; Walton, R. A., *Multiple Bonds Between Metal Atoms*. 3rd ed.; Springer Science and Business Media, Inc.: New York, 2005; p 817.

(9) Nguyen, T.; Sutton, A. D.; Brynda, M.; Fettinger, J. C.; Long, G. J.; Power, P. P., *Science* **2005,** *310*, 844.

Chapter 2

Introduction: Background and Outline

2.1 Trimetallic Compounds

Metal-metal multiply bonded compounds have been under investigation since the 1960s, starting with work on bimetallic quadruply bonded rhenium compounds. Since that time, a large number of metal-metal bonded species have been prepared, as shown in Table 2.1.[1] The structures and bonding of these compounds are interesting because high bond orders can be achieved and because these compounds are quite stable at ambient temperatures. Still, the addition of another metal center near the metal-metal multiply bonded unit further increases the allure of these compounds and spurs an investigation into the effects of the third metal center on the metal-metal bonded unit and vice versa. Triply-bridging ligands can stabilize three metal centers in a linear arrangement, leading to the formation of chain complexes.

Table 2.1. Number of compounds containing M_2^{n+} cores in 2003.

V *11*	Cr *>500*	Mn	Fe *3*	Co *8*	Ni *1-9*
Nb 7	Mo >1100	Tc >50	Ru >500	Rh >1500	Pd *3*
Ta	W >110	Re >550	Os ~70	Ir 9	Pt *>100*

Trimetallic chain compounds of the type $M_3(dpa)_4X_2$ (where dpa = 2,2'-dipyridylamine and X is an axial ligand such as chloride) have been studied extensively since the 1990s.[2] These compounds, which feature a linear chain of metal atoms coordinated by the bridging dpa ligand in a paddlewheel arrangement, have been

explored with a number of different transition metals, including chromium, molybdenum, tungsten, iron, cobalt, nickel, copper, rhodium and ruthenium and have been fully characterized by X-ray crystallographic and spectroscopic methods. These compounds typically have unpaired electrons and therefore are of interest for their magnetic properties.[1] In addition to varying the identity of M, it is also possible to alter the identity of X in these homometallic compounds, usually by metathesis with one equivalent of a silver or sodium salt (excess can cause either oxidation or demetallation).[1] Using this method, Cotton and coworkers have prepared compounds where X = Cl, Br, CN, NCS, acetylide, or acetonitrile.

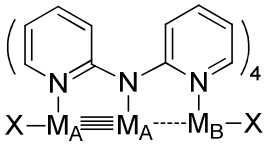

Figure 2.1. Heterotrimetallic compound framework where X is an axial ligand.

The library of chain compounds has been extended in recent years to include heterometallic compounds, shown in Figure 2.1. Although there has been substantial variation in the identity of the metal center, the identity of the axial ligand X has been limited in these heterometallic compounds, the primary body of work featuring chloride ligands in the axial positions. These compounds have been thoroughly studied by our group through crystallography and spectroscopy,[3] but we sought to expand the realm of this work to include variation in the X ligand, as was done with the homometallic compounds.

Recently, our group has become interested in exploring compounds featuring both metal-metal and metal-ligand multiple bonds, particularly metal-oxo and metal-nitrido

moieties. We discovered that a metal-metal bonded diruthenium azide complex can be photolyzed or heated to the corresponding metal-metal bonded nitrido unit, which subsequently undergoes N-atom insertion into a ligand C-H bond (Figure 2.2A). [4] In addition, we have prepared a ditungsten compound that contains a tungsten-oxo moiety (Figure 2.2B).[5] While tungsten-oxo compounds are not particularly rare, they are usually unreactive. Interestingly, the ditungsten-oxo reacts with tri-*tert*-butylphosphine to make the phosphonium salt and other products resulting from reaction with solvent, and it is likely that the second tungsten atom in the molecule increases the reactivity of the tungsten-oxo moiety. [5]

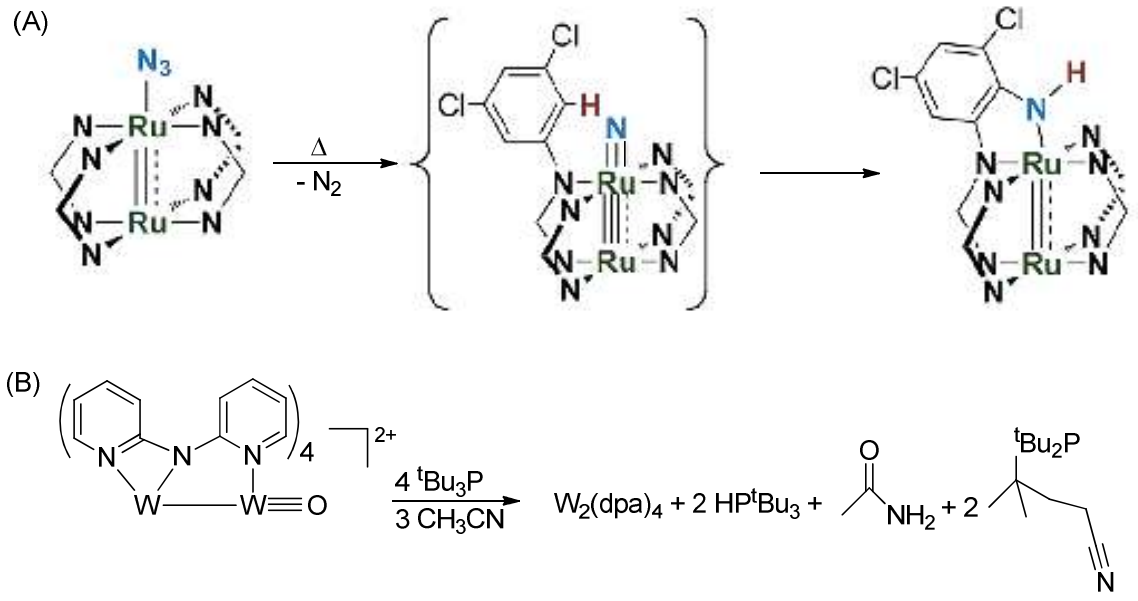

Figure 2.2. (A) Ruthenium-azide thermolysis to form the intramolecular insertion product.[4a] (B) A metal-metal and metal-ligand multiply bonded ditungsten oxo compound.

Inspired by these interesting compounds, we hypothesized that a trimetallic framework should also be able to stabilize metal-ligand multiple bonds, and that this

interaction might be supported by a metal-metal multiply bonded unit. The third metal center should have empty orbitals to facilitate a multiple bond with a ligand such as an oxo or nitrido. There are several methods for appending these moieties to the metal center, as will be discussed further in the next section.

2.2 Metal-Oxo and Metal-Nitrido Bonds

Synthetic efforts toward the preparation of metal-oxo and metal-nitrido moieties have been well-documented by a number of researchers, and an overview of these methods is presented here.

2.2.1 Metal-Oxo Synthesis

Terminal metal-oxo moieties are implicated as reactive intermediates in biologically relevant processes, such as the oxidation of inert C-H bonds by the heme iron(IV) oxo in the active site of cytochrome P450[6] and various peroxidases.[7] Taking a hint from nature, synthetic chemists have sought to prepare this reactive species to do similar oxidation reactions.

Although there are some examples of biomimetic heme-containing Fe^{IV} oxo compounds,[8] there was a dearth of non-heme Fe^{IV} oxo species until Wieghardt and co-workers reported ozonolysis of an Fe^{III} cyclam complex to generate an Fe^{IV} oxo species, as confirmed by absorption and Mössbauer spectroscopy.[9] Due to the low yield of this reaction, however, other synthetic methods were investigated. Later, it was found that reaction of an Fe^{III} TAML complex (TAML = tetraamido macrocyclic ligand) with *tert*-butyl hydroperoxide in basic water also leads to the formation of an Fe^{IV} oxo species.[10]

Another interesting technique for the generation of an Fe^{IV} oxo compound is oxygenation of an Fe^{II}(TMC-py) precursor (where TMC-py = 1-(2'pyridylmethyl)-4,8,11-trimethyl-1,4,8,11-tetrzazacyclotetradecane) in the presence of acid and tetraphenylborate anion (Figure 2.3).[11] The Que group further found that reaction of Fe^{II}(TMC-py) with 1 equivalent of hydrogen peroxide and 2,6-lutidine (which acts as an acid-base catalyst) in acetonitrile forms $[Fe^{IV}(O)(TMC\text{-}py)(CH_3CN)]^{2+}$ in >85% yield.[12] It is interesting to note that while the Fe^{IV} oxo unit may be generated directly from the Fe^{II} precursor, it is also possible to go stepwise through O-O bond cleavage of an Fe^{III} hydoperoxo compound (generated by reaction of an Fe^{II} reactant with excess peroxide).[13] Recently, a new Fe^{II} carboxylate-ligated starting material was reported and subsequently converted to a highly reactive Fe^{IV} oxo compound by reaction with oxygen atom transfer reagents such as $NaIO_4$, hydrogen peroxide or 3-chloroperoxybenzoic acid.[14] Overall, the the Que group has optimized several methods for the preparation of an Fe^{IV} oxo and can generate this reactive species via oxidation of Fe precursors that have rigid ligand platforms.

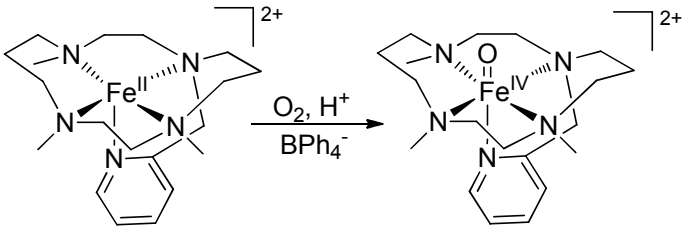

Figure 2.3. Synthesis of Fe(IV)-oxo from the Fe(II) precursor.

2.2.2 Metal-Nitrido Synthesis

There are several useful methods for the generation of terminal metal-nitrido moieties, as will be presented in this section. For the sake of brevity, only techniques that lead to terminal metal-nitrido compounds and have fewer than two steps will be presented. These methods can be grouped into three categories: photolysis, thermolysis, or reaction of an azide precursor, oxidation of an ammonia adduct, and N-atom transfer (Figure 2.4).

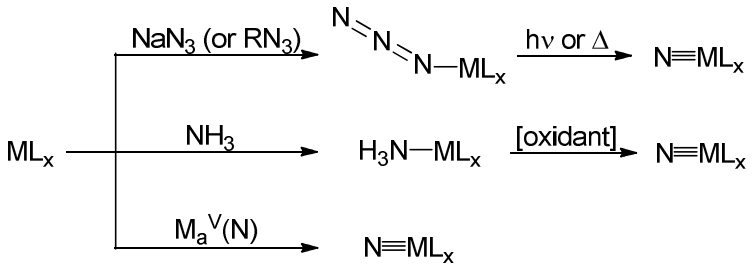

Figure 2.4. Synthetic routes for the formation of metal-nitrido compounds.

Perhaps the most common synthetic route toward the formation of metal-nitrido compounds is reaction with, or decomposition of, metal-azide compounds. Early work showed that reaction of a metal precursor with sodium azide or an organic azide at ambient conditions results in the formation of a metal-nitrido compound[15] and this method was used recently in the synthesis of the first uranium-nitrido complex.[16] Typically, reaction of a metal with sodium azide results in the formation of a metal azide, which must be heated or photolyzed to form the corresponding nitrido compound. This method has been used extensively in the formation of metal-nitrido compounds since the early 1980s.[4b,9,15c,17] Although this method is very effective, it can be problematic for late metal compounds, as photolysis of azides has been known to cause photoreduction

instead of photooxidation of the compound, which inhibits formation of the desired nitrido compound.[17a,18] As a result, other pathways for the formation of nitrido compounds are exploited by researchers in this field.

Another well-known synthetic method for the preparation of terminal metal-nitrido compounds is the oxidation of metal-ammonia compounds by oxidants such as cerium(IV) salts[19] or sodium hypochlorite.[15c,17b,20] This method is useful, but is limited to compounds that are tolerant of such highly oxidizing conditions.

To avoid the problems presented in the first two synthetic routes, it is useful to consider the N-atom transfer pathway, wherein the nitrogen atom of a metal-nitrido is transferred to another metal center. Bendix and co-workers have made a series of chromium-nitrido compounds using N-atom transfer from a manganese-nitrido compound of salen.[21] This method is useful because the starting materials are inexpensive and because the corresponding manganese chloride compound precipitates out of solution, driving the reaction. However, this work has thus far been limited to N-atom transfer to Cr, forming unreactive chromium nitrides and more work must be done to expand the utility of this pathway.

2.3 Outline

Chapter three of this work will detail efforts toward the preparation of new heterotrimetallic compounds containing variation in the axial ligand position. The impact of axial ligation on the bond distances of metal-ligand bonds and the induced “tilting” effect are discussed. Chapter four of this work will highlight the synthesis and characterization of a series of trimetallic diazide compounds. It will showcase efforts

toward the formation of a compound containing both metal-metal and metal-ligand multiple bonds through azide photolysis and thermolysis. Chapter five of this thesis details a simple N-atom transfer route for the preparation of a reactive iron-nitrido species and its reaction with triphenylphosphine. Chapter six will outline reactions of trimetallic compounds with oxygen atom transfer reagents and provide evidence for the formation of trimetallic aklyperoxo species.

References

(1) Cotton, F. A.; Murillo, C. A.; Walton, R. A., *Multiple Bonds Between Metal Atoms*. 3rd ed.; Springer Science and Business Media, Inc.: New York, 2005; p 817.

(2) Aduldecha, S.; Hathaway, B., *J. Chem. Soc., Dalton Trans.* **1991**, 993.

(3) (a) Nippe, M.; Berry, J. F., *J. Am. Chem. Soc.* **2007,** *129*, 12684; (b) Nippe, M.; Victor, E.; Berry, J. F., *Eur. J. Inorg. Chem.* **2008,** *2008*, 5569; (c) Nippe, M.; Wang, J.; Bill, E.; Hope, H.; Dalal, N. S.; Berry, J. F., *J. Am. Chem. Soc.* **2010,** *132*, 14261.

(4) (a) Musch Long, A. K.; Yu, R. P.; Timmer, G. H.; Berry, J. F., *J. Am. Chem. Soc.* **2010,** *132*, 12228; (b) Long, A. K. M.; Timmer, G. H.; Pap, J. z. S.; Snyder, J. L.; Yu, R. P.; Berry, J. F., *J. Am. Chem. Soc.* **2011,** *133*, 13138.

(5) Nippe, M.; Goodman, S. M.; Fry, C. G.; Berry, J. F., *J. Am. Chem. Soc.* **2011,** *133*, 2856.

(6) Schlichting, I.; Berendzen, J.; Chu, K.; Stock, A. M.; Maves, S. A.; Benson, D. E.; Sweet, R. M.; Ringe, D.; Petsko, G. A.; Sligar, S. G., *Science* **2000,** *287*, 1615.

(7) Sono, M.; Roach, M. P.; Coulter, E. D.; Dawson, J. H., *Chem. Rev.* **1996,** *96*, 2841.

(8) Groves, J. T.; Han, Y.-Z., Models and Mechanisms of Cytochrome P450 Action. In *Cytochrome P450: Structure, Mechanism, and Biochemistry*, Ortiz De Montellano, P. R., Ed. Springer: New York, 1995; pp 3.

(9) Grapperhaus, C. A.; Mienert, B.; Bill, E.; Weyhermüller, T.; Wieghardt, K., *Inorg. Chem.* **2000,** *39*, 5306.

(10) Chanda, A.; Shan, X.; Chakrabarti, M.; Ellis, W. C.; Popescu, D. L.; Tiago de Oliveira, F.; Wang, D.; Que, L.; Collins, T. J.; Münck, E.; Bominaar, E. L., *Inorg. Chem.* **2008,** *47*, 3669.

(11) Thibon, A.; England, J.; Martinho, M.; Young, V. G.; Frisch, J. R.; Guillot, R.; Girerd, J.-J.; Münck, E.; Que, L.; Banse, F., *Angew. Chem. Int. Ed.* **2008,** *47*, 7064.

(12) Li, F.; England, J.; Que, L., *J. Am. Chem. Soc.* **2010,** *132*, 2134.

(13) Li, F.; Meier, K. K.; Cranswick, M. A.; Chakrabarti, M.; Van Heuvelen, K. M.; Münck, E.; Que, L., *J. Am. Chem. Soc.* **2011,** *133*, 7256.

(14) McDonald, A. R.; Guo, Y.; Vu, V. V.; Bominaar, E. L.; Munck, E.; Que, L., *Chem. Sci.* **2012,** *3*, 1680.

(15) (a) Griffith, W. P.; Pawson, D., *J. Chem. Soc., Dalton Trans.* **1973**, 1315; (b) Chan, D. M. T.; Chisholm, M. H.; Folting, K.; Huffman, J. C.; Marchant, N. S., *Inorg. Chem.* **1986,** *25*, 4170; (c) Dehnicke, K.; Strähle, J., *Angew. Chem. Int. Ed.* **1992,** *31*, 955.

(16) King, D. M.; Tuna, F.; McInnes, E. J. L.; McMaster, J.; Lewis, W.; Blake, A. J.; Liddle, S. T., *Science* **2012**.

(17) (a) Meyer, K.; Bill, E.; Mienert, B.; Weyhermüller, T.; Wieghardt, K., *J. Am. Chem. Soc.* **1999,** *121*, 4859; (b) Eikey, R. A.; Abu-Omar, M. M., *Coord. Chem. Rev.* **2003,** *243*, 83; (c) Berry, J. F.; Bill, E.; Bothe, E.; George, S. D.; Mienert, B.; Neese, F.; Wieghardt, K., *Science* **2006,** *312*, 1937; (d) Vogel, C.; Heinemann, F. W.; Sutter, J.; Anthon, C.; Meyer, K., *Angew. Chem. Int. Ed.* **2008,** *47*, 2681; (e) Schöffel, J.; Rogachev, A. Y.; DeBeer George, S.; Burger, P., *Angew. Chem. Int. Ed.* **2009,** *48*, 4734; (f) Scepaniak, J. J.; Young, J. A.; Bontchev, R. P.; Smith, J. M., *Angew. Chem. Int. Ed.* **2009,** *48*, 3158.

(18) Song, Y.-F.; Berry, J. F.; Bill, E.; Bothe, E.; Weyhermüller, T.; Wieghardt, K., *Inorg. Chem.* **2007,** *46*, 2208.

(19) Buhr, J. D.; Winkler, J. R.; Taube, H., *Inorg. Chem.* **1980,** *19*, 2416.

(20) Du Bois, J.; Hong, J.; Carreira, E. M.; Day, M. W., *J. Am. Chem. Soc.* **1996,** *118*, 915.

(21) (a) Bendix, J.; Meyer, K.; Weyhermüller, T.; Bill, E.; Metzler-Nolte, N.; Wieghardt, K., *Inorg. Chem.* **1998,** *37*, 1767; (b) Bendix, J., *J. Am. Chem. Soc.* **2003,** *125*, 13348; (c) Birk, T.; Bendix, J., *Inorg. Chem.* **2003,** *42*, 7608.

Chapter 3

Remote Effects of Axial Ligand Substitution in Heterometallic Cr≡Cr···M Chains

The primary body of this paper was composed by both Michael Nippe and Yevgeniya Turov. Yevgeniya Turov developed the pathway for the synthesis of $Cr_2Fe(dpa)_4(OTf)_2$ and performed complete characterization on this compound. Additionally, the NMR and IR data for these compounds was collected by Yevgeniya Turov.

3.1 Abstract

The heterometallic complexes $CrCrM(dpa)_4Cl_2$ (dpa = 2,2'-dipyridylamide) featuring linear Cl−Cr≡Cr···M−Cl chains can regiospecifically be modified via axial ligand substitution to yield OTf−Cr≡Cr···M−Cl chains (OTf = triflate) with M being Fe, Mn or Co. The effect of OTf substitution on the Cr side of the molecule has an unusual and profound structural impact on the square-pyramidal transition metal M. Specifically, elongation of the four equatorial $M-N_{py}$ bonds and the axial M−Cl bonds by 0.03 and 0.09 Å for Fe and 0.07 and 0.11 Å for Mn is observed. The longer M−Cl and $M-N_{py}$ bonds result from subtle interactions between the equatorial dpa ligand and the three metal ions. The equatorial dpa ligand responds to the introduction of the more labile OTf ligand at Cr by binding more strongly to this Cr ion which in turn weakens bonding to M. The ligand field experienced by M can be tuned by changing the Cr axial ligand, and this effect is observed in electrochemical measurements of the iron compounds.

3.2 Introduction

The reactivity of heterometallic coordination complexes has recently been of interest,[1,2] especially with respect to models of heterometallic enzyme active sites.[3] In this respect, the differential reactivity of M–L vs M′–L bonds in heterometallic molecules containing both M and M′ deserves inquiry. Research efforts in our lab have afforded rational synthetic methods to access a class of heterometallic complexes $CrCrM(dpa)_4Cl_2$ that contain linear Cl−Cr≡Cr···M−Cl chains, with M = Mn^{II},[4] Fe^{II},[5] or Co^{II},[6] (here, dpa = the anion of 2,2'-dipyridylamine). The metal atoms are ligated equatorially by the nitrogen atoms of dpa and the outer metal atoms are ligated axially by chloride. These linear frameworks are ideally suited to allow for experiments probing the nature of secondary interactions at the N_4MCl square pyramidal transition metal center in response to differing axial ligands appended to the Cr≡Cr multiply bonded group (Scheme 3.1). Whether a specific change made at the Cr end of the molecule has any effect on the geometry of M may have important implications for the nature of charge distribution and Cr···M interactions in these molecules.

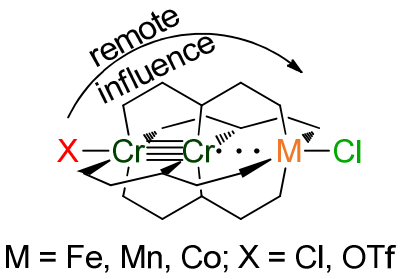

Scheme 3.1. Influence of axial ligation.

We report herein the preparation of new mixed chloride/triflate compounds and the novel ditriflate compound $CrCrFe(dpa)_4(OTf)_2$ ($OTf = {}^{-}OSO_2CF_3$) along with crystallographic, spectroscopic and electrochemical data. These data provide evidence that the geometry and properties of M are strongly influenced by ligand substitution on the Cr side of the linear framework. This *remote influence* is induced by a tilting of the dpa ligands about their central amido nitrogen atoms in response to the variable ligand field strength at the terminal Cr atom.

3.3 Experimental Section

3.3.1 Materials and Methods

All reactions were carried out under a dry N_2 atmosphere using Schlenk techniques and glovebox methods. Solvents diethyl ether (Et_2O), acetonitrile (CH_3CN) and hexanes were purified using a Vacuum Atmospheres solvent purification system. Dichloromethane was freshly distilled under an N_2 atmosphere over CaH_2 prior to use. $Fe(OTf)_2$ (Wako) and Tl(OTf) (Strem) were purchased and used as received. NaSCN (Sigma-Aldrich) was dried at 80°C for ~10 h under dynamic vacuum prior to use. The ligand dpaH (2,2′-dipyridylamine, Sigma-Aldrich) was recrystallized from hot hexanes prior to use. $Cr_2(dpa)_4$,[5] $CrCrFe(dpa)_4Cl_2$ (**1**),[5] $CrCrMn(dpa)_4Cl_2$ (**2**),[4] and $CrCrCo(dpa)_4Cl_2$ (**7**)[6] were prepared according to literature procedures. Cyclic voltammograms (CVs) were taken on a BAS Epsilon-EC instrument using CH_2Cl_2 solutions with 0.1 M NBu_4PF_6 and <1 mM substrate. The electrodes were as follows: glassy carbon (working), Pt wire (auxiliary) and Ag/Ag^+ in CH_3CN (reference). The potentials were referenced versus the ferrocene/ferrocenium redox couple, by externally

added ferrocene. Elemental analysis was carried out by Columbia Analytical Services in Arizona, USA and Midwest Microlab, LLC in Indiana, USA. X-Band EPR spectra of frozen solutions (CH_2Cl_2) of **8/8-iso** were recorded at 4 and 8 K temperature using a Bruker EleXsys EPR spectrometer: E-500-A console with ER 049SX SuperX Bridge and SuperX Cavity. The sample temperature was set using an Oxford Instruments ESR 900 continuous flow liquid helium cryostat regulated by an Oxford ITC4 temperature controller. The IR spectra were taken on a BRUKER TENSOR 27 using KBr techniques. ^{1}H-NMR spectra were recorded on a Varian INOVA-500 spectrometer. The magnetic susceptibility of compounds **3** and **5** were established using an Evans balance, with proper diamagnetic corrections calculated from Pascal's constants.[7]

OTfCrCrFeCl(dpa)$_4$ (3). *Route A.* A suspension of TlOTf (66 mg, 0.188 mmol) in CH_2Cl_2 (8 mL) was slowly added to a stirred solution of **1** (185 mg, 0.188 mmol) in CH_2Cl_2 (25 mL) at 0°C. The mixture was stirred for a minimum of 1 h during which it was allowed to warm to room temperature. Filtration through celite and subsequent diffusion of hexanes into the yellow-brown solution yielded crystalline material of **3**. Yield: 120 mg, 62%. Anal. Calcd. for $C_{41}H_{32}ClFeCr_2F_3N_{12}O_3S$ (**3**): C 48.04%, H 3.15%, N 16.40%; found C 47.64%, H 3.31%, N 16.05%. μ_{eff} (298 K, μ_B) = 4.37. ^{1}H-NMR (CD_2Cl_2, 500 MHz, ppm): δ 112.36, 70.66, 40.49, 6.39, 4.30, 4.09, 3.64, -1.97. IR (KBr, cm^{-1}): 1605 m, 1595 m, 1560 w, 1549 w, 1469 s, 1424 s, 1367 s, 1310 m, 1285 m, 1235 m, 1217 m, 1167 m, 1153 m, 1109 w, 1051 w, 1027 m, 1018 m, 920 w, 880 m, 860 w, 764 s, 740 m, 648 w, 634 m, 570 w, 517 m.

Route B. CH_2Cl_2 (30 mL) was added to a solid mixture of **1** (64 mg, 0.07 mmol) and **5** (80 mg, 0.07 mmol) and the resulting yellow-brown solution was stirred for a minimum of 2 h at room temperature. Subsequent filtration and diffusion of hexanes into the CH_2Cl_2 solution yielded crystalline material of **3**, in very high purity as determined by ^{1}H-NMR spectroscopy. Yield: 90 mg, 63%.

OTfCrCrMnCl(dpa)$_4$ (4). Compound **4** was prepared from **2** analogously to *Route A* for the preparation of **3**. Yield: 30 mg, 53%. Anal. Calcd. for $C_{46.2}H_{43.8}Cl_3Cr_2F_3MnN_{12}O_3S$ (**4·2CH$_2$Cl$_2$**): C, 43.25%; H, 3.04%; N, 14.08%. Found: C, 42.90%; H, 3.38%; N, 13.71%. IR (KBr, cm^{-1}): 1606 s, 1595 s, 1560 w, 1550 w, 1470 s, 1459 s, 1424 s, 1366 m, 1310 m, 1287 w, 1235 m, 1217 m, 1167 m, 1153 m, 1106 w, 1028 m, 1018 m, 1007 w, 920 w, 879 w, 860 w, 764 m, 748 w, 741 m, 668 w, 649 w, 635 m, 538 w, 517 w.

CrCrFe(dpa)$_4$(OTf)$_2$ (5). THF (35 mL) was added to a solid mixture of orange $Cr_2(dpa)_4$ (380 mg, 0.48 mmol) and off-white $Fe(OTf)_2$ (190 mg, 0.53 mmol). The suspension was heated to reflux whilst stirring for a minimum of 7 h, after which the formation of a lustrous gold-colored precipitate was observed. The crude product was isolated by filtration. X-ray quality crystals were grown by diffusion of hexanes into a solution of the compound in dichloromethane. Yield: 410 mg, 74%. Anal. Calcd. for $C_{43.5}H_{35}Cr_2F_6FeN_{12}O_6S_2Cl_3$ (**5·0.5CH$_2$Cl$_2$·0.15C$_4$H$_8$O**): C, 42.92%; H, 2.95%; N, 13.90%. Found: C, 43.43%; H, 2.89%; N, 14.10%. μ_{eff}(298 K, μ_B) = 4.78. ^{1}H-NMR (CD_2Cl_2, 500 MHz, ppm): δ 105.02, 71.23, 39.29, 4.49, 3.84, 2.47, -0.76, -2.65. IR (KBr,

cm^{-1}): 1607 m, 1598 m, 1551 w, 1471 s, 1430 , 1365 m, 1314 m, 1287 m, 1235 m, 1213 m, 1155 m, 1028 m, 1018 m, 881 w, 861 w, 766 m, 740 w, 636 m.

(SCN)CrCrFeCl(dpa)$_4$ (6). Compound **3** was formed *in situ* via route A, from **1** (140 mg, 0.14 mmol) and TlOTf (50 mg, 0.14 mmol). A solution (3.7 mL) of NaSCN (38 mM) was added dropwise over 4 minutes to the yellow-brown solution of **3** and a slight color change to red-brown was observed. Solvent was removed under reduced pressure, yielding a red-brown microcrystalline solid. The solid was washed with 10 mL Et_2O and extracted into 20 mL CH_2Cl_2. Solvent diffusion of Et_2O into the solution mixture yielded a small amount of crystalline material. Yield: 6.4 mg, 5%. Anal. Calcd. for $C_{41.5}H_{33}Cl_2FeCr_2F_3N_{13}S$ (**6**·$0.5CH_2Cl_2$): C 51.03%, H 3.38%, N 18.65%; found C 51.39%, H 3.60%, N 18.34%. IR (KBr, cm^{-1}): 2040 s, 1605 m, 1595 m, 1548 w, 1466 s, 1426 s, 1369 m, 1311 m, 1282 w, 1154 m, 1017 m, 880 w, 859 w, 764 m, 739 m, 647 w, 538 w, 518 w.

OTfCrCrCoCl(dpa)$_4$/ClCrCrCoOTf(dpa)$_4$ (8/8-iso). Compounds **8/8-iso** were prepared as a mixture from **7** analogously to *Route A* for the preparation of **3**. Yield: 70 mg, 42% Anal. Calcd. for Anal. Calcd. for $C_{41.1}H_{32.2}Cl_{1.2}CoCr_2F_3N_{12}O_3S$ (**8/8-iso**): C 47.89%, H 3.14%, N 16.35%; found C 47.37%, H 2.96%, N 15.73%. IR (KBr, cm^{-1}): 3070 w, 3031 w, 2972 w, 2853 w, 1607 s, 1596 s, 1550 w, 1469 s, 1429 s, 1371 s, 1313 s, 1286 s, 1234 s, 1213 s, 1155 s, 1112 w, 1018 s, 881 m, 861 m, 765 s, 740 s.

3.3.2 X-Ray Structure Determinations

Crystallographic data were measured at the Molecular Structure Laboratory of the Chemistry Department of the University of Wisconsin – Madison. Crystals were selected

under oil under ambient conditions. Block shaped single crystals were attached to the tip of a MiTeGen MicroMount©. The crystals were mounted in a stream of cold nitrogen at 100(1) K and centered in the X-ray beam using a video monitoring system. The crystal evaluation and data collection were performed on a Bruker Quazar SMART APEX-II diffractometer with Mo K_α ($\lambda = 0.71073$ Å) radiation. The data were collected using a routine to survey reciprocal space, and were indexed by the SMART program.[8] The structures were solved using direct methods and refined by least-squares refinement on F^2 followed by difference Fourier synthesis.[9] All hydrogen atoms were included in the final structure factor calculation at idealized positions and were allowed to ride on the neighboring atoms with relative isotropic displacement coefficients.

The crystal structure of **5** deserves additional comments: The structure was solved with space group *C*2/*c*, but was found to refine poorly. However, the model refines well in the space group *Cc* as an inversion twin with a minor component contribution of 19%. The two independent molecules were solved using the program smtbx with charge flipping and refined over several cycles to complete the ligands.[10] One of the four independent triflate ligands is disordered (18%/82%), as are the Cr and Fe atoms. The metal atoms (Fe and Cr) were not refined anisotropically except Cr2/Cr2A and Cr4/Cr4A, which were sufficiently far apart that anisotropic refinement was appropriate. The metal atoms had variable occupancy of 76%/24% ratio in one and 43%/57% ratio in the second molecule. The disordered triflate ions were also not refined anisotropically, except for O7, S4 and S4A atoms. There is also one partially occupied disordered tetrahydrofuran molecule in the asymmetric unit, which was not refined anisotropically.

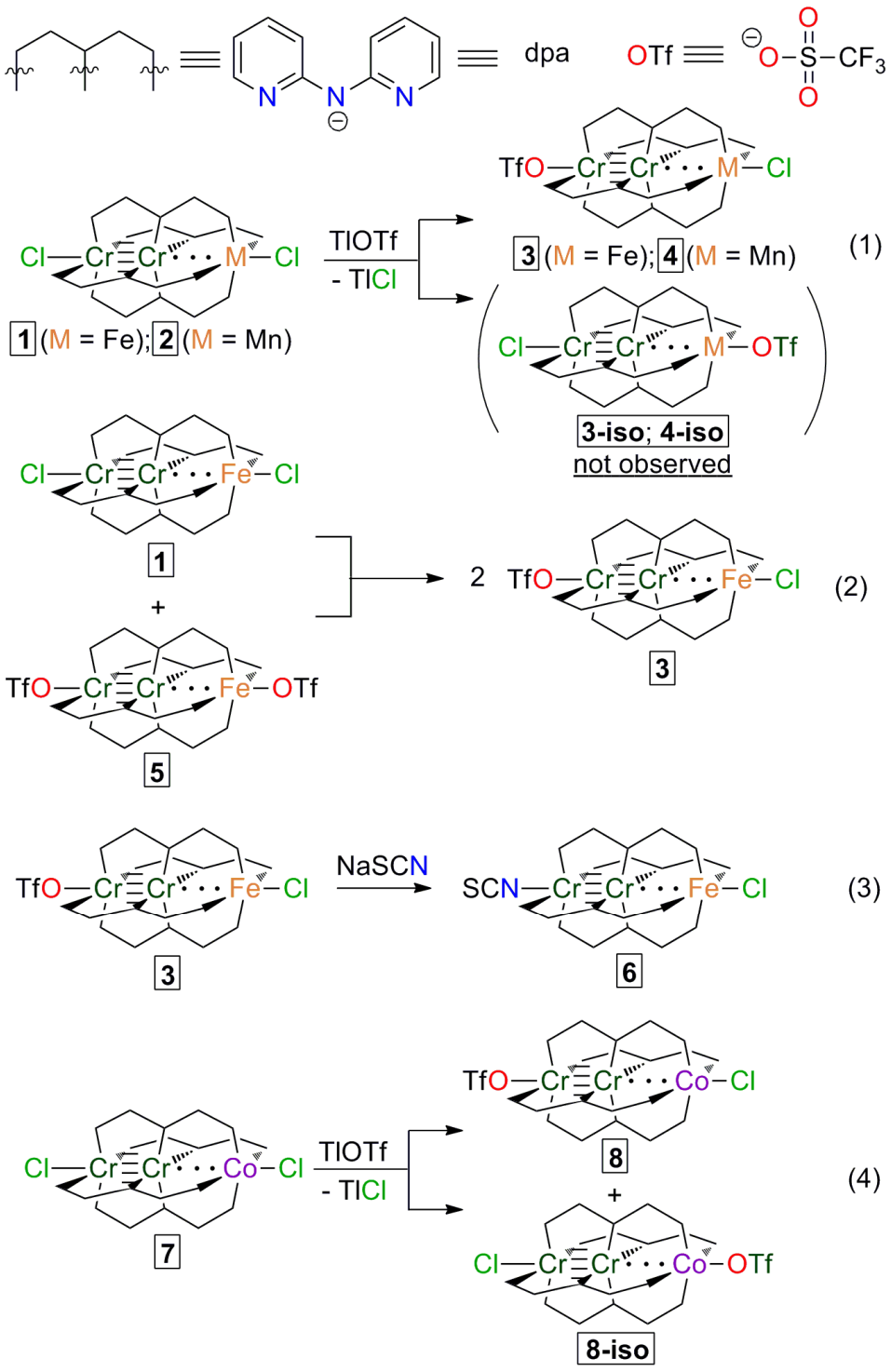

Scheme 3.2. Synthetic pathways.

3.4 Results and Discussion

3.4.1 Synthesis

The synthetic methods and numbering for the compounds reported here are outlined in Scheme 3.2. Reaction of **1** with one equivalent of thallium triflate (TlOTf) in CH_2Cl_2 at 0°C results in the regiospecific substitution of the Cr-bound chloride (Cl_{Cr}) ion for triflate, yielding the mono-triflate complex **3** in good yield (63%) and TlCl as a precipitate (equation 1, Scheme 3.2). The regioselectivity of the reaction and the characterization of the product as a single component was established via ^{1}H-NMR spectroscopy and X-ray crystallography (*vide infra*). The selectivity of this reaction is likely promoted by the kinetic lability of Cl_{Cr} (d(Cr−Cl) = ~2.7 Å) as compared to Cl_{Fe} (d(Fe−Cl) = ~2.3 Å) and the possible thermodynamic preference of the Cr_2 unit for the weaker axial σ donor OTf ligand in **3** *vs.* Cl. The same kinetic argument holds for the corresponding reaction of **2** with TlOTf to generate **4**, because of the large difference in bond distances for the metal-chloride bonds in **2**,[4] d(Cr−Cl) = ~2.7 Å as compared to d(Mn−Cl) = ~2.3 Å. Alternatively, **3** can be furnished in high purity via reaction of **1** with the ditriflate compound **5** (equation 2). This equilibration reaction is the preferred synthetic route to **3** because it avoids the use of thallium salts and can easily be scaled up.

Compound **5** is conveniently prepared in analogy to the dichloride compound **1** by metallation of $Cr_2(dpa)_4$ with ferrous ditriflate ($Fe(OTf)_2$) in tetrahydrofuran (THF) at elevated temperatures. The resulting solid material can be extracted with CH_2Cl_2 and crystallizes upon addition of hexanes. X-ray crystallographic examination of the crystalline sample is consistent with the molecular connectivity of **5** as drawn in Scheme

3.1 (*vide infra*). The ability of compound **3** to serve as a synthon for the selective generation of further heteroligated X−Cr≡Cr···Fe−Cl compounds was established by preparation of **6** (equation 3): careful addition of one equivalent of a dilute solution of sodium thiocyanate (NaNCS) in acetonitrile (CH_3CN) to a CH_2Cl_2 solution of **3** results in substitution of the labile OTf^- ligand by NCS^- to furnish the isothiocyanato complex **6**. The yield of this reaction is poor due to a side reaction including Fe demetallation; thus, reliable synthetic routes to heteroligated species still need to be found. Nevertheless, good quality single crystals of **6** were obtained via diffusion of Et_2O into CH_2Cl_2.

We also investigated the possibility of extending the initial synthetic protocol of generating **3** via Cl^- abstraction from **1** (using TlOTf) to structural analogs of **1**, namely $CrCrMn(dpa)_4Cl_2$, **2**, and $CrCrCo(dpa)_4Cl_2$, **7**. Like **1**, compound **2** undergoes regiospecific ligand exchange at the Cr end of the molecule with TlOTf furnishing **4** as the sole product (equation 1). In the case of **7**, however, no such selectivity can be reported, and it is of interest to note that in the low-spin form, the Co-Cl and Cr-Cl bond distances are equal (d(Co−Cl) = ~2.6 Å and d(Cr−Cl) = ~2.6 Å), whereas the high-spin form of **7** resembles **1** and **2** with d(Co−Cl) = ~2.4 Å and d(Cr−Cl) = ~2.6 Å.[6] A product mixture containing the mono-triflate compounds **8** and **8-iso** was obtained (equation 4) with OTf^- bound to either the terminal Cr or the Co ion, respectively. To our knowledge, this is the first report of two compounds that are heterometallic and heteroligated isomers. We have not been able to separate these isomers.

3.4.2 Crystal Structures

X-ray crystallographic results are presented in three parts: *(1)* a general discussion addresses metal atom disorder and intermolecular interactions between the trinuclear compounds and cocrystallized solvent molecules where applicable; *(2)* a detailed discussion addresses the assignment of the non-centrosymmetric space group *Cc* to structures of **3**, **4**, **5** and **8/8-iso**; *(3)* a detailed discussion of structural changes induced by ligand substitution is given. Crystallographic details and bond distances for all discussed compounds are given in Tables 3.1 and 3.2, respectively.

Table 3.1. Crystallographic Data.

Compound	**3**	**4**	**5**	**6**	**8/8-iso**
	100 K	100 K	100 K	100 K	100 K
Formula	$Cr_2Fe(C_{10}H_8N_3)_4(CF_3SO_3)Cl\cdot 2CH_2Cl_2$	$Cr_2Mn(C_{10}H_8N_3)_4(CF_3SO_3)Cl\cdot 2CH_2Cl_2$	$[Cr_2Fe(C_{10}H_8N_3)_4(CF_3SO_3)_2]_2\cdot CH_2Cl_2\cdot 0.3C_4H_8O$	$Cr_2Fe(C_{10}H_8N_3)_4(NCS)Cl\cdot Et_2O$	$Cr_2Co(C_{10}H_8N_3)_4(CF_3SO_3)Cl\cdot 2CH_2Cl_2$
Crystal system	Monoclinic	Monoclinic	Monoclinic	Monoclinic	Monoclinic
Space group	*C c*	*C c*	*C c*	*P 2₁ / c*	*C c*
a, Å	18.961(2)	18.981(2)	34.4912(9)	16.3144(5)	18.861(2)
b, Å	16.951(2)	16.917(2)	17.8894 (5)	16.1054(5)	16.999(2)
c, Å	15.607(1)	15.641(1)	16.8300(4)	17.5820(5)	15.574(2)
β, °	109.088(1)	108.931(1)	108.302(1)	103.998(2)	109.330(2)
V, Å^3	4740.3(7)	4750.8(7)	9859.3(4)	4482.5(2)	4712.0(9)
Z	4	4	8	4	4
ρ, Mg m^{-3}	1.674	1.669	1.593	1.494	1.689
R1[a], *w*R2[b] (*I* > 2σ(*I*))	0.0388, 0.1012	0.0315, 0.0791	0.0467, 0.1312	0.0531, 0.1414	0.0500, 0.1224
R1[a], *w*R2[b] (all data)	0.0511, 0.1168	0.0374, 0.0891	0.0484, 0.1323	0.0541, 0.1422	0.0563, 0.1274

[a]R1 = 3||Fo| - |Fc||/3|Fo|. [b]wR2 = $[3[w(F_o^2 - F_c^2)^2]/3[w(F_o^2)^2]]^{½}$, w = 1/σ2($F_o^2$) + (aP)2 + bP, where P = [max(0 or F_o^2) + 2(F_c^2)]/3.

(1) General discussion. Single-crystalline material of compounds **3**, **4**, and **8/8-iso** was obtained from CH_2Cl_2/hexanes solvent mixtures. The molecules crystallize as $M{\cdot}2CH_2Cl_2$ solvates in the monoclinic space group *Cc*. Because Cr and Fe (or Mn or Co) are crystallographically indistinguishable, the assignments of metal atom identities are based on expected distances for quadruply bonded Cr≡Cr units. The metal atoms in **3** (Figure 3.1, left) and **4** show no sign of metal atom disorder in contrast to their precursors **1** and **2**, respectively. The absence of disorder of the metal atom positions indicates that the crystals considered contain solely **3** (or **4**) and none of the possible structural isomer **3-iso** (or **4-iso**), because cocrystallization of the product mixture would be expected as in the case of **8/8-iso**; however, it is possible that isomers of **3-iso** and **4-iso** do form in the reaction and were simply not seen in the particular crystals that were examined crystallographically. But, ^{1}H NMR studies on **3** show the existence of only one species in solution of the bulk sample, and we may therefore discount the possibility that **3-iso** is formed. In the case of **8-iso**, both the high-spin and low-spin forms of **7** are present in solution and the low-spin case has elongated Co-Cl bond distances which results in the formation of the **8-iso**. Conversely, compounds **1** and **2** are present solely in the high-spin form in which the Cr-Cl bond is longer than the M-Cl bond and the formation of **3-iso** and **4-iso** is not probable.

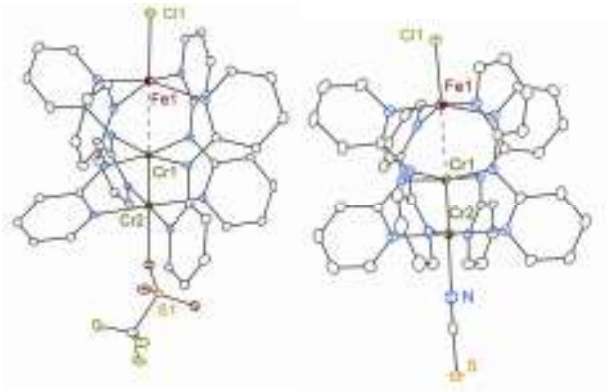

Figure 3.1. Molecular structures of **3** (left) and **6** (right) with displacement ellipsoids drawn at the 30% probability level. Hydrogen atoms have been omitted for clarity.

Cocrystallization of isomers is observed for the product mixture after reaction of **7** with TlOTf: the metal atoms in **8**/**8-iso** are clearly disordered with relative occupancies of 67%/33%, respectively, indicating cocrystallization of the two distinguished molecular entities, featuring either an N_4CoCl (in **8**) or N_4CoOTf (in **8-iso**) unit (Figure 3.2).

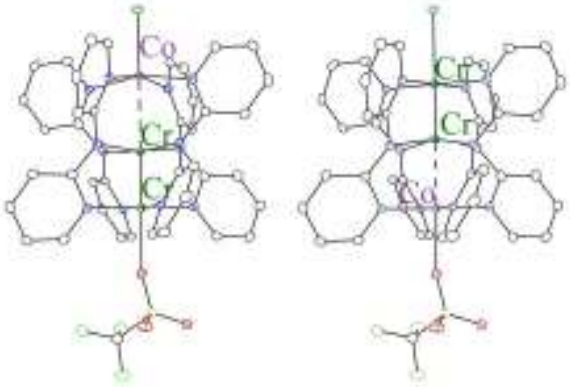

Figure 3.2. Molecular structures of cocrystallized **8** (left) and **8-iso** (right) with displacement ellipsoids drawn at the 30% probability level. Hydrogen atoms have been omitted for clarity.

Another important feature of the crystal structures of **3**, **4**, and **8** is the proximity of a solvent CH_2Cl_2 molecule ($d(Cl\cdots H(CH_2Cl_2) = 2.65$ Å) to the chloro ligand at a

distance less than the sum of their van der Waals radii (Figure 3.3), which is indicative of an intermolecular interaction (directional Cl···H−C angle = 152°). Similar interactions in crystalline material of **1** and **2** have recently been shown to have a significant influence on the spectroscopic properties of the paramagnetic metal.[4]

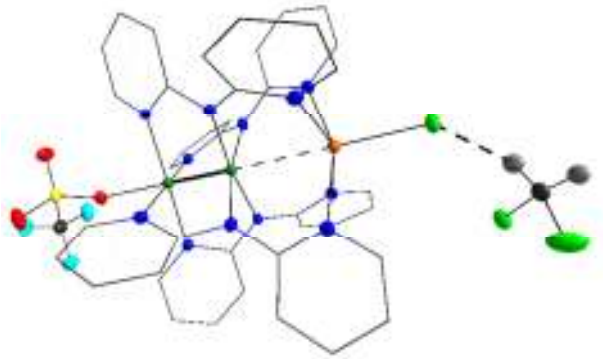

Figure 3.3. Molecular structure of **4** highlighting the intermolecular Mn−Cl···H(CH_2Cl_2) interaction on the right (Cr-dark green, Mn-orange, Cl-green, N-blue, F-light blue, O-red).

Compound **6** (Figure 3.1, right) was crystallized as **6·Et$_2$O**. The metal atoms are not disordered indicating that only the weakly bound OTf^- ligand of Cr in **3** was replaced by NCS^-. The Cr–NCS distance of 2.22 Å is only somewhat shorter than in the NCS adduct of dichromium tetrakispropionate (2.25 Å).[11] The Cr–N–C angle of 179° may indicate that the NCS ligand is also acting as a π donor in this compound, though the Cr≡Cr bond length of 2.02 Å remains short.

Compound **5** was crystallized as **5·0.5CH$_2$Cl$_2$** from CH_2Cl_2/hexanes (Figure 3.4). The crystal structure contains two molecules of **5** in the asymmetric unit. The metal atoms of each independent molecule are disordered with relative occupancies of 76%/24% for one, and 57%/43% for the other molecule. The metal-ligand and metal-metal distances in these four distinct molecules span an unusually broad range: Fe−O,

Cr···Fe, and Cr−Cr distances vary from 1.95 to 2.10 Å, 2.59 to 2.74 Å, and 1.84 to 2.01 Å, respectively. It is not clear at this point what causes these remarkable structural variations in the solid state, though the metal atom positions of the 24% occupied orientations are most likely inaccurate. We note that ^{1}H-NMR experiments (*vide infra*) show the presence of only one species in solution.

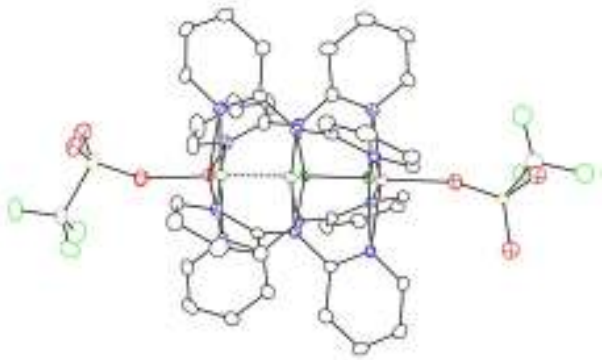

Figure 3.4. Molecular structure of one of the two independent trinuclear molecules in **5·0.5CH_2Cl_2·0.3C_4H_8O** showing the Fe (red) and Cr (green) disorder, with displacement ellipsoids drawn at the 30% probability level. Hydrogen atoms have been omitted for clarity.

(2) Assignment of the non-centrosymmetric space group Cc. The structures of compounds **3**, **4**, **5**, and **8/8-iso** were all solved in the space group *Cc*, which is a somewhat problematic space group because its systematic absences also fit the centrosymmetric space group *C2/c*. Intensity statistics for the X-ray data can be inconclusive; thus, a discussion of the choice of space group and refinement is warranted. For compounds **3**, **4** and **8/8-iso**, the statistics favor a non-centrosymmetric structure, indicating that the *Cc* space group provides a better fit for the data. Deeper inquiry reveals the structures to be pseudosymmetric and, in all cases, the triflate moiety breaks the center of symmetry. The refinement in *Cc*, however, is not straightforward, since **3**, **4**, and **8/8-iso** refine with Flack parameter[12] values of 0.495(13), 0.50(11) and 0.54(13),

respectively, suggesting that the centrosymmetric structure may indeed be correct. Our best attempts to refine these structures in *C2/c* with disordered triflates led to unstable refinements with wR2 values of 0.4038, 0.4201, 0.3491, and 0.4691 for **3**, **4**, **5**, and **8/8-iso**, respectively, which we deemed unacceptable. The only structure solution for each of these data sets that produced chemically reasonable and computationally stable refinements was a refinement in space group *Cc* as a racemic twin.

Using similar methods, compound **5** was found to be a racemic twin with a minor component contribution of 0.19(3). Attempts to refine the structure in the centrosymmetric space group *C2/c* were unfruitful and were not computationally stable. In addition, inspection of the correlation matrices for these structures does not reveal any correlation between would-be symmetry-related parameters, which is a strong indication that the structure is not centrosymmetric. The identities of important atoms such as the metal centers were consistent with structures of the dichloro precursor molecules.

(3) Structural changes induced by ligand substitution. Regiospecific substitution of the chromium bound Cl_{Cr} of **1** and **2** by OTf^- in **3** and **4** or NCS^- in **6** causes a variety of structural changes. As one would anticipate from the substantial work previously done on Cr≡Cr bonded compounds,[13] changing the Cr axial ligand has a meaningful effect on the Cr≡Cr bond distance[14] and, to a lesser extent, the outer Cr–N bond distances. Specifically, the Cr≡Cr bond distance decreases in length from 2.025(2) to 2.0187(8) to 1.9641(7) Å as the axial ligand is changed from chloride (**1**) to thiocyanate (**6**) to triflate (**3**). The shortening of the metal-metal bond distance is accompanied by a concomitant decrease in the equatorial Cr_{outer}–N distances of ~0.05 Å. The Cr≡Cr and Cr_{outer}–N

distances of the manganese analogs shorten consistently from 2.040(1) to 1.9573(6) Å (by ~ 0.08 Å) and from 2.130[5] to 2.076[3] Å (by ~ 0.05 Å), respectively, upon substituting Cl_{Cr} by OTf.

Although the interrelatedness of Cr−Cr, Cr−axial ligand, and Cr−equatorial ligand bonding has been established,[13] the different Cr axial ligands also remotely and unexpectedly influence the geometry of Fe or Mn center. As the Cr_{outer} –N bond distances become shorter, the Fe–N and Mn−N bond distances uniformly become longer by as much as 0.04 Å and 0.07 Å, respectively, in a more or less linear relationship. The changes in the Fe–N and Mn−N bond distances may be described as a teeter-totter-like "tilting" of the ligand about its central Cr–N bond. Thus, the identity of the Cr axial ligand may be used here to tune the ligand field of the Fe or Mn atoms in these compounds.

We may define a "degree of tilting" (δ) of the dpa ligand in these compounds as $\delta = d(M{-}N) - d(Cr{-}N_{outer})$ with M = Mn, Fe or Co. From the δ values listed in Table 3.2, we can see a clear correlation with Cr≡Cr bond distances, stemming from the established direct relationship between Cr−equatorial ligand bond distance and Cr≡Cr bond distance. Notably, there is no correlation between values of δ and the heterometallic Cr···M separations. We have recently provided evidence that the magnetic anisotropy of M is affected by the quadruple bond,[4] but it is important to point out here that no relationship between the heterometallic separations and any of the geometric features of M are apparent, although the axial M−Cl distances are, in certain cases, obscured by an intermolecular interaction with a solvent molecule. Further, although it would be useful

to quantify the magnitude of the "tilting" effect on the ligand field of M by probing the metal ligand field transitions with UV-Vis spectroscopy, the Fe ligand field transitions have not been observable in these compounds and Mn^{II} does not have spin-allowed bands.

Table 3.2. Selected bond distances in **1** (**1**·CH_2Cl_2, 100 K), **2**, **3**, **4**, **6** and **8/8-iso**.

Compound	M–Cl, Å	M–N_{avg}, Å	M···Cr, Å	Cr≡Cr, Å	Cr_{inner}-N_{avg}, Å	Cr_{outer}-N_{avg}, Å	δ, Å
1 (M = Fe)	2.300(2)	2.157[4]	2.715(2)	2.025(2)	2.028[2]	2.119[5]	0.038(5)
2 (M = Mn)	2.259(2)	2.190[1]	2.781(1)	2.040(1)	2.03[2]	2.130[5]	0.060(3)
3 (M = Fe)	2.3966(9)	2.190[3]	2.7317(7)	1.9641(7)	2.029[3]	2.077[3]	0.113(3)
4 (M = Mn)	2.3707(8)	2.262[3]	2.8528(6)	1.9573(6)	2.036[2]	2.076[3]	0.186(3)
6 (M = Fe)	2.354(1)	2.173[3]	2.6957(7)	2.0187(8)	2.034[3]	2.110[3]	0.063(3)
8 (M = Co)	2.360(2)	2.161[5]	2.715(2)	1.939(3)	2.019[3]	2.032[6]	0.129(6)
8-iso (M = Co)	2.641(6)	2.034[1]	2.543(7)	1.964(6)	2.030[4]	2.141[1]	-0.107(1)

Additionally, the axial Fe−Cl and Mn−Cl distances elongate by 0.09 and 0.11 Å in going from **1** and **2** to **3** and **4**, respectively. This elongation is presumably due to some extent to the above-mentioned interaction between the axial Cl^- and a CH_2Cl_2 solvent molecule and it is therefore somewhat ambiguous in these compounds as to whether the change is due to the exchange of Cr axial ligands. However, the Fe–Cl bond in **6** is not perturbed by any intermolecular interactions, and its elongation by ~ 0.05 Å as compared to **1** is therefore a clear result of the remote effect of substituting Cl^- for NCS^- at Cr.

Similar structural changes are observed for the N_4CoCl unit in compound **8** although structural comparison to the dichloro compound **7** is complicated by the temperature-dependence of the spin-state of the Co^{II} ion in **7**. It has been shown by variable temperature (VT) magnetic susceptibility and VT crystallography that the Co^{II} ion in **7** is low-spin (S = 1/2) at low temperature (~100 K) and high-spin (S = 3/2) at room-temperature.[6] The Co−N and Co−Cl distances (at 100 K) in **8** of 2.161[5] Å and 2.359(2) Å, respectively, are indicative of high-spin Co^{II} and can be compared to the room temperature structure of **7**, having shorter Co−N distances of 2.125[3] Å and a rather long Co−Cl bond length of 2.370(1) Å. Thus, the "tilting" of the dpa ligand away from Co is also observed in going from **7** to **8** and, more importantly, the tilt of the dpa ligand in **8** causes the Co^{II} ion to remain high-spin at 100 K, whereas the Co^{II} ion in **7** is mostly low-spin at this temperature. This effect is a clear indication of a weaker ligand field being exerted in **8** than in **7**.

The N_4CoOTf unit in **8-iso** has short Co−N distances of 2.03[2] Å which are indicative of low-spin Co^{II} and similar to the Co−N bond lengths in the low-spin form of **7** (2.054(2) Å). The axial Co−O distance of 2.18(1) Å in **8-iso** is shorter than the $Co-OSO_2CF_3$ bond lengths of 2.244(3) Å and 2.223(3) Å in the homometallic pentanuclear ditriflate compound $Co_5(tpda)_4(OTf)_2$ (tpda = the dianion of *N*,*N*-bis(α-pyridyl)-2,6-diaminopyridine)[15] and the hexanuclear $[Co_6(\mu_6\text{-bpyany})_4(OTf)_2](OTf)_2$ (bpyany = dianion of 2,7-bis(a-pyridylamino)-1,8-naphthyridine),[16] respectively. It is remarkable that the substitution of the stronger σ donor chloro ligand by the weaker OTf^- ligand at Co causes the Co^{II} ion in **8-iso** to be low-spin at 100 K, but this is likely due to

the lesser π-donation of triflate as compared to chloride. The presence of two Co ions of different spin states in the **8**/**8-iso** mixture in frozen solution was also evidenced by EPR spectroscopy (*vide infra*).

3.4.3 ^{1}H-NMR and EPR spectroscopy

The Fe-ligand bond distances in **1**, **3**, **5**, and **6** are all suggestive of a high-spin Fe^{II} ion with an $S = 2$ magnetic ground state. This ground state assignment has been verified by room temperature magnetic susceptibility measurements on **1**, **3**, and **5**. Despite their paramagnetism, ^{1}H NMR spectra could be measured for these Fe^{II} compounds. ^{1}H-NMR spectra of the paramagnetic compounds **1**, **3**, **5**, and **6** in CD_2Cl_2 display eight well-resolved signals in the range of 115 to -6 ppm (Table 3.3). The peaks corresponding to the protons of the Fe-bound pyridine moiety of the dpa ligand were assigned considering the characteristic ^{1}H-NMR signal pattern of iron/pyridine complexes.[17] These signals show a remarkable sensitivity to Cl_{Cr} substitution for OTf^- and SCN^- in going from **1** to **3** and **3** to **6**, respectively. The chemical shift of the Cr-bound pyridine protons in **1**, **3** and **6** are less affected by the paramagnetism in that they appear at a more intuitive, "diamagnetic" region of the ^{1}H-NMR spectrum. However, in **5** we find these proton resonances to be significantly shifted upfield and note that the chemical shifts of the individual Cr-bound pyridine protons vary more than what would be expected based on the diamagnetic anisotropy of the quadruple bond.[13,18] Most importantly, compound **3** shows only one set of ^{1}H NMR signals, verifying that it is a pure compound and that **3-iso** is not present. Also, the proposed altered bonding of the dpa ligand upon regioselective ligand substitution in going from **1** to **3** and **3** to **6**, as deduced from the

solid state crystallographic results above, appears to be present in solution as well, as all the Fe-pyridine NMR signals shift monotonically **1** to **6** to **3**.

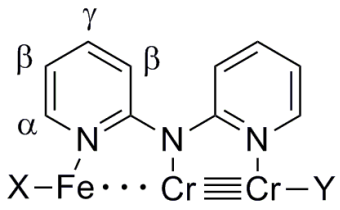

Table 3.3. ^{1}H resonances (ppm) in **1**, **3**, **5** and **6** and their assignments.

compound	α	β	γ	Cr bound pyridine protons
1	107.35	68.26	-5.54	6.36, 5.61, 3.21, 1.86
X = Y = Cl		39.36		
3	112.36	70.66	-1.97	6.39, 4.30, 4.09, 3.64
X = Cl, Y = OTf		40.49		
5	105.02	71.23	-2.65	4.49, 3.84, 2.47, -0.76
X = Y = OTf		39.29		
6	108.06	69.08	-4.51	5.92, 4.90, 2.88, 1.52
X = Cl, Y = SCN		39.27		

The ^{1}H-NMR spectrum of the paramagnetic compound **8/8-iso** CD_2Cl_2 displays many signals in the range of 120 to -10 ppm, indicating the presence of two compounds, a major product and minor product. Accurate integrations of these signals were inaccessible due to broadening of the signals. The peaks corresponding to the protons of the Co-bound pyridine moiety of the dpa ligand of the major product appear at α = 117.86

ppm, β = 49.45 and 74.57 ppm, and the minor product at α = 108.24 ppm, β = 46.37 and 68.76 ppm. The γ protons were obscured by resonances from the other pyridine ring and could not be assigned unambiguously. The positions of these peaks are markedly similar to those of compound **3** and are therefore assigned analogously. It is remarkable that the pyridine resonances for both **8** and **8-iso** appear in a similar range to each other. Due to the two different spin of **8** and **8-iso** suggested by the crystal structure, one might expect high-spin and low-spin resonances in significantly different chemical shift ranges. Instead, this is not observed and the peak positions suggest that at room temperature in solution, both **8** and **8-iso** are high spin. The chemical shifts of the Cr-bound pyridine protons of the major and minor products are difficult to distinguish because of the broadening of the signals caused by paramagnetism, although they fall in range from -8 to 8 ppm, which is a similar, albeit larger, range compared to that of compounds **1**, **3**, **5**, and **6**.

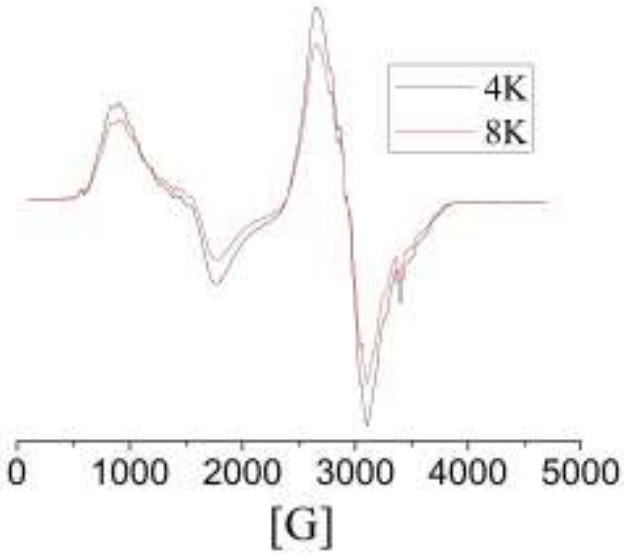

Figure 3.5. X-band EPR spectrum of a frozen solution (CH_2Cl_2) of the **8**/**8-iso** mixture.

The 4 K X-band EPR spectrum of a frozen solution of the **8**/**8-iso** mixture in CH_2Cl_2 (Figure 3.5) displays one signal at g_{obs} = 4.81 and one more intense signal at g_{obs} = 2.29. The major signal is clearly due to a slightly axial $S = 2$ system, and the g value of 2.29 is in good agreement with low-spin Co^{II} (indicative of **8-iso**) since the more than half-filled set of d orbitals gives rise to g values greater than 2. The g = 4.8 signal is assigned to a Co^{II} high-spin ($S = 3/2$) ion in **8**. This assignment is made based on similar assignments for the corresponding Mn^{II} compounds.[4] In the case of the Co^{II} and Mn^{II} compounds, the axial zero-field splitting parameter D is larger than the microwave quantum and therefore, effective g values of 6 for the $S = 5/2$ state and 4 for the $S = 3/2$ state are expected from rhombograms for the fully axial case (E/D = 0). The splitting of the g = 4 signal of **8** is consistent with a deviation from true axial symmetry, roughly to E/D ~ 0.12.

3.4.4 Electrochemistry

We also investigated how the Cr axial ligand exchange affects the redox properties of Fe in **3** (Figure 3.6). The cyclic voltammogram (CV) of **1** in CH_2Cl_2 exhibits a reversible iron centered oxidation wave at -236 mV and an irreversible wave at 538 mV.[5] The dominant features of the cyclic voltammogram of **3** are two oxidation waves, which appear both quasireversible and of the same peak height. The first oxidation wave is observed at -4 mV and the second at 720 mV (potentials referenced vs. Fc/Fc^+). The first oxidation event in **3** is proposed to be the $Fe^{II/III}$ redox couple of the N_4FeCl unit in analogy to the redox properties of **1**. The shift to higher potential is likely due to both the less electron donating ability of OTf^- in **3** as compared to **1** and the longer

Fe–dpa bond distances (weaker ligand field), which renders the Fe^{II} ion in **3** more difficult to oxidize as compared to **1**. The second oxidation wave in the CV of **3** shows reversible features and may be ascribed to either the $Cr_2^{IV/V}$ or the $Fe^{III/IV}$ redox couple. The CV of the ditriflate compound **5** displays one non-reversible oxidation at 156 mV and further oxidation events at even higher potential.

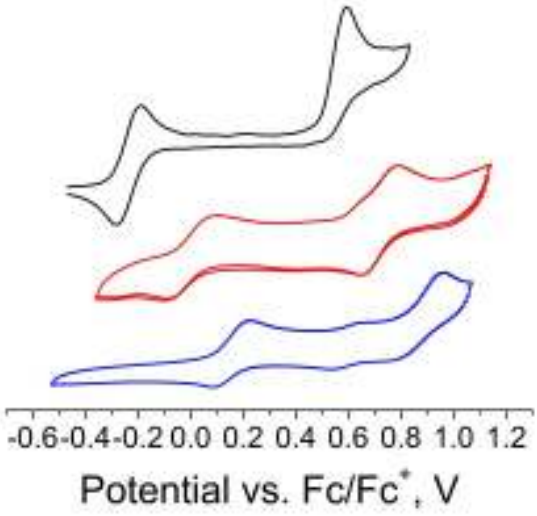

Figure 3.6. Cyclic voltammogram of **1** (top), **3** (middle), and **5** (bottom) in CH_2Cl_2.

3.5 Summary

Substitution of the axial chloride ligand in **1** and **2** with OTf^- occurs regiospecifically at Cr yielding the monotriflate compounds **3** and **4**. For **7** no such selectivity was found. Most importantly, we found that the environment of the hetero-metal Fe, Mn, or Co can be altered without changing its primary coordination sphere. In detail, the introduction of a weaker axial ligand (OTf) to the Cr_2 unit causes a physical tilting of the dpa ligand towards its Cr_2 bound region thereby weakening its binding to Fe, Mn, or Co. This effect significantly alters the ligand field strength and the redox properties of Fe^{II} in the CrCrFe chains, elongates the axial Fe-Cl bond, and makes the Fe more difficult to oxidize.

3.6 Acknowledgement

We thank the National Science Foundation for support under CHE-0745500.

3.7 Supporting Information

Crystallographic data in CIF format. This information is available via the Internet at www.acs.org.

References

(1) (a) Berry, J. F., Metal Metal Bonds in Chains of Three or More Metal Atoms: From Homometallic to Heterometallic Chains. In *Metal-Metal Bonding*, 2010; Vol. 136, pp 1; (b) Meng, X.; Wang, F. S.; Jin, G. X., *Coord. Chem. Rev.* **2010,** *254*, 1260; (c) Diaconescu, P. L., *Acc. Chem. Res.* **2010,** *43*, 1352; (d) Diaconescu, P. L., *Comments Inorg. Chem.* **2010,** *31*, 196; (e) Marinescu, G.; Andruh, M.; Lloret, F.; Julve, M., *Coord. Chem. Rev.* **2011,** *255*, 161; (f) Mandal, S. K.; Roesky, H. W., *Acc. Chem. Res.* **2010,** *43*, 248.

(2) (a) Sculfort, S.; Welter, R.; Braunstein, P., *Inorg. Chem.* **2010,** *49*, 2372; (b) Navulla, A.; Tsirlin, A. A.; Abakumov, A. M.; Shpanchenko, R. V.; Zhang, H. T.; Dikarev, E. V., *J. Am. Chem. Soc.* **2011,** *133*, 692; (c) Li, B.; Zhang, H. T.; Huynh, L.; Diverchy, C.; Hermans, S.; Devillers, M.; Dikarev, E. V., *Inorg. Chem.* **2009,** *48*, 6152; (d) Dikarev, E. V.; Li, B.; Rogachev, A. Y.; Zhang, H. T.; Petrukhina, M. A., *Organometallics* **2008,** *27*, 3728; (e) Dikarev, E. V.; Li, B.; Zhang, H. T., *J. Am. Chem. Soc.* **2006,** *128*, 2814; (f) Bruce, M. I.; Humphrey, P. A.; Zaitseva, N. N.; Nicholson, B. K.; Skelton, B. W.; White, A. H., *Dalton Trans.* **2010,** *39*, 8801; (g) Colson, A. C.; Whitmire, K. H., *Organometallics* **2010,** *29*, 4611; (h) Stavila, V.; Thurston, J. H.; Whitmire, K. H., *Inorg. Chem.* **2009,** *48*, 6945; (i) Ould-Ely, T.; Thurston, J. H.; Whitmire, K. H., *C. R. Chim.* **2005,** *8*, 1906; (j) Huang, W.; Carver, C. T.; Diaconescu, P. L., *Inorg. Chem.* **2011,** *50*, 978; (k) Cooper, B. G.; Fafard, C. M.; Foxman, B. M.; Thomas, C. M., *Organometallics* **2010,** *29*, 5179; (l) Thomas, C. M.; Napoline, J. W.; Rowe, G. T.; Foxman, B. M., *Chem. Commun.* **2010,** *46*, 5790; (m) Greenwood, B. P.; Forman, S. I.; Rowe, G. T.; Chen, C. H.; Foxman, B. M.; Thomas, C. M., *Inorg. Chem.* **2009,** *48*, 6251; (n) Rampersad, M. V.; Zuidema, E.; Ernsting, J. M.; van Leeuwen, P.; Darensbourg, M. Y., *Organometallics* **2007,** *26*, 783; (o) Zhou, W.; Napoline, J. W.; Thomas, C. M., *Eur. J. Inorg. Chem.* **2011,** *2011*, 2029.

(3) (a) Huang, D. G.; Holm, R. H., *J. Am. Chem. Soc.* **2010,** *132*, 4693; (b) Groysman, S.; Majumdar, A.; Zheng, S. L.; Holm, R. H., *Inorg. Chem.* **2010,** *49*, 1082; (c) Hlavinka, M. L.; Miyaji, T.; Staples, R. J.; Holm, R. H., *Inorg. Chem.* **2007,** *46*, 9192; (d) Sun, J. B.; Tessier, C.; Holm, R. H., *Inorg. Chem.* **2007,** *46*, 2691; (e) Pesavento, R. P.; Berlinguette, C. P.; Holm, R. H., *Inorg. Chem.* **2007,** *46*, 510; (f) Berlinguette, C. P.; Holm, R. H., *J. Am. Chem. Soc.* **2006,** *128*, 11993; (g) Osterloh, F.; Achim, C.; Holm, R. H., *Inorg. Chem.* **2001,** *40*, 224; (h) Osterloh, F.; Segal, B. M.; Achim, C.; Holm, R. H., *Inorg. Chem.* **2000,** *39*, 980; (i) Osterloh, F.; Sanakis, Y.; Staples, R. J.; Munck, E.; Holm, R. H., *Angew. Chem. Int. Ed.* **1999,** *38*, 2066; (j) Darensbourg, M. Y.; Weigand, W., *Eur. J. Inorg. Chem.* **2011**, 994; (k) Almaraz, E.; Foley, W. S.; Denny, J. A.; Reibenspies, J. H.; Golden, M. L.; Darensbourg, M. Y., *Inorg. Chem.* **2009,** *48*,

5288; (l) Barton, B. E.; Whaley, C. M.; Rauchfuss, T. B.; Gray, D. L., *J. Am. Chem. Soc.* **2009,** *131*, 6942; (m) Barton, B. E.; Rauchfuss, T. B., *J. Am. Chem. Soc.* **2010,** *132*, 14877; (n) Nayak, S.; Pada, H.; Dehnen, S.; Powell, A. K.; Reedijk, J., *Dalton Trans.* **2011**, 2699; (o) Mishra, A.; Yano, J.; Pushkar, Y.; Yachandra, V. K.; Abboud, K. A.; Christou, G., *Chem. Commun.* **2007**, 1538; (p) Ogo, S.; Kabe, R.; Uehara, K.; Kure, B.; Nishimura, T.; Menon, S. C.; Harada, R.; Fukuzumi, S.; Higuchi, Y.; Ohhara, T.; Tamada, T.; Kuroki, R., *Science* **2007,** *316*, 585; (q) Kure, B.; Ogo, S.; Inoki, D.; Nakai, H.; Isobe, K.; Fukuzumi, S., *J. Am. Chem. Soc.* **2005,** *127*, 14366; (r) Ogo, S.; Suzuki, T.; Ozawa, Y.; Isobe, K., *Inorg. Chem.* **1996,** *35*, 6093.

(4) Nippe, M.; Wang, J.; Bill, E.; Hope, H.; Dalal, N. S.; Berry, J. F., *J. Am. Chem. Soc.* **2010,** *132*, 14261.

(5) Nippe, M.; Berry, J. F., *J. Am. Chem. Soc.* **2007,** *129*, 12684.

(6) Nippe, M.; Victor, E.; Berry, J. F., *Eur. J. Inorg. Chem.* **2008,** *2008*, 5569.

(7) Bain, G. A.; Berry, J. F., *J. Chem. Educ.* **2008,** *85*, 532.

(8) Bruker-AXS, APEX2, SADABS, and SAINT Software Reference Manuals. Madison, Wisconsin, USA, 2009.

(9) Dolomanov, O. V.; Bourhis, L. J.; Gildea, R. J.; Howard, J. A. K.; Puschmann, H., *J. Appl. Crystallogr.* **2009,** *42*, 339.

(10) Spek, A., *J. Appl. Crystallogr.* **2003,** *36*, 7.

(11) Ford, P. D.; Larkworthy, L. F.; Povey, D. C.; Roberts, A. J., *Polyhedron* **1983,** *2*, 1317.

(12) Flack, H., *Acta. Cryst.* **1983,** *A39*, 876.

(13) Cotton, F. A., In *Multiple Bonds Between Metal Atoms*, Cotton, F. A.; Murillo, C. A.; Walton, R. A., Eds. Springer Science and Business Media: New York, 2005; Vol. 3rd, pp 57.

(14) The nature of the Cr−Cr multiple bond is defined by the distribution of states of different configurations with different populations of bonding and antibonding molecular orbitals; e.g., $\sigma^2\pi^4\delta^2$, $\sigma^2\pi^4\delta^1\delta^{*1}$,... . The length of the Cr-Cr quadruple bond is generally regarded to be highly affected by the extent to which an axial ligand modifies electron density in the antibonding orbitals of this multiple bond.

(15) Yeh, C.-Y.; Chou, C.-H.; Pan, K.-C.; Wang, C.-C.; Lee, G.-H.; Su, Y. O.; Peng, S.-M., *J. Chem. Soc., Dalton Trans.* **2002**, 2670.

(16) Chien, C.-H.; Chang, J.-C.; Yeh, C.-Y.; Lee, G.-H.; Fang, J.-M.; Peng, S.-M., *Dalton Trans.* **2006**, 2106.

(17) (a) Zang, Y.; Kim, J.; Dong, Y.; Wilkinson, E. C.; Appelman, E. H.; Que, L., *J. Am. Chem. Soc.* **1997,** *119*, 4197; (b) Klinker, E. J.; Kaizer, J.; Brennessel, W. W.; Woodrum, N. L.; Cramer, C. J.; Que, L., *Angew. Chem. Int. Ed.* **2005,** *44*, 3690.

(18) (a) Collman, J. P.; Barnes, C. E.; Swepston, P. N.; Ibers, J. A., *J. Am. Chem. Soc.* **1984,** *106*, 3500; (b) Collman, J. P.; Garner, J. M.; Hembre, R. T.; Ha, Y., *J. Am. Chem. Soc.* **1992,** *114*, 1292.

Chapter 4

Synthesis, Characterization and Thermal Properties of Trimetallic N_3-Cr≡Cr···M-N_3 Azide Complexes with M = Cr, Mn, Fe, and Co

Reprinted with permission. Yevgeniya Turov and John F. Berry *Dalton Trans.*, **2012**, *41*, 8153-8161.

4.1 Abstract

We report here two novel synthetic pathways toward the preparation of a family of trimetallic diazide compounds of the type $Cr_2M(dpa)_4(N_3)_2$, with M = Cr (**10**), Mn (**4**), Fe (**5**), and Co (**11**). Reaction of either $Cr_2M(dpa)_4(OTf)_2$ (for M = Mn and Fe) or $[Cr_2M(dpa)_4(MeCN)_2](PF_6)_2$ (for M = Cr and Co) with sodium azide in methanol leads to the formation of the corresponding diazide compounds, and single crystal X-ray diffraction measurements confirm the predicted structures. Compounds **4**, **5**, and **10** are all high-spin compounds, but **11** is a spin-crossover compound exhibiting low-spin behavior at low temperatures (~100 K). Thermolytic characterization by DSC and TGA reveals an exothermic reaction corresponding to loss of two dinitrogen molecules from compound **5**, **10**, and **11**. Further characterization by solution NMR measurements and cyclic voltammetry are also presented.

4.2 Introduction

Transition metal azide complexes are currently of considerable interest for their ability to mediate magnetic coupling between paramagnetic metal ions,[1] as well as their ability to serve as precursors to transition metal nitrides.[2] Recently, our group has investigated the isolation, characterization and chemical reactivity of terminal nitrido compounds

containing metal-metal multiple bonds.[3] Heterometallic nitride complexes are generally rare,[4] and we have sought synthetic routes to heterometallic nitrido compounds that contain metal-metal bonds. As a first step to such compounds, we report here the synthesis and characterization of heterometallic azide complexes containing the quadruply bonded dichromium unit, and examine their potential for thermal activation to form nitrido species.

4.3 Results and Discussion

4.3.1 Synthesis

Homometallic Cr_3 chain complexes of the type $Cr_3(dpa)_4X_2$ (where dpa = 2,2'-dipyridylamine) have been studied since their discovery in 1997.[5] In recent years, we and others have employed the $Cr_2(dpa)_4$ molecule as a precursor for heterometallic chain compounds having a linear Cr≡Cr···M backbone with M = Mn, Fe, Co, Ni, and Zn.[6] Axial ligand substitution in these chain compounds poses significant synthetic challenges. For example, we have recently reported that the $Cr_2M(dpa)_4Cl_2$ complexes with M = Mn or Fe react cleanly with AgOTf to replace only the Cr-bound chloride ion for triflate.[7] However, the analogous reaction using $Cr_2Co(dpa)_4Cl_2$ yields a mixture of TfO–Cr≡Cr···Co–Cl and Cl–Cr≡Cr··Co–OTf isomeric products.[7] Furthermore, axial ligand replacement by simple sodium salt metathesis fails for Cr_2M chains due to demetallation of M in the presence of excess pseudohalide ions, yielding $Cr_2(dpa)_4$ and, presumably, a hexakis-pseudohalometallate ion.[7] In order to achieve clean axial substitution reactions, new chemistry needed to be developed, as discussed here. We

recently showed that the axial triflate ion in $Cr_2Fe(dpa)_4Cl(OTf)$ could be substituted for NCS^-.[7] We therefore hypothesized that $Cr_2M(dpa)_4(OTf)_2$ species may be suitable precursors for $Cr_2M(dpa)_4(N_3)_2$ complexes and that the latter may be obtained using stoichiometric amounts of NaN_3, rather than the excess quantities that lead to demetallation. Additionally, axial acetonitrile complexes have been shown to be very good precursors to axially substituted homotrimetallic chain complexes.[5b] We therefore outlined two preparative routes to $Cr_2M(dpa)_4(N_3)_2$ molecules, proceeding either through a diacetonitrile or a ditriflate intermediate, as outlined in Scheme 4.1, pathway A and pathway B, respectively.

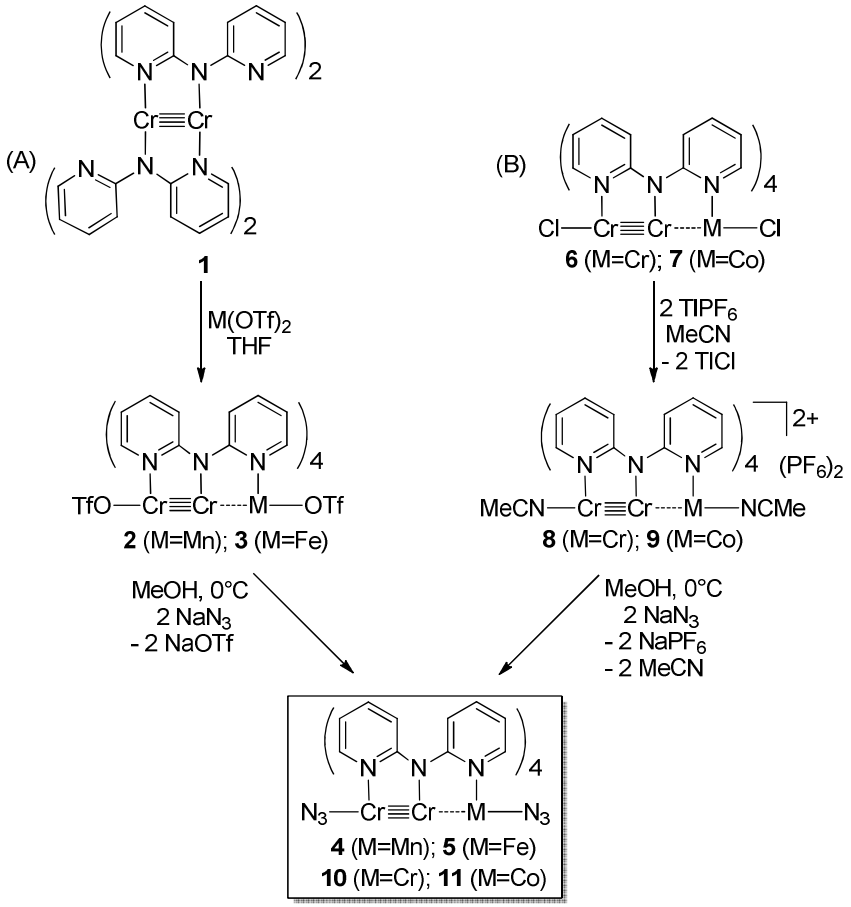

Scheme 4.1. Synthesis of $Cr_2M(dpa)_4(N_3)_2$ compounds.

In pathway A, $Cr_2(dpa)_4$ (**1**) reacts with either $Mn(OTf)_2$ or $Fe(OTf)_2$ in refluxing tetrahydrofuran to yield $Cr_2Mn(dpa)_4(OTf)_2$ (**2**) and $Cr_2Fe(dpa)_4(OTf)_2$ (**3**),[7] respectively. Addition of a methanolic solution of sodium azide to a solution of ditriflate compounds **2** and **3** in methanol at 0ºC produces the diazide complexes $Cr_2Mn(dpa)_4(N_3)_2$ (**4**) and $Cr_2Fe(dpa)_4(N_3)_2$ (**5**), respectively, as brown precipitates. Although **4** is formed in poor yield due to demetallation of the Mn^{II} ion, Pathway A is useful for the preparation of **5** in good yields. Pathway B stems from the reaction of $Cr_2M(dpa)_4Cl_2$ complexes with $TlPF_6$ in acetonitrile to produce $[Cr_2M(dpa)_4(NCCH_3)_2](PF_6)_2$ species.[5b] Notably, this thallium metathesis reaction was found to proceed only in the case of M = Cr and M = Co; reactions of the Mn or Fe complexes with $TlPF_6$ did not produce the desired compounds. The labile acetonitrile solvent ligands of $[Cr_3(dpa)_4(NCCH_3)_2](PF_6)_2$ (**8**) and $[Cr_2Co(dpa)_4(NCCH_3)_2](PF_6)_2$ (**9**) are easily displaced by azide ligands upon reaction with a methanolic solution of sodium azide to generate the corresponding diazide compounds $Cr_3(dpa)_4(N_3)_2$ (**10**) and $Cr_2Co(dpa)_4(N_3)_2$ (**11**) in good yields (>60%).

It is interesting to note that Pathway B does not lead to the formation of demetallation product, and also generates higher yields than Pathway A. One possibility for this result is that the ditriflate compounds have poorer stability in methanol than the diacetonitrile compounds, and this might result in some demetallation prior to the formation of the azide compound. Another possibility for the poor yield of **4** via Pathway A is the inherent lability of high-spin Mn^{II} and the lack of ligand field stabilization energy for this ion. Despite the shortcomings of Pathway A, we are able to report

characterization of the products of this pathway (**4** and **5**) and compare their properties with those of **10** and **11**, formed via pathway B.

4.3.2 Crystal Structures

Crystal structures of the new compounds **2**, **4**, **5**, **9**, **10**, and **11** are reported here. Crystallographic data are shown in Table 4.1 and selected bond distances are shown in Table 4.2.

Table 4.1. Crystallographic Data.

Compound	**2**	**4**	**5**	**9**	**10**	**11**	**11a**
	100 K	100 K	100 K	100 K	100 K	100 K	296 K
Formula	$[Cr_2Mn(C_{10}H_8N_3)_4(CF_3SO_3)_2]\cdot 2CH_2Cl_2$	$Cr_2Mn(C_{10}H_8N_3)_4(N_3)_2$	$Cr_2Fe(C_{10}H_8N_3)_4(N_3)_2\cdot Et_2O$	$[Cr_2Co(C_{10}H_8N_3)_4(NCCH_3)_2](PF_6)_2\cdot 2MeCN$	$Cr_3(C_{10}H_8N_3)_4(N_3)_2\cdot Et_2O$	$Cr_2Co(C_{10}H_8N_3)_4(N_3)_2\cdot Et_2O$	$Cr_2Co(C_{10}H_8N_3)_4(N_3)_2\cdot Et_2O$
Crystal system	Monoclinic	Monoclinic	Monoclinic	Monoclinic	Monoclinic	Monoclinic	Monoclinic
Space group	*C c*	*P 2₁ / c*	*P 2₁ / c*	*C 2/c*	*P 2₁ / c*	*P 2₁ / c*	*P 2₁/c*
a, Å	34.4980(8)	13.8889(7)	15.9450(5)	27.791(1)	15.9804(3)	15.9020(3)	16.0970(3)
b, Å	17.8985(4)	16.5572(8)	16.2777(5)	10.0388(4)	16.2292(3)	16.1624(3)	16.3036(3)
c, Å	16.8592(4)	17.0566(8)	17.6430(6)	22.7492(8)	17.6685(3)	17.5796(3)	17.7674(4)
β, °	108.144(1)	96.002(3)	104.433(2)	125.337(1)	104.626(1)	104.688(1)	104.627(1)
V, Å^3	9892.3(4)	3900.9(3)	4434.7(2)	5177.5(3)	4433.8(1)	4370.6(1)	4511.7(2)
Z	8	4	4	4	4	4	4
ρ, Mg m^{-3}	1.539	1.573	1.495	1.665	1.489	1.523	1.475
R1[a], *w*R2[b] ($I > 2\sigma(I)$)	0.0663, 0.1945	0.0422, 0.1063	0.0403, 0.1443	0.0489, 0.1499	0.0330, 0.0878	0.0336, 0.0843	0.0402, 0.0924
R1[a], *w*R2[b] (all data)	0.0730, 0.1999	0.0583, 0.1150	0.0496, 0.1513	0.0507, 0.1516	0.0368, 0.0919	0.0427, 0.0900	0.0727, 0.1072

Table 4.2. Selected bond distances in **2**-**11**. All data were taken at 100 K unless otherwise noted. All units are reported in angstroms, Å.

Compound	M–X_{axial}	M–N_{avg}	M···Cr	Cr≡Cr	Cr_{inner}-N_{avg}	Cr_{outer}-N_{avg}	Cr-X_{axial}	Ref
2 $Cr_2Mn(dpa)_4(OTf)_2$	1.968[6]	2.165[7]	2.740[5]	1.954[5]	2.025[7]	2.128[6]	2.376[6]	[a]
3 $Cr_2Fe(dpa)_4(OTf)_2$	2.020[5]	2.136[5]	2.728[6]	1.868[8]	2.02[1]	2.114[5]	2.369[3]	[7]
4 $Cr_2Mn(dpa)_4(N_3)_2$	2.021[8]	2.16[1]	2.706[8]	2.082[8]	2.032[4]	2.13[1]	2.348[8]	[a]
5 $Cr_2Fe(dpa)_4(N_3)_2$	1.985[3]	2.139[4]	2.636[4]	2.046[4]	2.036[6]	2.113[5]	2.295[3]	[a]
7 $Cr_2Co(dpa)_4Cl_2$	2.567(5)	2.054(2)	2.491(1)	2.0358(7)	2.012[2]	2.056[2]	2.5671(5)	[6c]
7 $Cr_2Co(dpa)_4Cl_2$ (296 K)	2.370(1)	2.125(3)	2.623(5)	2.067(5)	2.025[7]	2.117[3]	2.620(1)	[6c]
8 $[Cr_3(dpa)_4(MeCN)_2](PF_6)_2$	2.339(2)	2.101[1]	2.464(3)	2.143(3)	2.036[4]	2.101[1]	2.339(2)	[5b]
9 $[Cr_2Co(dpa)_4(MeCN)_2](PF_6)_2$	2.249(2)	2.037[2]	2.4665(8)	2.0127(7)	2.017[2]	2.037[2]	2.249(2)	[a]
10 $Cr_3(dpa)_4(N_3)_2$	2.114[2]	2.114[2]	2.534[1]	2.131[1]	2.048[1]	2.102[2]	2.265[2]	[a]
11 $Cr_2Co(dpa)_4(N_3)_2$	2.174[2]	2.026[2]	2.444(2)	2.050(2)	2.016[5]	2.060[2]	2.175[2]	[a]
11a $Cr_2Co(dpa)_4(N_3)_2$ (296 K)	2.041[3]	2.091[3]	2.577[2]	2.019[3]	2.025[3]	2.076[3]	2.257[3]	[a]

[a]This work.

Compound **2** is the Mn analog of $Cr_2Fe(dpa)_4(OTf)_2$, **3**, whose crystal structure was reported earlier.[7] Important interatomic distances for **2**, **3**, and the other compounds reported here are given in Table 3. Like **3**, the structure of **2** (Figure 4.1) contains a linear heterometallic array of Cr≡Cr···Mn atoms wrapped in a helical manner by four triply-bridging dpa ligands. The axial sites of the chain are capped by triflate anions, which bond to each outer metal atom in a monodentate fashion through one oxygen atom. The structure contains disorder in the metal atom positions such that a superposition of two oppositely pointed Cr≡Cr···Mn chains is observed. As in the structure of compound **3**, there is disorder in one of the triflate ligands.

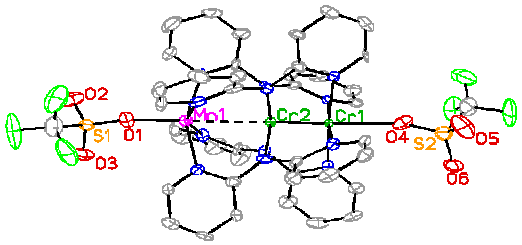

Figure 4.1. Structure of **2** with ellipsoids drawn at 50% probability. Hydrogen atoms, solvent molecules and alternative orientations of disordered metal atoms are omitted for clarity.

The Mn-N distances to the equatorial dpa pyridyl rings in **2** are 2.165[7] Å, similar to the Fe-N distances of 2.136[5] Å in **3**, and allow us to assign the Mn ion as high-spin Mn^{II} as confirmed by EPR data (*vide infra*). The Mn-O distance to the triflate ion, 1.968[6] Å, is notable shorter than the Fe-O distance of 2.020[5] Å in **3**, indicating a stronger interaction of the triflate ions in **2**. The heterometallic Mn···Cr separation of 2.740[5] Å is similar to those found in other CrCrMn compounds. The Cr≡Cr distance,

1.954[5] Å, is notably shorter than that in $Cr_2Mn(dpa)_4Cl_2$ (2.023[4] Å), consistent with the presence of a more significant Cr-O interaction of 2.376[6] Å in the triflate compound. Interestingly, the Cr≡Cr distance in the Fe compound **3** (1.868[8] Å) is even shorter than that in **3**. The unusual flexibility of the Cr≡Cr distances in these compounds is in agreement with the very shallow potential energy well associated with the Cr≡Cr quadruple bond.[8]

The azide complexes **4**, **5**, **10**, and **11** (with M = Mn, Fe, Cr, and Co) are isostructural and crystallize in the monoclinic space group $P2_1/c$. As shown in Figure 4.2, each compound contains a linear Cr≡Cr···M chain with axial azide ligands capping each terminal metal atom. As expected, all of the metal-azide linkages are bent with an average M-N-N angle of 135.7[2]°. In all of the azide structures, the metal atoms are disordered in a similar way to what is observed in compound **2**. For **4**, **5**, and **11**, the Cr≡Cr distances lie within the narrow range of 2.05-2.08 Å.

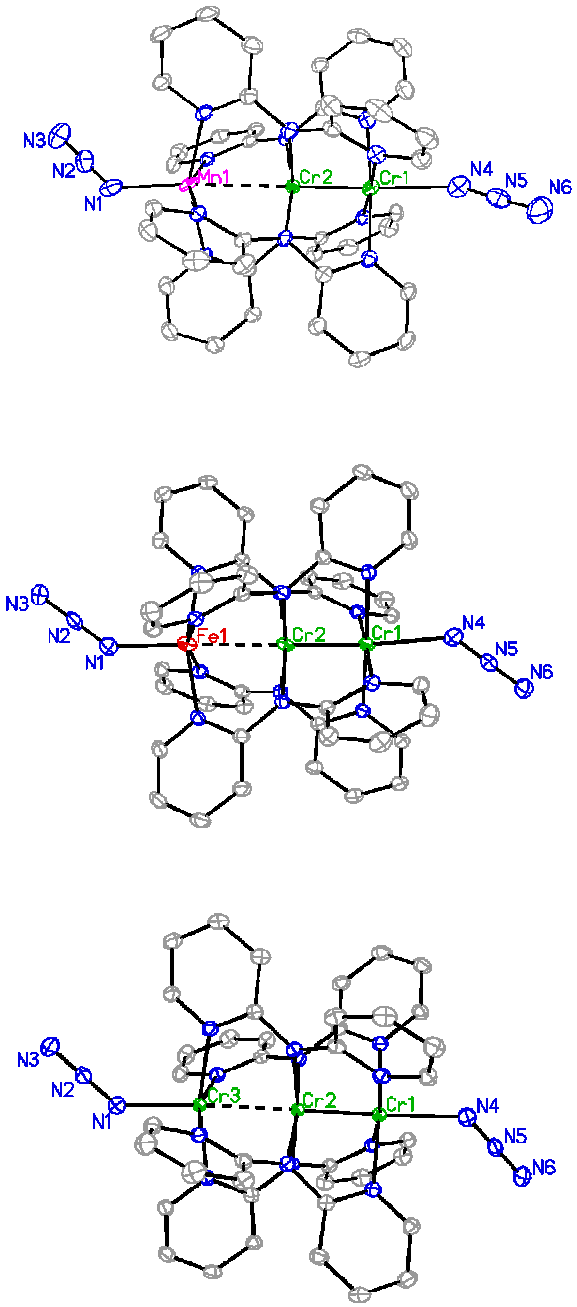

Figure 4.2. Structures of **4**, **5**, and **10** with ellipsoids drawn at 50% probability. Hydrogen atoms, solvent molecules and alternative orientations of disordered metal atoms are omitted for clarity.

The homometallic complex **10** is different, however, having a much longer Cr≡Cr distance of 2.13 Å. This longer distance is in accord with a greater σ delocalization in the homometallic species, as is observed for other Cr_3 molecules.[5b,9] In accord with this observation is the relatively short Cr···Cr separation of 2.53 Å in **10**. The M···Cr separations in **4** and **5**, 2.71 Å and 2.64 Å, respectively, are in agreement with the M···Cr separations in other CrCrM compounds with M = Mn or Fe.

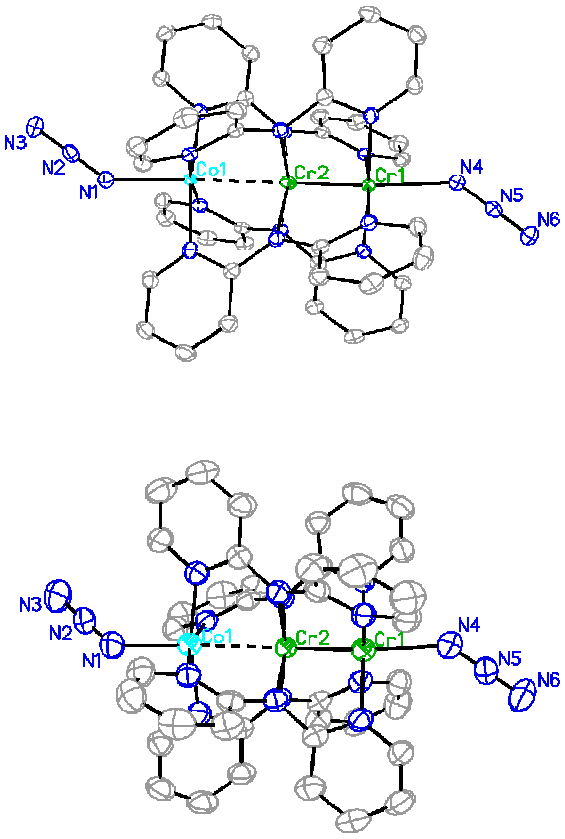

Figure 4.3. Structures of **11** (top) and **11a** (bottom) with ellipsoids drawn at 50% probability. Hydrogen atoms, solvent molecules and alternative orientations of disordered metal atoms are omitted for clarity.

Compound **11** (Figure 4.3) has a prominently short Co···Cr separation of 2.44 Å. This distance, along with the other Co-N bond distances suggests the presence of the low-spin Co^{II} ion, in contrast to all of the other azide complexes, which are high-spin. We may compare the structure of **11** with that of the low-spin form of $Cr_2Co(dpa)_4Cl_2$, in which the Co···Cr distance of 2.49 Å is observed.[6c] In order to determine if **11** is a spin-crossover compound as is the case with $Cr_2Co(dpa)_4Cl_2$, we obtained the room temperature crystal structure, **11a**. In **11a**, as in the room temperature structure of $Cr_2Co(dpa)_4Cl_2$, the Co···Cr distance is elongated to 2.58 Å, the Co-X_{axial} distance is shortened from 2.17 Å to 2.04 Å, and the Cr-N distance is elongated from 2.03 Å to 2.09 Å. While the Cr-N distances are elongated as well, the Cr≡Cr distance is shortened from 2.05 Å to 2.02 Å. We observe that the CrCrCo acetonitrile complex **9** (Figure 4.4) has a short Co···Cr separation of 2.47Å, similar to that in **11**, and may be likewise assigned as a low-spin Co^{II} complex.

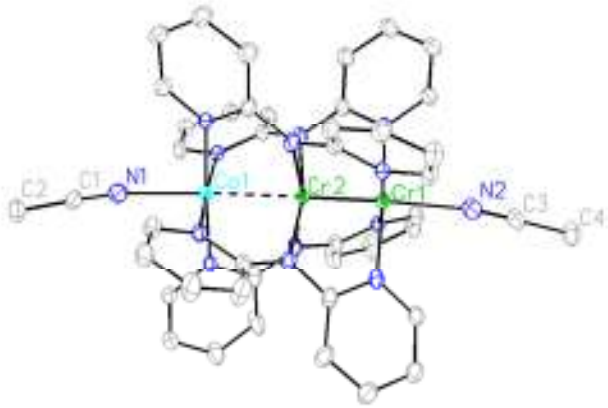

Figure 4.4. Structure of the dication in **9** with ellipsoids drawn at 50% probability. Hydrogen atoms, anions, solvent molecules and alternative orientations of disordered metal atoms are omitted for clarity.

4.3.3 Magnetic Properties

The ground state magnetic properties of compounds **3**,[7] **6**,[5b] **7**,[6c] and **8**[5b] have been previously established. In general, these complexes may be described as containing a diamagnetic Cr≡Cr quadruply bonded unit in the proximity of a high-spin M^{II} ion. EPR measurements of the manganese-containing compounds **2** and **4** show broad signals with g_{eff}>4.7, consistent with those of previously reported S = 5/2 Cr_2Mn compounds, as anticipated from the crystal structure geometries.[6b] Compound **5** has μ_{eff} = 5.20 μ_B, which is consistent with an S = 2 system, indicating that iron is high-spin. $Cr_2Co(dpa)_4Cl_2$ differs somewhat from this description in that the Co^{II} ion in this complex has been shown to undergo temperature-driven spin equilibrium.[6c] Thus, at low temperatures (below ~100 K), the compound contains the low-spin Co^{II} ion and has an S = 1/2 ground state. At room temperature, the Co^{II} ion becomes high-spin with S = 3/2.[6c] Room-temperature solid-state magnetic measurements on compound **9** yield μ_{eff} = 1.60 μ_B, which is consistent with an S = 1/2 system, indicating that cobalt is low-spin. This is also in agreement with the discussion above of the crystal structure. For compound **11**, the crystal structure at 100 K indicates that the compound is low-spin, but at room temperature, the crystal structure indicates that the Co^{II} ion in compound **11** becomes high-spin. Solution magnetic measurements of **11** yield μ_{eff} = 3.31 μ_B, which is between the values anticipated of a high-spin (μ_{eff} = 3.87 μ_B) and low-spin compound (μ_{eff} = 1.73 μ_B) and is consistent with the proposed spin equilibrium. Compound 10 has μ_{eff} = 4.61 μ_B, which is indicative of an S = 2 system, as expected from the crystal structure and similar homometallic trichromium compounds.

4.3.4 Solution Properties

Although all the compounds described here are paramagnetic, they (with the exception of the M = Mn compounds) show interesting, and generally interpretable, NMR spectra. Compound 10 (Figure 4.5) shows only three broad resonances in its ^{1}H NMR spectrum at 12.96 ppm, -0.42 ppm, and -15.00 ppm, corresponding to dpa ligand protons. The observation of only three signals is unusual, since one would expect eight distinct ^{1}H resonances based on the unsymmetrical Cr≡Cr···Cr solid state structure. It is possible, however, that the molecule could be symmetrical with equivalent Cr–Cr–Cr distances in solution. A symmetrical isomer of Cr_3 chains has been invoked to explain some of the unusual electron transport behavior of Cr_3 chains,[10] so far without solid experimental evidence**.**

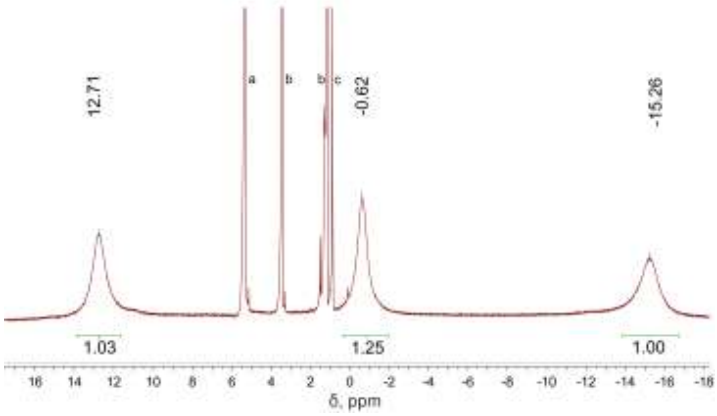

Figure 4.5. Paramagnetic ^{1}H NMR spectrum of **10**, with broad peaks corresponding to **10**. [a]CD_2Cl_2 residual solvent peak, [b]diethyl ether, [c]grease.

The three resonances observed by ^{1}H NMR for **10** could indicate that there are four inequivalent protons (as expected for a symmetrical structure), and that one signal is too broad to be observed. The other possible interpretation is that there are eight

inequivalent protons of an unsymmetrical structure, and that five of them are too broad to be observed. Of the two interpretations listed above, the former seems more likely (in the sense of Occam's razor). There are two possible explanations for why only four resonances would be seen (as shown in Figure 4.6): 1) the solution structure of the compound could truly be symmetrical, or 2) the compound could exist in equilibrium in solution such that the quadruple bond switches back and forth between two unsymmetrical forms faster than the time scale of the NMR experiment. In order for the latter to be true, there would need to be a low barrier for this "switching," which should result in a deconvolution of the spectrum at sufficiently low temperatures. Spectra of compound **10** in CD_2Cl_2 at temperatures as low as -50°C showed no deconvolution of the peaks, giving an upper limit for the "switching" of $\Delta G^{\ddagger} = 8.8$ kcal/mol. At this oscillation barrier, the half-life would be less than a millisecond, which is faster than the NMR time scale. Although this data does not conclusively rule out either option in Figure 4.6, it does provide some explanation for the effects seen in this spectrum.

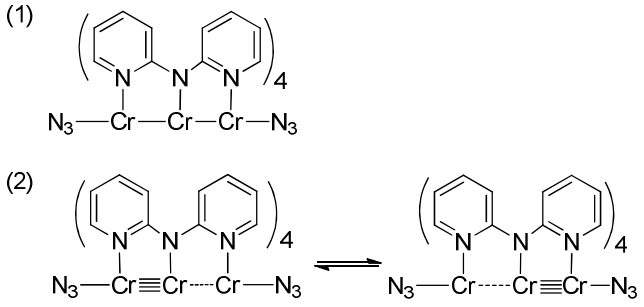

Figure 4.6. Possible solution structures of $Cr_3(dpa)_4(N_3)_2$.

Attempts to study the solution behavior of **11** were somewhat hindered by its instability to chlorinated solvents. To examine the magnetic properties of this compound,

it was dissolved in either deuterated dichloromethane or deuterated chloroform. In the former case, very small peaks (relative to the intensity of the main product peaks) were seen corresponding to the $Cr_2Co(dpa)_4Cl_2$ compound, indicating some decomposition of the diazide. In the latter case, the peaks were much larger and continued to grow in over a period of 24 hours. This result is somewhat surprising because compounds **4**, **5**, **9**, and **10** do not show any indication of decomposition. Although the NMR spectrum of **5** does not show any evidence of dichloride formation, there is surprising evidence of a small amount of **10** present in the ^{1}H NMR spectrum; however, at this time, we do not have mechanistic insight into its formation under these conditions.

4.3.5 Electrochemistry

The redox behavior of the azide precursors, as well as the novel diazide compounds was studied by cyclic voltammetry, as shown below in Figure 4.7 and in Figure 4.8. Compound **9** shows a reversible one-electron wave at $E_{1/2}$ = 266 mV, as well as an irreversible wave at -1050 mV, which may be assigned as oxidation and reduction, respectively, of the Co^{II} ion. Compound **2** shows only irreversible waves that onset at 200 mV, similar to what has been shown before for other Cr≡Cr···Mn compounds. Compound **10** has a reversible wave at $E_{1/2}$ = -518 mV, which may be assigned to the $Cr^{II/III}$ redox couple[6d] and also displays a second reversible redox wave at $E_{1/2}$ = 460 mV. Compound **5** also shows a reversible $Fe^{II/III}$ wave at $E_{1/2}$ = -270 mV, but has a small fore-feature at -518 mV due to the impurity of **10** noted above. Larger scan ranges result in large, irreversible peaks that affect the reversibility of the redox waves of compound **5**. Compound **11** shows one quasi-reversible wave at $E_{1/2}$ = 0 mV that likely corresponds to the $Co^{II/III}$

redox couple. The $Co^{II/III}$ couple most probably is accompanied by a spin-state change from high spin to low spin, the large structural rearrangements of which are likely to cause the quasi-reversibility.

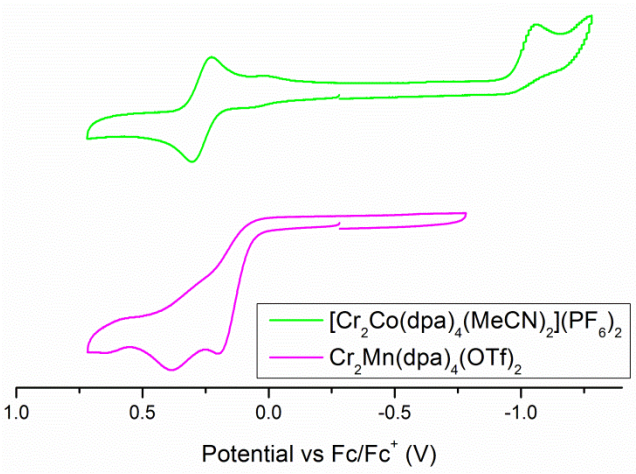

Figure 4.7. Cyclic voltammograms of **2** (bottom) and **9** (top) in dichloromethane.

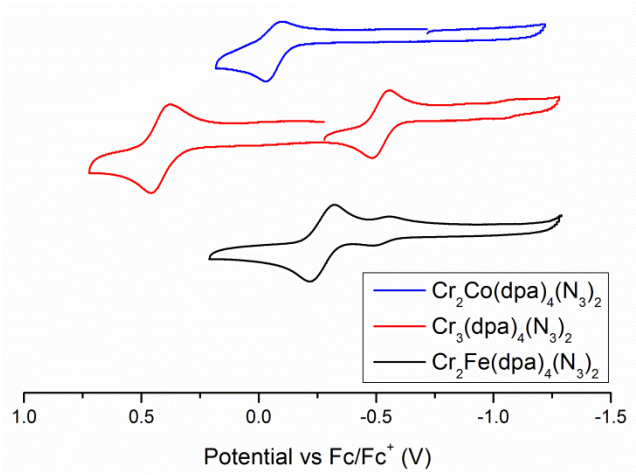

Figure 4.8. Cyclic voltammograms of **5** (bottom), **10** (middle), and **11** (top) in dichloromethane.

4.3.6 Thermal Properties: TGA and DSC

Compound **5**, **10**, and **11** are sufficiently stable in air to allow for thermogravimetric analysis (TGA), as well as differential scanning calorimetry (DSC) measurements. These measurements serve as a probe of possible thermolytic cleavage of the azide ligands to form nitrido products. As shown in Figure 4.9, the TGA traces of these compounds are remarkably similar. These compounds undergo weight loss of roughly 1% at 75°C, which we attribute to loss of residual solvent from the structure of the compound during the TGA process.

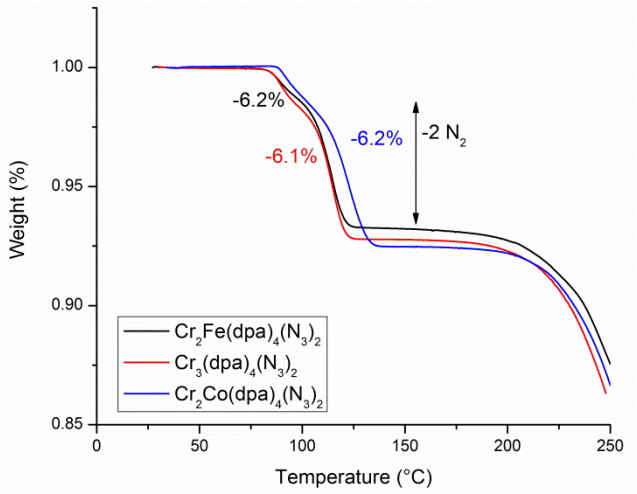

Figure 4.9. TGA of compounds **5**, **10** and **11** after drying under vacuum overnight at 30°C.

Compounds **5**, **10**, and **11** subsequently lose about 6% of their mass in a second step that occurs between 93-100°C. The loss of 6% weight is consistent with the loss of two dinitrogen molecules from the diazide precursor compounds, as shown in Table 4.3. This unexpected result suggests that formation of new heterometallic nitrido compounds from these diazide precursors is likely. The new products are stable up to at least 200°C,

based on the plateau observed in the TGA traces.

Table 4.3. Calculated mass difference corresponding to loss of two dinitrogen molecules.

	5	**10**	**11**
Starting Mass (g/mol)	924.12	920.13	927.12
Final Mass (g/mol)	868.11	864.11	871.11
Mass Loss: Calc	6.1%	6.1%	6.0%
Mass Loss: Expt	6.2%	6.1%	6.2%

To gain some structural insight into the products of thermolysis, samples were investigated by IR spectroscopy following TGA measurements. For compound **10** the stretches in the region from 1600 cm^{-1} to 600 cm^{-1} do not change substantively after heating to 300°C, but the azide stretch near 2050 cm^{-1} changes both in frequency and intensity, disappearing completely upon heating above 300°C (as shown in Figure 4.10). Similar results were obtained for **11**, although at higher temperatures (*e.g.*, 300°C) the characteristic signals from the dpa ligand are lost, signifying destruction of the compound.

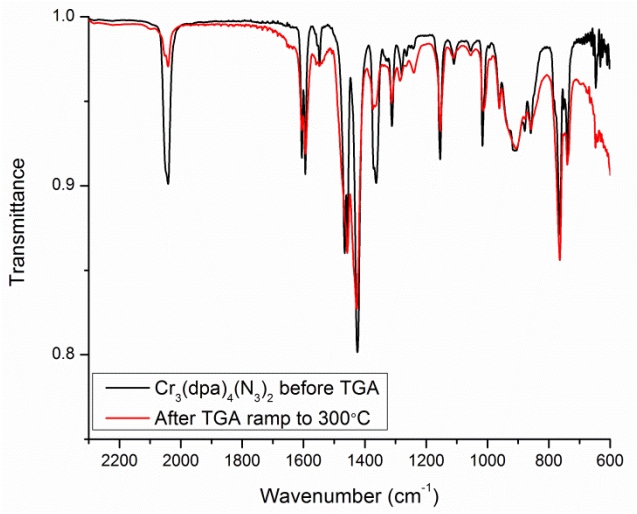

Figure 4.10. IR of **10** and the products resulting from heating to 300°C by TGA.

Differential scanning calorimetry measurements of compounds **5** and **10** show an endothermic reaction below 150°C for both compounds, likely from thermolysis of the azide groups, as shown in Figure 4.11. Similarly, heating **11** results in a small endothermic reaction, starting at 100°C, followed by a larger step at 126°C, which likely corresponds to N_2 loss. At 225°C and above, compounds **5** and **11** undergo multiple stepwise exothermic reactions, which appear to involve degradation of the compound, since this temperature correlates with significant (>10%) mass loss by TGA. Conversely, the decomposition of compound **10** proceeds by a single clean, highly exothermic reaction at 295°C.

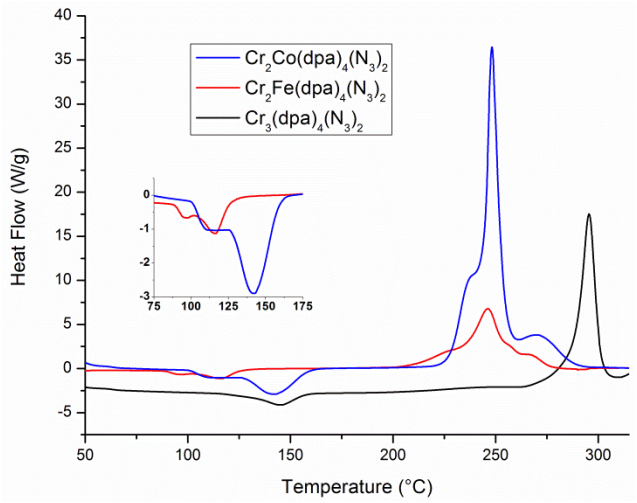

Figure 4.11. DSC of $Cr_2Fe(dpa)_4(N_3)_2$ (**5**), $Cr_3(dpa)_4(N_3)_2$ (**10**), and $Cr_2Co(dpa)_4(N_3)_2$ (**11**).

From the DSC data, ΔH values can be extracted for the proposed azide thermolysis step. These values fall between +16 kJ/mol (4 kcal/mol) and +24 kJ/mol (6 kcal/mol) for the three compounds investigated. It is interesting that these reactions are endothermic. This result signifies that the thermolysis is purely entropy-driven and that the products of thermolysis are inherently less stable than their azide precursors. This situation contrasts with what we have seen in the formation of diruthenium nitrido complexes from azido precursors, which are always exothermic reactions.[3b, 3c] Burger and coworkers also use DSC and TGA to examine N_2 loss from an iridium azide precursor to form the corresponding nitrido complex, and they have found that the loss of dinitrogen is exothermic, with ΔH = -6 kcal/mol.[11] One reason for the exothermicity of the ruthenium and iridium systems may be that in those complexes, triply-bonded nitrido units result.[3b,11a] In the complexes reported here, however, it is not clear that M≡N triple bonds would be formed because of the metal-metal multiply bonded units. As a result, it

is not altogether surprising that the loss of two dinitrogen molecules in complexes **5**, **10**, and **11** is endothermic.

4.4 Conclusions

New diazide complexes of the type $Cr_2M(dpa)_4(N_3)_2$ where M = Cr, Mn, Fe or Co have been prepared and characterized crystallographically, spectroscopically, electrochemically, and thermochemically. When M = Cr, Fe, or Co, thermolysis of the diazide compounds results in the endothermic loss of two dinitrogen molecules. These results lead us to believe that new nitride compounds can be accessed, and future efforts will be devoted to exploring the properties and reactivity of such species.

4.5 Experimental Section

4.5.1 Materials and Methods

All reactions were carried out under a dry N_2 atmosphere using Schlenk techniques and glovebox methods. Solvents diethyl ether (Et_2O), acetonitrile (CH_3CN) and hexanes were purified using a Vacuum Atmospheres solvent purification system. Dichloromethane was freshly distilled under an N_2 atmosphere over CaH_2 prior to use. $Fe(OTf)_2$ (Wako), $Mn(OTf)_2$ (Sigma-Aldrich) and Tl(OTf) (Strem) were purchased and used as received. NaN_3 (Sigma-Aldrich) was dried at 80°C for ~10 h under dynamic vacuum prior to use. The ligand dpaH (2,2´-dipyridylamine, Sigma-Aldrich) was recrystallized from hot hexanes prior to use. $Cr_2(dpa)_4$,[6a] $Cr_2Fe(dpa)_4Cl_2$,[6a] $Cr_2Fe(dpa)_4(OTf)_2$,[7] $Cr_2Mn(dpa)_4Cl_2$,[6b] $Cr_2Co(dpa)_4Cl_2$,[6c] and $[Cr_3(dpa)_4(NCCH_3)_2](PF_6)_2$[5b] were prepared according to literature procedures.

Cyclic voltammograms (CVs) were taken on a BAS Epsilon-EC instrument using CH_2Cl_2 solutions with 0.1 M NBu_4PF_6 and ~1 mM substrate. The electrodes were as follows: glassy carbon (working), Pt wire (auxiliary) and Ag/Ag^+ in CH_3CN (reference). The potentials were referenced versus the ferrocene/ferrocenium redox couple by externally added ferrocene. Elemental analysis was carried out by Columbia Analytical Services in Arizona, USA and Midwest Microlab, LLC in Indiana, USA. X-Band EPR spectra of frozen dichloromethane solutions were recorded at 8 K using a Bruker EleXsys EPR spectrometer: E-500-A console with ER 049SX SuperX Bridge and SuperX Cavity. The sample temperature was set using an Oxford Instruments ESR 900 continuous flow liquid helium cryostat regulated by an Oxford ITC4 temperature controller. IR spectra were taken on a BRUKER TENSOR 27 spectrometer using an ATR adapter. ^{1}H-NMR spectra were recorded on a Varian INOVA-500 spectrometer. The magnetic susceptibility of compound **9** was established using an Evans balance, and by the ^{1}H NMR method[12] for compounds **5**, **10**, and **11** with proper diamagnetic corrections calculated from Pascal's constants.[13]

Differential scanning calorimetry (DSC) measurements were performed on a Thermal Advantage Q-100 differential scanning calorimeter fitted with a TA refrigerated cooling system and TA autosampler. TGA was monitored on a TA Instruments TGA Q-500 build model 203 using the TA Instruments Universal Analysis 2000 software package. Compounds **5**, **10** and **11** all have diethyl ether in the crystal lattice and drying overnight under vacuum helps to remove most of the residual solvent. Drying under these conditions was found not to cause loss of the dinitrogen ligands, as IR spectra indicate

that the azide stretches were present prior to TGA or DSC analysis.

4.5.2 X-Ray Structure Determinations

Crystallographic data were measured at the Molecular Structure Laboratory of the Chemistry Department of the University of Wisconsin – Madison. Crystals were selected under oil under ambient conditions. Single crystals were attached to the tip of a MiTeGen MicroMount©. The crystals were mounted in a stream of cold nitrogen at 100(1) K and centered in the X-ray beam using a video monitoring system. The crystal evaluation and data collection were performed on a Bruker Quazar SMART APEX-II diffractometer with Mo K_α (λ = 0.71073 Å) radiation. The data were collected using a routine to survey reciprocal space, and were indexed by the SMART program.[14] The structures were solved using direct methods and refined by least-squares refinement on F^2 followed by difference Fourier synthesis.[15] All hydrogen atoms were included in the final structure factor calculation at idealized positions and were allowed to ride on the neighboring atoms with relative isotropic displacement coefficients. Note: The crystal structure of compound **2** was solved in the *Cc* space group; attempts to solve the structure in the centrosymmetric space group *C2/c* were unfruitful since the triflate ligands break the center of symmetry, as seen previously for the crystal structure of **3**.[7]

Compounds **5**, **10**, **11**, and **11a** crystallize as M·Et_2O solvates in the monoclinic space group $P2_1/c$. Because Cr and Fe (or Co) are crystallographically indistinguishable, the assignments of metal atom identities are based on expected distances for quadruply bonded Cr≡Cr units. In these compounds, as well as in **2**, **4**, and **9**, the metal atoms show

some disorder and are separated into parts, with a 180° difference in the orientation of the Cr≡Cr···M chain. In these structures, anisotropic refinement of some metal atoms led to large coalesced ellipsoids. When this occurred, we refined these metal atoms with an isotropic thermal parameter. Attempts to split the outer metal atoms of compound **11** were unfruitful, and we therefore constrained the outer Cr and Co atoms to have the same coordinates and thermal parameters.

4.5.3 Synthesis of Complexes

$Cr_2Mn(dpa)_4(OTf)_2$ (2). To a flask containing $Cr_2(dpa)_4$ (0.86 g, 1.1 mmol) and $Mn(OTf)_2$ (0.62 g, 1.8 mmol) was added 85 mL of dry THF. The resulting mixture was heated to reflux overnight, resulting in the formation of a golden microcrystalline precipitate. The brown filtrate was decanted and the precipitate was dried under vacuum. The solid was then extracted into 80 mL of dichloromethane and the solution was filtered and layered with diethyl ether. Diffusion of ether into the dichloromethane solution produced gold crystals suitable for X-ray diffraction after 2 days. Yield: 0.70 g (56%). Found C 43.46%, H 2.91%, N 14.19% Calcd. for $C_{42.5}H_{33}ClCr_2F_6MnN_{12}O_6S_2$ (**$2\cdot0.5CH_2Cl_2$**): C 43.25%, H 2.82%, N 14.24% IR (cm^{-1}): 1608 m, 1598 m, 1463 s, 1425 s, 1363 m, 1328 w, 1311 m, 1288 w, 1233 m, 1210 m, 1154 m, 1025 m, 1018 m, 885 w, 768 m, 743 w, 633 s.

$Cr_2Mn(dpa)_4(N_3)_2$ (4). A solution of NaN_3 (0.08 g, 1 mmol) in 5 mL of MeOH was added to a solution of **3** (0.15 g, 0.13 mmol) in 20 mL of MeOH at 0ºC. The mixture was stirred for 1 hour at 0ºC, resulting in the formation of a brown solid. The methanol

was decanted and the solid was dried under reduced pressure, dissolved in 20 mL of dichloromethane and filtered to remove $Cr_2(dpa)_4$. Diffusion of diethyl ether into the dichloromethane solution resulted in the formation of brown crystals suitable for X-ray diffraction after 2 days, along with bright orange needles of $Cr_2(dpa)_4$. Yield: 10 mg (8%). IR (cm^{-1}): 2078 w, 2050 m (N_3), 1604 m, 1593 m, 1457 s, 1422 s, 1367 m, 1308 w, 1150 m, 1017 m, 903 br, 767 s, 732 m. The poor yield of this compound precluded more extensive characterization.

$Cr_2Fe(dpa)_4(N_3)_2$ (5). $Cr_2Fe(dpa)_4(OTf)_2$ (0.12 g, 0.10 mmol) was dissolved in 25 mL of dry MeOH and cooled to 0°C. To this solution was added a solution of NaN_3 (0.02 g, 0.3 mmol) in 8 mL of dry MeOH at room temperature. The resulting mixture was stirred for 2 hours at 0ºC, after which time the methanol was decanted using a cannula, leaving a brown solid that was dried under reduced pressure, dissolved in 25 mL of dichloromethane, filtered and layered with 30 mL diethyl ether. Small black block crystals formed after 1 day. Note: This reaction also forms a small amount of bright orange $Cr_2(dpa)_4$ crystals that co-crystallize with the product and can be removed from the bulk product by manual separation. Yield: 90 mg (93%). μ_{eff} (298 K, μ_B) = 5.20. Found C 52.14%, H 4.24%, N 23.86%. Calcd. for $C_{44}H_{42}Cr_2FeN_{18}O$ (**$1 \cdot 0.5Et_2O$**): C 52.45%, H 3.85%, N 26.22%. IR (cm^{-1}): 3070 w, 3027 w, 2964 w, 2043 s (N_3), 1605 s, 1593 s, 1547 w, 1467 s, 1426 s, 1361 m, 1311 m, 1263 m, 1154 m, 1107 m, 1016 m, 801 m, 740 m. ^1H NMR (500 MHz, CD_2Cl_2): δ = 117.02 (1H, br), 69.99 (1H, s), 39.74 (1H, s), 8.42 (1H, s), 5.14 (1H, s), 3.69 (1H, s), 2.29 (1H, s), -6.00 (1H, s).

$[Cr_2Co(dpa)_4(MeCN)_2](PF_6)_2$ (9). To a flask containing solid $Cr_2Co(dpa)_4Cl_2$

(0.337 g, 0.368 mmol) and solid $TlPF_6$ (0.299 g, 0.856 mmol) was added 25 mL of dry acetonitrile. The resulting brown reaction mixture was stirred for 4 hours at room temperature, after which point a white precipitate was observed. The mixture was then filtered over celite, resulting in a dark green-brown filtrate, which was layered with diethyl ether. Small green-black crystals of $[Cr_2Co(dpa)_4(NCCH_3)_2](PF_6)_2 \cdot 2CH_3CN$ suitable for X-ray diffraction formed after 1 hour. Yield: 200 mg (45%). μ_{eff} (298 K, μ_B) = 1.60. Found C 43.72%, H 3.49%, N 15.93%. Calcd. for $C_{44}H_{38}CoCr_2F_{12}N_{14}P_2$ (**9**): C 43.47%, H 3.15%, N 16.13%. IR (cm^{-1}): 1610 w, 1600 w, 1470 m, 1430 m, 1364 w, 1318 w, 1157 w, 1023 w, 834 s, 764 m, 740 m. ^1H NMR (500 MHz, CD_3CN): δ = 11.92 (1H, s), 11.45 (1H, s), 8.65 (1H, br), 5.99 (1H, s), 5.77 (1H, s), 4.94 (1H, s), 4.34 (1H, s), -1.80 (1H, br).

$Cr_3(dpa)_4(N_3)_2$ (10). To a solution of $[Cr_3(dpa)_4(NCCH_3)_2](PF_6)_2$ (0.23 g, 0.19 mmol) in 15 mL of MeOH at 0ºC was added a solution of NaN_3 (0.03 g, 0.5 mmol) in 5 mL of MeOH at room temperature. Upon stirring at 0ºC for several minutes, the initial clear green solution became cloudy green and eventually cloudy brown. After 1 hour, the solvent was decanted, leaving behind a green-gray microcrystalline solid that was dried under vacuum, dissolved in 15 mL of dichloromethane, filtered and layered with ether. Green-black crystals of $Cr_3(dpa)_4(N_3)_2 \cdot Et_2O$ formed overnight. Yield: 90 mg (50%). μ_{eff} (298 K, μ_B) = 4.61. Found C 52.85%, H 4.14%, N 25.00%. Calcd. for $C_{44}H_{42}Cr_3N_{18}O$ (**$10 \cdot Et_2O$**): C 53.12%, H 4.25%; N 25.34%. IR (cm^{-1}): 2041 m (N_3), 1605 m, 1594 m, 1466 s, 1457 s, 1424 s, 1363 m, 1312 w, 1154 m, 1017 m, 912 br, 764 s, 741 m. ^1H NMR (500 MHz, CD_2Cl_2): δ = 12.96 (1H, br), -0.42 (1H, br), -15.00 (1H, br).

$Cr_2Co(dpa)_4(N_3)_2$ (11). To a solution of $[Cr_2Co(dpa)_4(NCCH_3)_2](PF_6)_2$ (0.277 g, 0.228 mmol) in 15 mL of MeOH at 0ºC was added a solution of NaN_3 (0.04 g, 0.5 mmol) in 8 mL of MeOH at room temperature. After stirring for 2 hours at 0ºC, the solvent was decanted, leaving behind a brown microcrystalline solid that was dried under vacuum, dissolved in 25 mL of dichloromethane, filtered and layered with ether. Black crystals of $Cr_2Co(dpa)_4(N_3)_2 \cdot Et_2O$ formed immediately and were grown over 2 days. Yield: 126 mg (60%). μ_{eff} (298 K, μ_B) = 3.31. Found C 51.75%, H 4.17%, N 24.61%. Calcd. for $C_{44}H_{42}Cr_2CoN_{18}O$ (**$11 \cdot Et_2O$**): C 52.75%, H 4.23%; N 25.17%. IR (cm^{-1}): 2051 m (N_3), 1605 m, 1593 m, 1550 w, 1465 s, 1457 s, 1425 s, 1362 m, 1311 w, 1280 w, 1149 m, 1107 w, 1017 m, 886 br, 860 w, 766 s, 741 m. ^1H NMR (500 MHz, CD_2Cl_2): δ = 100.65 (1H, s), 67.18 (1H, s), 41.81 (1H, s), 19.42 (1H, s), 8.31 (1H, s), 4.65 (1H, s), 4.11 (1H, s), -14.55 (1H, s).

References

(1) (a) Aromí, G.; Aguila, D.; Gamez, P.; Luis, F.; Roubeau, O., *Chem. Soc. Rev.* **2012,** *41*, 537; (b) Escuer, A.; Aromí, G., *Eur. J. Inorg. Chem.* **2006,** *2006*, 4721; (c) Adhikary, C.; Koner, S., *Coord. Chem. Rev.* **2010,** *254*, 2933.

(2) (a) Sieh, D.; Schoffel, J.; Burger, P., *Dalton Trans.* **2011,** *40*, 9512; (b) Thomson, R. K.; Cantat, T.; Scott, B. L.; Morris, D. E.; Batista, E. R.; Kiplinger, J. L., *Nat. Chem.* **2010,** *2*, 723; (c) Eikey, R. A.; Abu-Omar, M. M., *Coord. Chem. Rev.* **2003,** *243*, 83; (d) Berry, J. F., *Comments Inorg. Chem.* **2009,** *30*, 28.

(3) (a) Pap, J. S.; DeBeer George, S.; Berry, J. F., *Angew. Chem. Int. Ed.* **2008,** *47*, 10102; (b) Long, A. K. M.; Timmer, G. H.; Pap, J. S.; Snyder, J. L.; Yu, R. P.; Berry, J. F., *J. Am. Chem. Soc.* **2011,** *133*, 13138; (c) Musch Long, A. K.; Yu, R. P.; Timmer, G. H.; Berry, J. F., *J. Am. Chem. Soc.* **2010,** *132*, 12228.

(4) (a) García, M. E.; Melón, S.; Ruiz, M. A.; López, R.; Sordo, T.; Marchiò, L.; Tiripicchio, A., *Inorg. Chem.* **2008,** *47*, 10644; (b) Hedegaard, E. D.; Schau-Magnussen, M.; Bendix, J., *Inorg. Chem. Commun.* **2011,** *14*, 719.

(5) (a) Cotton, F. A.; Daniels, L. M.; Murillo, C. A.; Pascual, I., *J. Am. Chem. Soc.* **1997,** *119*, 10223; (b) Berry, J. F.; Cotton, F. A.; Lu, T.; Murillo, C. A.; Roberts, B. K.; Wang, X., *J. Am. Chem. Soc.* **2004,** *126*, 7082.

(6) (a) Nippe, M.; Berry, J. F., *J. Am. Chem. Soc.* **2007,** *129*, 12684; (b) Nippe, M.; Wang, J.; Bill, E.; Hope, H.; Dalal, N. S.; Berry, J. F., *J. Am. Chem. Soc.* **2010,** *132*, 14261; (c) Nippe, M.; Victor, E.; Berry, J. F., *Eur. J. Inorg. Chem.* **2008,** *2008*, 5569; (d) Nippe, M.; Bill, E.; Berry, J. F., *Inorg. Chem.* **2011,** *50*, 7650; (e) Aydin-Cantürk, D.; Nuss, H., *Z. Anorg. Allg. Chem.* **2011,** *637*, 543.

(7) Nippe, M.; Turov, Y.; Berry, J. F., *Inorg. Chem.* **2011,** *50*, 10592.

(8) Cotton, F. A., In *Multiple Bonds Between Metal Atoms*, Editon ed.; Cotton, F. A.; Murillo, C. A.; Walton, R. A., Eds. Springer: New York, 2005.

(9) Georgiev, V. P.; McGrady, J. E., *J. Am. Chem. Soc.* **2011,** *133*, 12590.

(10) Chen, I. W. P.; Fu, M.-D.; Tseng, W.-H.; Yu, J.-Y.; Wu, S.-H.; Ku, C.-J.; Chen, C.-h.; Peng, S.-M., *Angew. Chem. Int. Ed.* **2006,** *45*, 5814.

(11) (a) Schöffel, J.; Rogachev, A. Y.; DeBeer George, S.; Burger, P., *Angew. Chem. Int. Ed.* **2009,** *48*, 4734; (b) Schöffel, J.; Šušnjar, N.; Nückel, S.; Sieh, D.; Burger, P., *Eur. J. Inorg. Chem.* **2010,** *2010*, 4911.

(12) (a) Evans, D. F., *J. Chem. Soc.* **1959**, 2003; (b) Piguet, C., *J. Chem. Educ.* **1997,** *74*, 815; (c) Grant, D. H., *J. Chem. Educ.* **1995,** *72*, 39.

(13) Bain, G. A.; Berry, J. F., *J. Chem. Educ.* **2008,** *85*, 532.

(14) Bruker-AXS *Bruker-AXS*, Madison, Wisconsin, USA, 2009.

(15) Dolomanov, O. V.; Bourhis, L. J.; Gildea, R. J.; Howard, J. A. K.; Puschmann, H., *J. Appl. Crystallogr.* **2009,** *42*, 339.

Chapter 5

Nitrogen Atom Transfer from Manganese to Iron

Yevgeniya Turov, Elizabeth Hillard, Rodolphe Clérac, John F. Berry *Angew. Chem. Int. Ed.*, Submitted.
E. Hillard and R. Clérac assisted with magnetic measurements. All other data and text is the original work of Yevgeniya Turov.

5.1 Abstract

Reaction of $FeCl_3(THF)$ with one equivalent of the N-atom transfer reagent MnN(salen) in acetonitrile results in the formation of a metastable brown intermediate in solution and precipitation of the insoluble MnCl(salen)·MeCN. Addition of triphenylphosphine to the above solution yields the binuclear phosphinimato complex $Fe_2Cl_4(\mu\text{-}NPPh_3)_2$ (**1**). In the absence of a suitable substrate, spontaneous bimolecular reduction to Fe^{II} occurs. These observations present strong circumstantial evidence for the formation of a reactive Fe-nitride species via N-atom transfer to $FeCl_3$ under very mild conditions.

5.2 Introduction

Reactive Fe intermediates are of considerable interest to the chemical community, especially in reference to the mechanisms of iron-containing enzymes in biological systems. Iron nitride species are of particular significance and relevance to nitrogen fixation via nitrogenase enzymes or the Haber-Bosch process.[1] Investigations of molecular iron nitride systems began with experiments by Nakamoto[2] on heme systems and Wieghardt[3] on non-heme systems. They showed that reactive Fe^{V} nitrido species could be generated by low-temperature photolysis of Fe^{III} azide precursors under demanding reaction conditions (-196°C). Although spectroscopic characterization of the

Fe^{V} species,[3a,4] and even an Fe^{VI} species,[5] could be attained, the demanding preparative conditions precluded both isolation of the nitrido compounds and exploration of their reactivity. These shortcomings have been largely overcome in recent years by gas-phase exploration of Fe-nitrido reactivity by Schwarz and coworkers,[6] preparation of stable complexes with bridging nitrido ligands,[7] dinitrogen activation by low-coordinate iron complexes,[8] and the synthesis of ligand-stabilized pseudo-tetrahedral Fe^{IV} nitrido complexes.[9] With this synthetic advance, a four-coordinate Fe^{V} nitrido complex has even been characterized crystallographically by Smith and coworkers.[1c] Despite these successes, it should be noted that Fe-nitride formation via azide photolysis is not entirely reliable; often photoreduction occurs instead.[3a,10] Thus, alternative methods to install the Fe-nitride unit, as reported here, are of great potential utility.

Electrophilic reactivity is a hallmark of high-valent Fe nitride chemistry. Nucleophiles such as phosphines,[1d,9a] isonitriles,[11] CO,[11] and H_2,[1a] can add to the N atom to yield $–N=PR_3$ phosphiniminato species, –N=C=NR carbodiimides, isocyanate, or ammonia. Additionally, Peters and coworkers have noted that terminal nitrido complexes may undergo bimolecular coupling to form an N_2-bridged metal dinuclear complex in a spectacular six-electron redox reaction.[9a] In this work, we show that a new species displaying characteristic Fe-nitride reactivity can be generated in solution at room temperature from a simple $FeCl_3$ starting material without any stabilizing ligands via an N-atom transfer protocol inspired by related Cr-nitrido chemistry pioneered by Bendix and coworkers.[12] Expansion of this N-atom transfer to iron is significant in that, while Cr^{V} nitrido compounds are unreactive towards N-atom transfer, Fe nitrides are much

more reactive. We explore the identity of this reactive intermediate whose structure is postulated to be a manganese-iron nitrido-bridged species, abbreviated as "{Fe(N)"$^{2+}$ in this work for brevity.

5.3 Results and Discussion

Reaction of yellow $Fe^{III}Cl_3(THF)$ with green $Mn^{V}N(salen)$ in acetonitrile instantly yields a deep brown mixture. After filtering the precipitate, the brown color of the filtrate changes within an hour to a dark red-brown color, indicating formation and loss of a metastable species in solution. To test this hypothesis, we attempted to trap the intermediate species by reaction with triphenylphosphine since high-valent Fe nitride compounds are known to react with this substrate.

Reaction of the dark brown "$\{Fe(N)\}^{2+}$" solution, prepared as described above, with a solution of triphenylphosphine in acetonitrile without stirring results in the formation of dark red needle-shaped crystals of the known compound $Fe^{III}_2Cl_4(\mu\text{-}NPPh_3)_2$ (**1**) in close to 50% yield, according to Scheme 5.1. The identity of **1** was unambiguously assigned based on a crystallographic unit cell determination,[13] elemental analysis, and IR and NMR spectroscopy. Although **1** was reported previously by Roesky and coworkers,[14] their synthetic method involved using a pre-existing N=P bond (from $Me_3SiNPPh_3$) and required refluxing a toluene solution for 48 hours to achieve formation of this iron complex. Thus, the synthetic route reported here is advantageous because the reaction proceeds at ambient temperatures and uses simple reagents. Furthermore, this result indicates that the "$\{Fe(N)\}^{2+}$" solution not only contains a reactive nitride species, but that this species is oxidizing, as it is able to oxidize $P^{III}Ph_3$ to $(\text{-}NP^{V}Ph_3)^{-}$ via N-atom transfer and that it can react to form well-defined products.

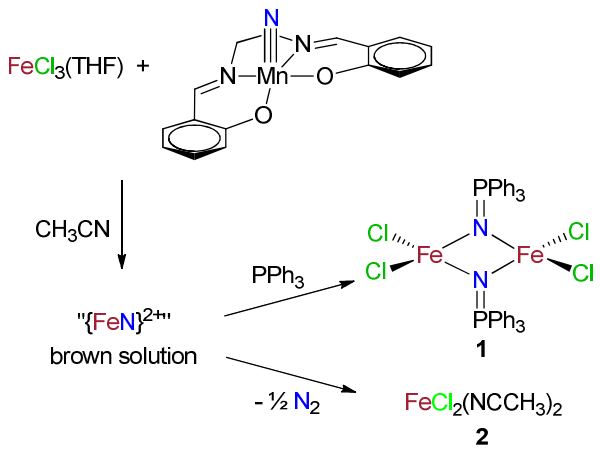

Scheme 5.1. Formation of 1 and 2.

Since no magnetic characterization of **1** had been reported, we have characterized **1** by magnetic susceptibility measurements (Figure 5.1). A plot of χT versus T has a value of $\chi T \sim 0.15$ cm^3 K/mol at temperatures below 50 K indicating that **1** possesses a diamagnetic ground state.[15] The value of χT increases with temperature to a value of 1.1 cm^3 K/mol at 270 K, and the overall shape of the curve is consistent with what is expected for a compound having two high-spin Fe^{III} nuclei that are antiferromagnetically coupled. A fit of the magnetic susceptibility data yielded $J/k_B = -120.5(2)$ K. Thus, the phosphiniminato ligands are good mediators of strong antiferromagnetic exchange between the $S = 5/2$ Fe^{III} centers and **1** possesses a diamagnetic ground state.

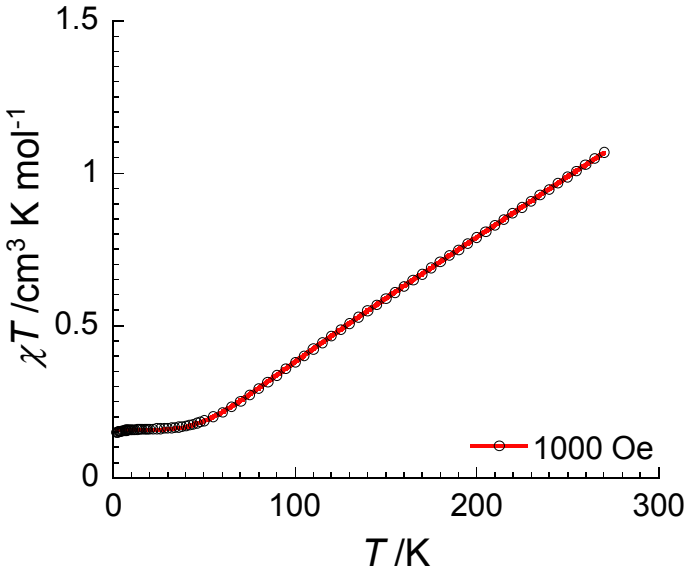

Figure 5.1. χT vs. T plot at 1000 Oe for **1**; the red line is the fit using an isotropic high spin Fe^{III} ($S_1 = S_2 = 5/2$) dinuclear model. The experimental data are well fitted to this model in the whole range of temperatures. The $S = 5/2$ model was employed using the following isotropic Heisenberg spin Hamiltonian: $H = -2JS_1 \cdot S_2$. In the frame of this model using the weak field approximation ($g\mu_B H << k_B T$), an analytical expression of the magnetic susceptibility can be obtained applying the van Vleck equation:

$$\chi_{(dimer)} = \frac{Ng^2\mu_B^2}{k_B T} \frac{2\exp(2x) + 10\exp(6x) + 28\exp(12x) + 60\exp(20x) + 110\exp(30x)}{1 + 3\exp(2x) + 5\exp(6x) + 7\exp(12x) + 9\exp(20x) + 11\exp(30x)}$$

where $x = J/k_B T$ and $g = 2$. The fitting parameters were $J/k_B =$ -120.5(2) K, and a 3.6% $S = 5/2$ paramagnetic impurity.

We have tested the possibility that the MnN(salen) starting material (rather than a reactive iron nitride) performs the reaction with PPh_3. A control reaction was performed in which MnN(salen) was added to triphenylphosphine in deuterated acetonitrile in the absence of Fe. The reaction was monitored by ^{31}P NMR spectroscopy and after 1 hour, the triphenylphosphine signal remained unchanged, indicating that there is no reaction between the MnN(salen) species and the substrate (Figure 5.2). This experiment strongly suggests that it is the Fe-nitride species that performs N-atom transfer to triphenylphosphine.

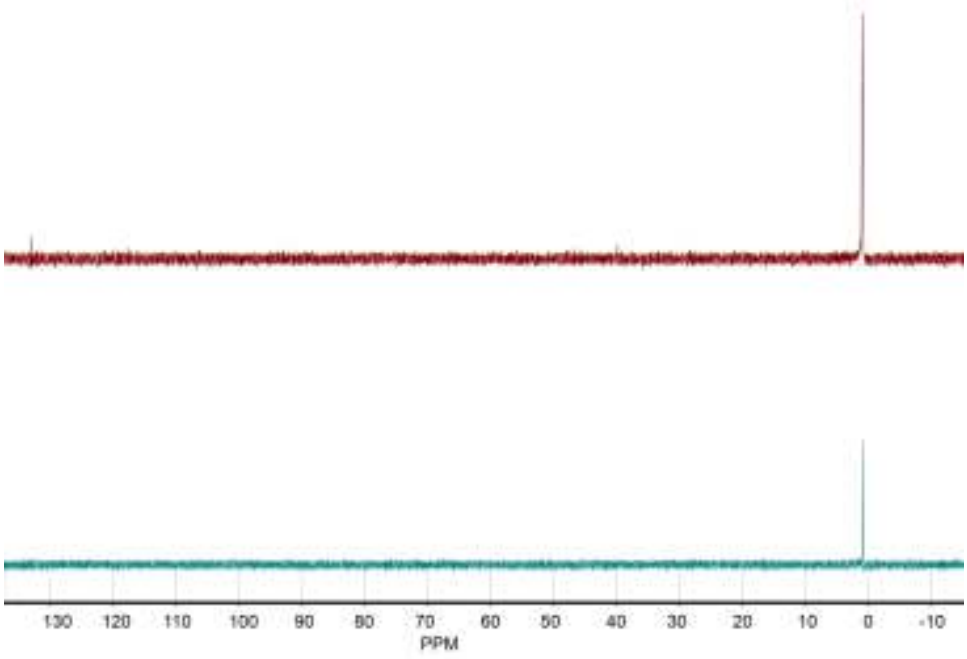

Figure 5.2. ^{31}P NMR spectrum of PPh_3 (bottom) and the reaction of PPh_3 and MnN(salen) in CD_3CN after 1 hour (top). A small peak begins to grow in at about 130 ppm after 1 hour, but this signal integrates to <0.01 and is not relevant on the time-scale of the reported reaction.

Interestingly, in the absence of substrate, the brown "$\{Fe(N)\}^{2+}$" solution changes color to red-brown and colorless block-shaped crystals of the known[16] compound $FeCl_2(NCCH_3)_2$ (**2**) form in 69% yield (Scheme 5.1). The identity of this compound was confirmed by X-ray crystallographic methods.[17] The formation of Fe^{II} under these conditions is surprising, but can be rationalized as the product formed when two "$\{Fe(N)\}^{2+}$" species dimerize to form a dinitrogen bridged intermediate, followed by elimination of dinitrogen, as shown in Scheme 5.2. If this is indeed the case, the decomposition of the "$\{Fe(N)\}^{2+}$" intermediate should be bimolecular and follow second order kinetics.

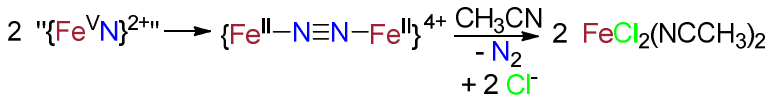

Scheme 5.2. *Proposed mechanism for the formation of* ***2.***

To test this hypothesis, the decomposition of "$\{Fe(N)\}^{2+}$" was studied by UV-Vis spectroscopy at room temperature using different concentrations of $FeCl_3(THF)$ in acetonitrile. In each run, the "$\{Fe(N)\}^{2+}$" species was generated as described above, and the disappearance of the signal at 757 nm was monitored over 2 hours. Plots of inverse absorbance over time give linear fits (Figures 5.3 and S5.1), consistent with the bimolecular mechanism proposed in Scheme 5.2. The decomposition of the reactive "$\{Fe(N)\}^{2+}$" explains the lower than quantitative yield for the reaction with triphenylphosphine. This reaction is extremely concentration-dependent, and it is very important to control the concentration and reaction time in order to mediate the delicate balance between the kinetics of the N-atom transfer from Mn^V to form the Fe-nitrido species and the bimolecular coupling that forms **2**.

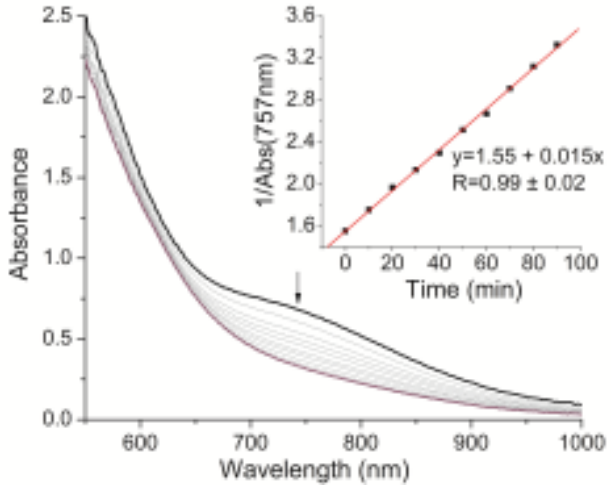

Figure 5.3. Kinetics of the second-order decomposition of "$\{Fe(N)\}^{2+}$" in acetonitrile at room temperature, prepared from a 10.2 mM solution of starting material (note: error bars are smaller than the data points).

Further, to confirm the formation of dinitrogen in this proposed decomposition, we labeled the Mn(N)salen starting material with ^{15}N. We then examined the head space of a reaction mixture to determine whether $^{30}N_2$ was observed. As predicted, one hour after starting the reaction, GC-MS head space analysis reveals a peak at M/Z = 30 with an area 730 times greater than that present in air (Figure 5.4).

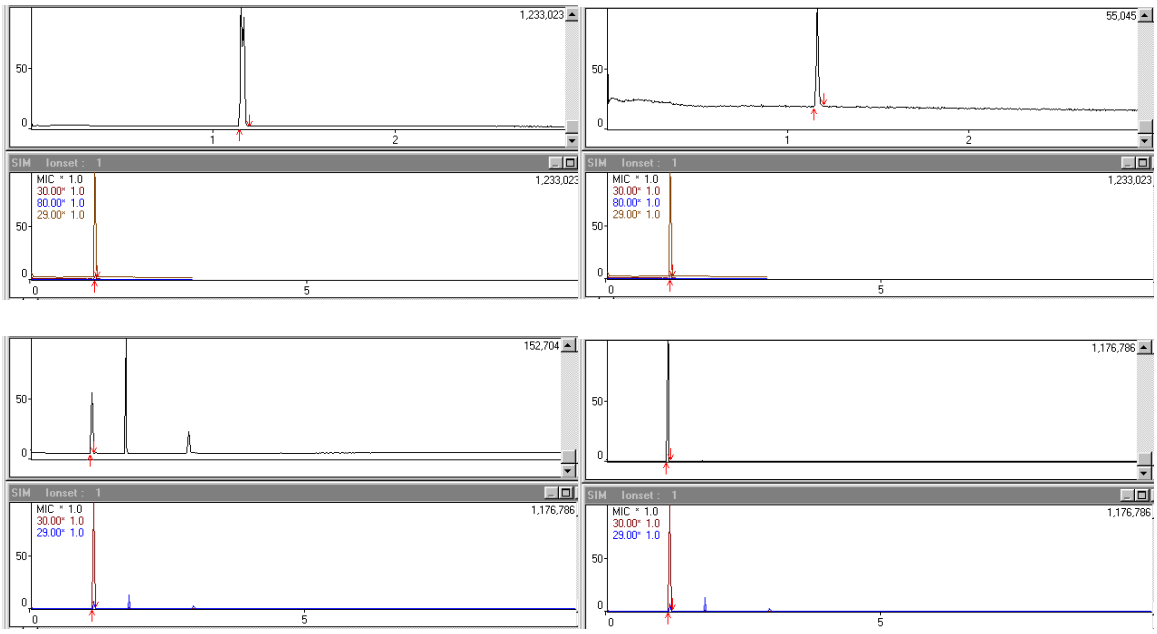

Figure 5.4. Air ($^{29}N_2$, top left), Air ($^{30}N_2$, top right), Reaction ($^{29}N_2$, bottom left), Reaction ($^{30}N_2$, bottom right).

The reactivity profile of "$\{Fe(N)\}^{2+}$" is suggestive of an Fe^{V} species and preliminary EPR data support this assignment. The EPR spectrum of a freshly prepared and rapidly frozen "$\{Fe(N)\}^{2+}$" solution shows a main broad isotropic signal from the Fe^{III} starting material with additional features at $g_{\perp} = 4$ and $g_{\parallel} = 2$ (Figure 5.5), consistent with an axial $S = 3/2$ species, likely indicating high-spin Fe^{V}. The spectrum can be modeled as a 20:7 mixture of Fe^{III}:Fe^{V} species.

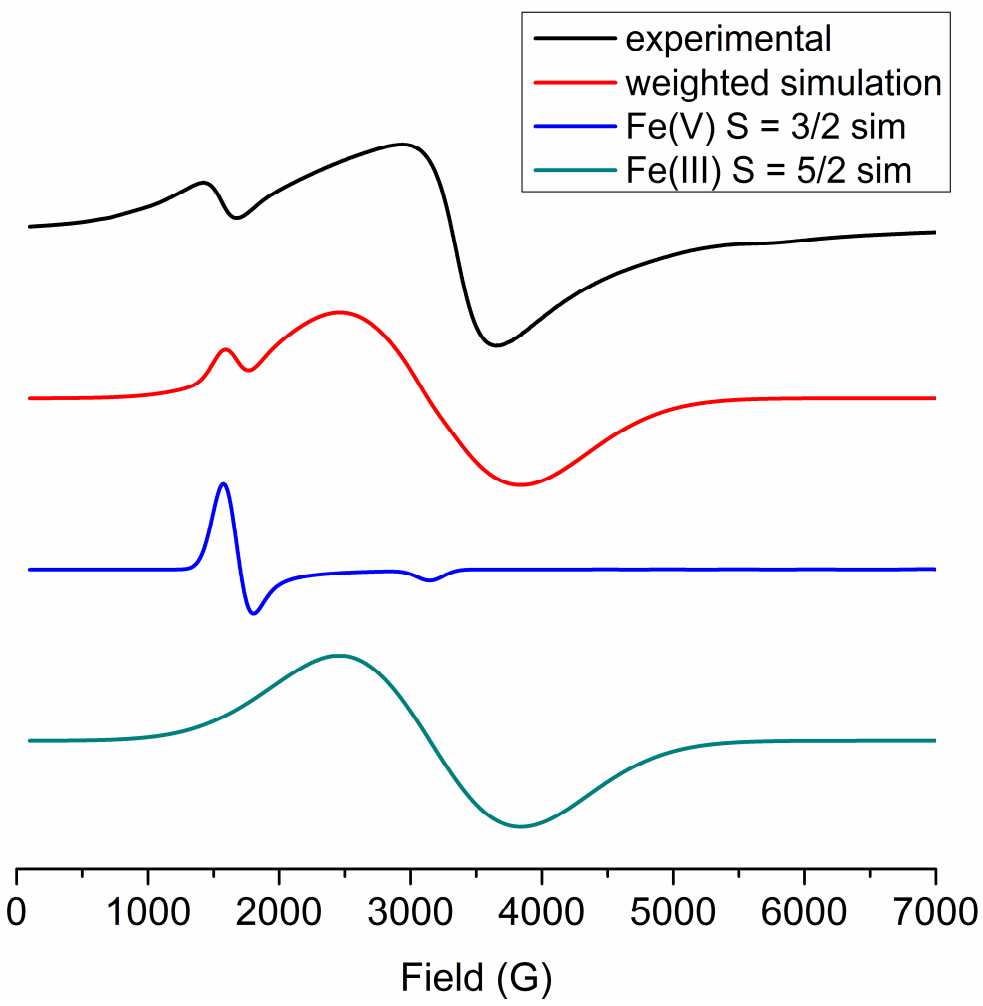

Figure 5.5. X-band EPR spectrum of "{Fe(N)}$^{2+}$" in frozen MeCN at 4 K (black). Simulated spectrum with $g_{\perp} = 4$ and $g_{\parallel} = 2$ for the minor component ($S = 3/2$ species), and $g_{iso} = 2$ for the major component ($S = 5/2$) (red). Simulated spectra of individual minor (blue) and major components (green).

The simulation was modeled with a minor component, an Fe^{V} $S = 3/2$ system (based on the g values) which is assigned a weight of seven and the major component, which is assigned a weight of twenty and is based on the Fe^{III} $S = 5/2$ system corresponding to the excess starting material present in solution.

5.4 Conclusions

In summary, we present a new method for the preparation of Fe-nitrido species via N-atom transfer from Mn^{V}. This observation has allowed us to make a preliminary exploration of fundamental Fe-nitride chemistry in the absence of stabilizing ligands. Reactivity studies show that this "$\{Fe(N)\}^{2+}$" unit reacts readily with triphenylphosphine to produce a phosphiniminato species that crystallizes from acetonitrile solution. UV-Vis and crystallographic studies confirm the decomposition of this intermediate to an Fe^{II} species through a bimolecular pathway. We suggest that this synthetic route may be extremely useful for the preparation of a number of new ligand-stabilized iron nitride species.

5.5 Experimental Section

All reactions were carried out under a dry N_2 atmosphere using Schlenk techniques and glovebox methods. Reagents were purchased from Sigma-Aldrich and used as received unless otherwise noted. Triphenylphosphine was purchased from Sigma-Aldrich and dried under vacuum overnight at 80°C before use. Acetonitrile (CH_3CN) was purified using a Vacuum Atmospheres solvent purification system and degassed prior to use. $FeCl_3$(THF) was prepared according to a slight variation on a literature method.[18] $FeCl_3$ was dissolved in THF, the solution was filtered, and the THF was removed under vacuum. The solid was then extracted into a minimal amount of benzene, filtered, and the benzene was removed under vacuum. The solid was then dried under vacuum at 50°C overnight to ensure full removal of solvent, leaving a yellow-brown solid. Sublimation at 70°C led to isolation of the desired bright yellow solid, $FeCl_3$(THF). MnCl(salen) and

MnN(salen) were prepared according to literature procedures.[19] $Mn^{15}N$(salen) was prepared analogously to MnN(salen) except $^{15}NH_4OH$ was used to introduce the labeled nitrogen. $Mn^{15}N$(salen) and MnN(salen) were purified by Soxhlet extraction into dichloromethane, followed by removal of the solvent under reduced pressure to yield a green solid. Without this purification step, MnN(salen) does not dissolve well in acetonitrile and the desired "$\{Fe(N)\}^{2+}$" species does not form.

Elemental analysis was carried out by Midwest Microlab, LLC in Indiana, USA. X-Band EPR spectra of frozen acetonitrile solutions were recorded at 8 K using a Bruker EleXsys EPR spectrometer: E-500-A console with ER 049SX SuperX Bridge and SuperX Cavity. The sample temperature was set using an Oxford Instruments ESR 900 continuous flow liquid helium cryostat regulated by an Oxford ITC4 temperature controller. EPR simulations were conducted using the Easyspin 4.0.0 toolbox[20] for MATLAB. IR spectra were taken on a BRUKER TENSOR 27 spectrometer using an ATR adapter. Inductively coupled plasma optical emission spectroscopy (ICP-OES) was performed on a Perkin Elmer Optical Emission Optima 2000 DV instrument, using Solid State RFGenerator, and AS-90 autosampler, and WinLab22 for data processing and samples of 1 mg/L concentration in water.

Gas chromatography – mass spectrometry (GC-MS) samples were prepared by reaction of $FeCl_3$(THF) and $Mn^{15}N$(salen) in degassed acetonitrile under argon atmosphere, and both air and argon were used as blanks in the analysis. Analysis was performed on a Shimadzu GC-17A Gas Chromatograph with Shimadzu Mass Spectrometer model QP-5000 instrument and analyzed using CLASS-5000 software.

Magnetic susceptibility measurements were obtained using a Quantum Design MPMS-XL SQUID magnetometer. The measurements were performed on a freshly filtered polycrystalline sample of **1** introduced in a polyethylene bag (3 × 0.5 × 0.02 cm). The dc measurements were conducted from 280 to 1.8 K at 1000 Oe applied dc field. An *M* vs *H* measurement was performed at 100 K to confirm the absence of ferromagnetic impurities.

$Fe_2Cl_4(\mu\text{-}NPPh_3)_2$ (1). In a glove box, $FeCl_3(THF)$ (57.6 mg, 0.246 mmol) was combined with Mn(N)salen (82.6 mg, 0.246 mmol) and 15 mL of acetonitrile in a round-bottom flask. This mixture instantly turned brown and a brown precipitate formed. After stirring for ten minutes, the precipitate was filtered off over glass wool and the filtrate ("$\{Fe(N)\}^{2+}$") was added to a 50 mL Schlenk flask. PPh_3 (172.8 mg, 0.659 mmol) was dissolved in 10 mL of acetonitrile. The triphenylphosphine solution was added to the "$\{Fe(N)\}^{2+}$" solution slowly via cannula, without stirring. Brown needles of **1** formed after 1 day and were suitable for X-ray crystallography. Yield: 0.0896 g (45%). Found C 53.24%, H 4.01%, N 3.08%. Calcd. for $C_{36}H_{30}Cl_4Fe_2N_2P_2$: C 53.64%, H 3.75%; N 3.48%. IR (cm^{-1}): 3181 br, 1622 s, 1601 m, 1542 m, 1439 s, 1394 w, 1338 w, 1296 m, 1261 w, 1117 s, 1012 m, 963 m, 937 m, 904 m, 865 m, 800 m, 749 s, 724 s, 690 s, 669 m, 655 m.

5.6 Supplementary Information

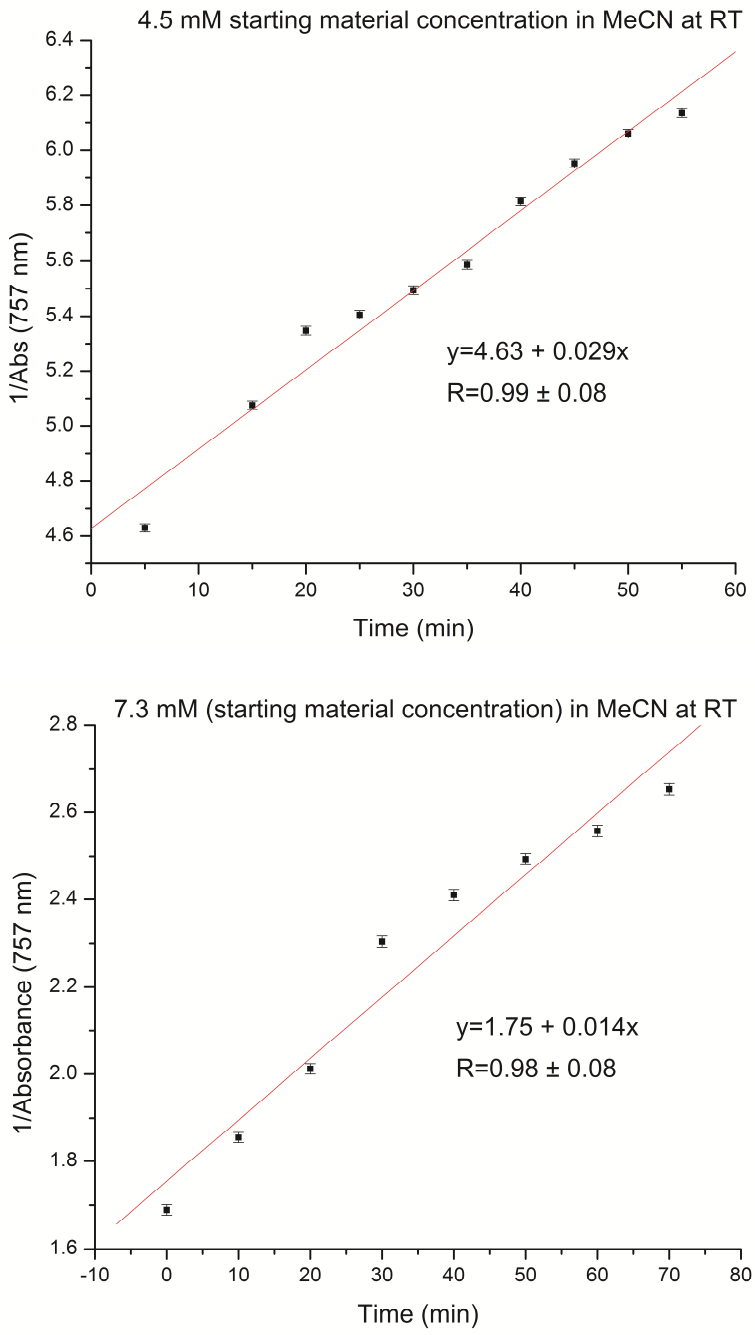

Figure S5.1. Kinetics measurements of the decomposition of 4.5 mM starting material concentration (top) and 7.3 mM starting material concentration (bottom) in MeCN at room temperature.

References

(1) (a) Scepaniak, J. J.; Young, J. A.; Bontchev, R. P.; Smith, J. M., *Angew. Chem. Int. Ed.* **2009,** *48*, 3158; (b) Scepaniak, J. J.; Young, J. A.; Bontchev, R. P.; Smith, J. M., *Angew. Chem.* **2009,** *121*, 3204; (c) Scepaniak, J. J.; Vogel, C. S.; Khusniyarov, M. M.; Heinemann, F. W.; Meyer, K.; Smith, J. M., *Science* **2011,** *331*, 1049; (d) Smith, J. M.; Subedi, D., *Dalton Trans.* **2012,** *41*, 1423.

(2) Nakamoto, K., *Coord. Chem. Rev.* **2002,** *226*, 153.

(3) (a) Meyer, K.; Bill, E.; Mienert, B.; Weyhermüller, T.; Wieghardt, K., *J. Am. Chem. Soc.* **1999,** *121*, 4859; (b) Grapperhaus, C. A.; Mienert, B.; Bill, E.; Weyhermüller, T.; Wieghardt, K., *Inorg. Chem.* **2000,** *39*, 5306.

(4) Petrenko, T.; DeBeer George, S.; Aliaga-Alcalde, N.; Bill, E.; Mienert, B.; Xiao, Y.; Guo, Y.; Sturhahn, W.; Cramer, S. P.; Wieghardt, K.; Neese, F., *J. Am. Chem. Soc.* **2007,** *129*, 11053.

(5) Berry, J. F.; Bill, E.; Bothe, E.; George, S. D.; Mienert, B.; Neese, F.; Wieghardt, K., *Science* **2006,** *312*, 1937.

(6) (a) Boyd, J. P.; Schlangen, M.; Grohmann, A.; Schwarz, H., *Helv. Chim. Acta* **2008,** *91*, 1430; (b) Schlangen, M.; Neugebauer, J.; Reiher, M.; Schröder, D.; López, J. P.; Haryono, M.; Heinemann, F. W.; Grohmann, A.; Schwarz, H., *J. Am. Chem. Soc.* **2008,** *130*, 4285.

(7) (a) Jüstel, T.; Müller, M.; Weyhermüller, T.; Kressl, C.; Bill, E.; Hildebrandt, P.; Lengen, M.; Grodzicki, M.; Trautwein, A. X.; Nuber, B.; Wieghardt, K., *Chem. Eur. J.* **1999,** *5*, 793; (b) Powers, T. M.; Fout, A. R.; Zheng, S.-L.; Betley, T. A., *J. Am. Chem. Soc.* **2011,** *133*, 3336.

(8) Rodriguez, M. M.; Bill, E.; Brennessel, W. W.; Holland, P. L., *Science* **2011,** *334*, 780.

(9) (a) Betley, T. A.; Peters, J. C., *J. Am. Chem. Soc.* **2004,** *126*, 6252; (b) Hendrich, M. P.; Gunderson, W.; Behan, R. K.; Green, M. T.; Mehn, M. P.; Betley, T. A.; Lu, C. C.; Peters, J. C., *Proc. Natl. Acad. Sci. USA* **2006,** *103*, 17107; (c) Vogel, C.; Heinemann, F. W.; Sutter, J.; Anthon, C.; Meyer, K., *Angew. Chem. Int. Ed.* **2008,** *47*, 2681; (d) Vogel, C.; Heinemann, F. W.; Sutter, J.; Anthon, C.; Meyer, K., *Angew. Chem.* **2008,** *120*, 2721; (e) Scepaniak, J. J.; Margarit, C. G.; Harvey, J. N.; Smith, J. M., *Inorg. Chem.* **2011,** *50*, 9508.

(10) Song, Y.-F.; Berry, J. F.; Bill, E.; Bothe, E.; Weyhermüller, T.; Wieghardt, K., *Inorg. Chem.* **2007,** *46*, 2208.

(11) (a) Scepaniak, J. J.; Bontchev, R. P.; Johnson, D. L.; Smith, J. M., *Angew. Chem. Int. Ed.* **2011,** *50*, 6630; (b) Scepaniak, J. J.; Bontchev, R. P.; Johnson, D. L.; Smith, J. M., *Angew. Chem.* **2011,** *123*, 6760.

(12) (a) Birk, T.; Bendix, J., *Inorg. Chem.* **2003,** *42*, 7608; (b) Bendix, J., *J. Am. Chem. Soc.* **2003,** *125*, 13348.

(13) Unit cell dimensions: a = 10.720 Å, b = 10.891 Å, c = 18.020 Å. α = 77.82°, β = 73.21°, γ = 64.90°.

(14) Roesky, H. W.; Seseke, U.; Noltemeyer, M.; Sheldrick, G. M., *Z. Naturforsch., B: Chem. Sci.* **1988,** *43*, 1130.

(15) The presence of a residual paramagnetic signal (0.15 cm3 K/mol) is commonly observed for magnetic complexes with a diamagnetic ground state and reveals the presence of intrinsic defects or surface effects of the sample. In the present case, this paramagnetic contribution represents only 3.6% of an S = 5/2 spin species in the measured sample.

(16) Pokhodnya, K. I.; Bonner, M.; DiPasquale, A. G.; Rheingold, A. L.; Her, J.-H.; Stephens, P. W.; Park, J.-W.; Kennon, B. S.; Arif, A. M.; Miller, J. S., *Inorg. Chem.* **2007,** *46*, 2471.

(17) Unit cell dimensions: a = 3.75 Å, b = 8.14 Å, c = 13.40 Å. α = β = γ = 90°.

(18) Benner, L. S.; Root, C. A., *Inorg. Chem.* **1972,** *11*, 652.

(19) (a) Idage, B. B.; Idage, S. B.; Kasegaonkar, A. S.; Jadhav, R. V., *Mater. Sci. Eng., B* **2010,** *168*, 193; (b) Du Bois, J.; Hong, J.; Carreira, E. M.; Day, M. W., *J. Am. Chem. Soc.* **1996,** *118*, 915.

(20) Stoll, S.; Schweiger, A., *J. Magn. Reson.* **2006,** *178*, 42.

Chapter 6

Reactions of Trimetallic Triflate Compounds with Oxygen Atom Transfer Reagents

6.1 Abstract

Reported here are reactions of oxygen-atom donors with trimetallic $M_2Fe(dpa)_4(OTf)_nCl_{2-n}$ compounds, where M = Cr or Mo, n = 1 or 2, and dpa = 2,2'-dipyridylamine. Reaction of $Cr_2Fe(dpa)_4(OTf)_2$ with *tert*-butyl hydroperoxide results in the formation of an intermediate likely to be a trimetallic Fe^{III}-*tert*-butylperoxo moiety, which is characterized by UV-Vis and EPR studies. Reaction of $Mo_2Fe(dpa)_4(OTf)_2$ with *tert*-butyl hydroperoxide results in demetallation of the iron and formation of the two-electron oxidized $[Mo_2(dpa)_4]^{2+}$ compound. Attempts to synthesize $Cr_2Fe(depa)_4(OTf)_2$ using the more basic depa ligand (depa = di-4,4'-ethyl-2,2'-pyridylamide) to stabilize the iron center in its low-spin form are reported.

6.2 Introduction

Terminal transition metal-oxo compounds, especially of iron, are of considerable interest, both because of their biological relevance and because of their ability to facilitate O atom transfer reactions.[1] Fe^{IV} oxo compounds have proved to be especially challenging to synthesize and well-characterized compounds were first prepared the 1990s.[2] Since then, the field has grown tremendously, particularly following the synthesis and crystallization of a non-heme Fe^{IV} oxo compound by Que and coworkers.[3] The main body of work in this area has focused on the use of bulky ligands that stabilize the terminal Fe^{IV} oxo moieties and allow for systematic study of their reactivity.

Research by Que and coworkers has shown that ligands containing multiple pyridine rings stabilize the Fe^{IV} oxo moiety. There are several methods for the generation of mononuclear Fe^{IV} oxo compounds stabilized by pyridine-based ligands. Oxidation of the iron triflate compound, $[Fe(TMC)(OTf)_2]$ (where TMC = 1,4,8,11-tetramethyl-1,4,8,11-tetraazacyclotetradecane), with stoichiometric iodosylbenzene or excess hydrogen peroxide in acetonitrile results in the formation of the Fe^{IV} oxo compound $[Fe(O)(TMC)(NCCH_3)](OTf)_2$.[3b] Under the same oxidation conditions, $[Fe^{II}(N4Py)(CH_3CN)]^{2+}$ (where N4Py = N,N-bis(2-pyridylmethyl)-N-(bis-2-pyridylmethyl)amine) is converted to $[Fe^{IV}(O)(N4Py)]^{2+}$, an Fe^{IV} oxo species capable of cyclohexane oxidation at room temperature.[4] In these cases, the Fe^{IV} oxo unit is stabilized by amine or pyridine-based macrocyclic or multidentate ligands, and triflate is used as a leaving group for the reactions with oxidants such as iodosylbenzene, *m*-CPBA, or peroxides.[2]

In addition to Fe^{IV} oxo compounds, Que[5] and others[6] have also investigated the structures and reactivities of Fe^{III} alkylperoxo and hydroperoxo compounds. Reaction of $[Fe^{II}(6\text{-}Me_3TPA)(CH_3CN)_2]^{2+}$ (where Me_3TPA = *N,N,N*-tri(6-methyl-2-pyridylmethyl)amine)) with excess *tert*-butyl hydroperoxide results in the formation of the high-spin iron compound, $[Fe^{III}(6\text{-}Me_3TPA)(OH_2)(OO^tBu)]^{2+}$.[5b] Low-spin Fe^{III} hydroperoxo compounds have also been synthesized and characterized, typically via reaction of a Fe^{II} precursor with hydrogen peroxide.[7] These compounds require excess hydrogen peroxide to form, so it is thought that the reaction proceeds via a two-step process.[7b]

Research in our group has focused on the use of the pyridine-based ligand 2,2'-dipyridylamine (dpa) to stabilize trimetallic units. We have also shown that a dichromium quadruply-bonded unit can act as a ligand to iron.[8] As a result, we can draw an analogy between our compounds and those of Que and postulate that an Fe center with equatorial dpa ligands and an axial dichromium (or dimolybdenum) ligand may support an Fe^{IV} oxo unit. In this chapter, we present our first exploratory synthetic work targeting high-valent iron-oxo or peroxo species, as depicted in Figure 6.1.

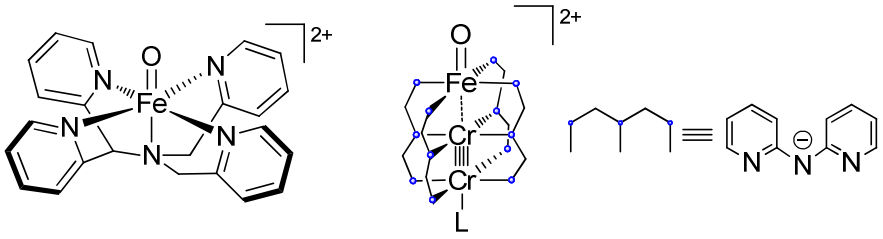

Figure 6.1. $[Fe^{IV}(O)(N4Py)]^{2+}$ (left), prepared by Que and coworkers and $[Fe^{IV}(O)Cr_2(dpa)_4L]^{2+}$ (right), the trimetallic analogue proposed in this work.

We have shown that triflate is a good leaving group in the trimetallic compounds.[9] The compounds $Cr_2Fe(dpa)_4(OTf)_2$ (**1**),[9] $Cr_2Fe(dpa)_4(OTf)Cl$ (**2**),[9] and $Mo_2Fe(dpa)_4(OTf)_2$ (**3**) have been prepared and characterized and are useful starting materials for reactions with O-atom donors. With compound **1**, it is possible that an oxygen atom transfer can occur at either the Cr or Fe side. To gain insight into the site of ligand replacement, one metal can be "blocked" by the presence of a less labile ligand such as chloride. Using compound **2**, the Fe side is blocked due to the presence of the less labile Cl ligand and we may expect oxidation to occur at the Cr side. Comparison of the reactions between both **1** and **2** with oxygen atom transfer reagents such as *m*-CPBA or *tert*-butyl hydroperoxide should indicate the site of reactivity and the likely oxidation

product(s). We also compare the analogous Mo_2 complex **3** and its oxidation chemistry (Scheme 6.1).

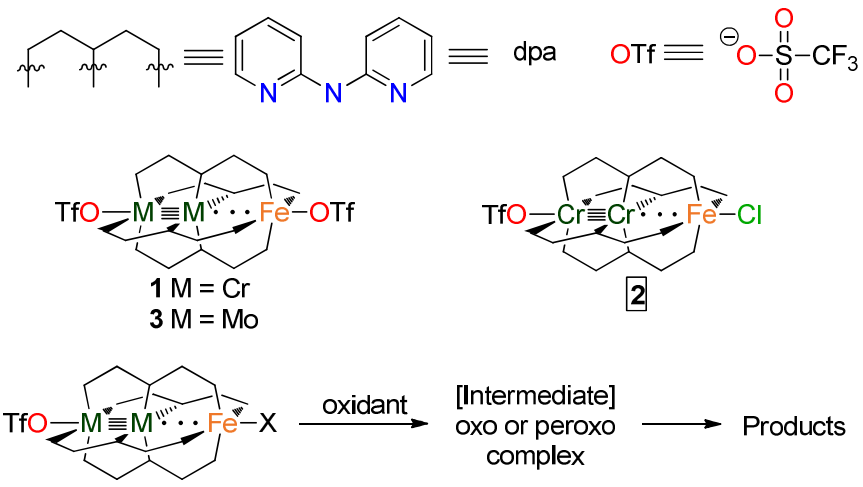

Scheme 6.1. Compounds **1**-**2** and their possible reactions with an oxidant.

We sought to further understand the reactivity of the Fe center by changing the equatorial ligand set. We hypothesized that introduction of the depa ligand (di-4,4'-ethyl-2,2'-pyridylamine, Figure 6.2) would enhance the stability of the starting material (and its oxidation products) since this ligand has been shown to decrease oxidation potentials in other trimetallic systems due to its increased basicity.[10] Efforts toward the synthesis of $Cr_2Fe(depa)_4(OTf)_2$ are described herein.

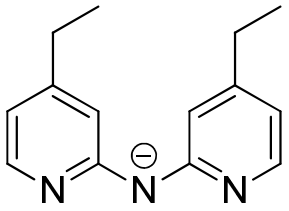

Figure 6.2. The depa ligand.

6.3 Experimental Section

6.3.1 Materials and Methods

All reactions were carried out under a dry N_2 atmosphere using Schlenk techniques and glovebox methods. Solvents acetonitrile (CH_3CN) and tetrahydrofuran (C_4H_8O) were purified using a Vacuum Atmospheres solvent purification system. Dichloromethane was freshly distilled under an N_2 atmosphere over CaH_2 prior to use. Naphthalene was sublimed and dried overnight before use. $Fe(OTf)_2$ (Wako) and *tert*-butyl hydroperoxide (Sigma-Aldrich) were purchased and used as received. Oxidants *m*-chloroperoxybenzoic acid (*m*-CPBA, Sigma-Aldrich) and (diacetoxyiodo)benzene (Sigma-Aldrich) were dried under vacuum at 40°C overnight before use. The ligand Hdpa (2,2′-dipyridylamine, Sigma-Aldrich) was recrystallized from hot hexanes prior to use. $Cr_2(dpa)_4$,[8] Hdepa,[10b] $Cr_2Fe(dpa)_4(OTf)_2$,[9] $Cr_2Fe(dpa)_4(OTf)Cl$,[9] $Cr_3(depa)_4Cl_2$[11] and $Mo_2(dpa)_4$[12] were prepared according to literature procedures. X-Band EPR spectra of frozen solutions (CH_2Cl_2 or CH_3CN) of oxidized products were recorded at 8 K temperature using a Bruker EleXsys EPR spectrometer: E-500-A console with ER 049SX SuperX Bridge and SuperX Cavity. The sample temperature was set using an Oxford Instruments ESR 900 continuous flow liquid helium cryostat regulated by an Oxford ITC4 temperature controller. UV/Vis spectroscopic measurements were performed with a StellarNet miniature fiber-optic dip-probe spectrometer and spectrum analyzer, with SpectraWiz software for processing.

$Mo_2Fe(dpa)_4(OTf)_2$ (3). To a Schlenk flask containing 4 g of dry napthalene were added $Mo_2(dpa)_4$ (490 mg, 0.56 mmol) and $Fe(OTf)_2$ (410 mg, 1.2 mmol). The mixture

was heated in a sand bath at 200°C for 25 minutes. During heating, the reaction mixture changes from brick red to dark green. After cooling to room temperature, the solid was washed with hot hexanes (3x50 mL) to remove the naphthalene. After drying under vacuum, the dark green solid was extracted in dichloromethane, filtered, and layered with hexanes. Green block crystals suitable for X-ray diffraction form after 2 days. Yield: 320 mg, 47%. Analysis calculated for $C_{42}H_{32}F_6FeMo_2N_{12}O_6S_2$: C 41.12%, H 2.63%, N 13.70%. Found: C 41.61%, H 3.35%, N 13.42%. MALDI MS: M/Z = 876 [$Mo_2(dpa)_4$]. IR (cm^{-1}): 1600 m, 1466 s, 1434 s, 1273 s, 1155 m, 1031 m, 962 w, 908 m, 767 s, 668 m, 637 s.

$Cr_2Fe(depa)_4(OTf)_2$ (4) attempt. To a flask containing Hdepa (160 mg, 0.70 mmol) were added 15 mL of tetrahydrofuran. This solution was cooled to -78°C and MeLi (0.45 mL, 0.70 mmol) was added, causing an instant color change to bright yellow. The solution was warmed to room temperature, at which point it was added to a flask containing $CrCl_2$ (39.6 mg, 0.32 mmol), causing a fast color change to orange. The orange mixture was stirred for 3 minutes at room temperature, until most of the $CrCl_2$ solid had dissolved and the solution was bright cherry red in color. The cherry red solution was cooled to -78°C and added to $Fe(OTf)_2$ (60 mg, 0.17 mmol) via cannula. The mixture was stirred at -78°C for 1 hour, followed by stirring overnight at room temperature, causing a change to dark brown-red. The solvent was then removed under reduced pressure and the brown solid was extracted into dichloromethane, filtered and layered with hexanes. After 2 days, no crystals formed, but a brown solid precipitated from solution.

6.3.2 EPR Sample Preparation

Samples for EPR spectroscopy were prepared as follows. An aliquot of a 0.25 mM solution of compound **1** in CH_2Cl_2 was transferred via cannula to an EPR tube under N_2 flow and frozen in liquid nitrogen immediately – this was labeled the "before" sample. To the stirring solution of **1** in CH_2Cl_2 at -20°C were added 3.20 mL of 0.055 M *tert*-butyl hydroperoxide (~10 equivalents). The solution was allowed to react for periods of 0 minutes, 7 minutes, 12 minutes, and 20 minutes. After each allotted time, an aliquot was transferred to an EPR tube and immediately frozen in liquid nitrogen. A 0.14 mM solution of compound **2** in CH_2Cl_2 was prepared and an aliquot was removed for the "before" sample and 2.00 mL of 0.055 M *tert*-butyl hydroperoxide (~10 equivalents) were then added at -20°C. Samples for EPR were prepared analogously to compound **1** except the time intervals were changed to 0 minutes, 3 minutes, and 20 minutes.

6.4 Results and Discussion

6.4.1 Synthesis

Compounds **1** and **2** were synthesized as reported earlier.[13] Compound **3** is new, and is easily prepared by addition of $Fe(OTf)_2$ to $Mo_2(dpa)_4$ at high temperatures. It is anticipated that oxidation of compounds **1**-**3** will proceed by the pathway outlined in Scheme 6.1, in which the starting material reacts with an oxygen atom transfer reagent to yield a product via an intermediate.

The course of the reaction can be monitored by absorption spectroscopy and, depending on the choice of starting material and oxidant, the intermediate can either be clearly visible or unobserved in the experiment. The intermediates and products of the oxidation reactions are characterized as presented below.

We hypothesized that the dpa ligand, which keeps the Fe center in its labile high spin form, could be changed to examine the effect of equatorial ligation on the formation of oxidation products. The depa ligand is more basic and should allow Fe to be present in its low spin state. To this end, we sought to synthesize $Cr_2Fe(depa)_4(OTf)_2$ (**4**) and to perform analogous oxidation studies on this compound.

There are two possible routes for the synthesis of **4**, as outlined in Scheme 6.2. Pathway A follows the same synthetic route as for the analogous dpa compound $Cr_2Fe(dpa)_4(OTf)_2$,[9] beginning with $Cr_3(depa)_4Cl_2$, prepared according to literature methods.[11] We anticipated that the trimetallic compound could be demetallated by excess sodium cyanide to yield $Cr_2(depa)_4$, in analogy to the preparation of $Cr_2(dpa)_4$.[8] The bimetallic depa compound would then react with iron ditriflate to yield the trimetallic

$Cr_2Fe(depa)_4(OTf)_2$. This synthetic method does not work as outlined, however, because the proposed NaCN demetallation reaction results only in the complete decomposition of $Cr_3(depa)$ rather than demetallation. As a result, we attempted Pathway B, which proceeds via generation of $Cr_2(depa)_4$, trapping of this species at -78°C, and immediate addition of this solution to $Fe(OTf)_2$. This pathway removes the possibility of generating any $Cr_3(depa)_4Cl_2$ (which forms along with $Cr_2(depa)_4$ at elevated temperatures) and also bypasses the unsuccessful demetallation step needed in Pathway A.

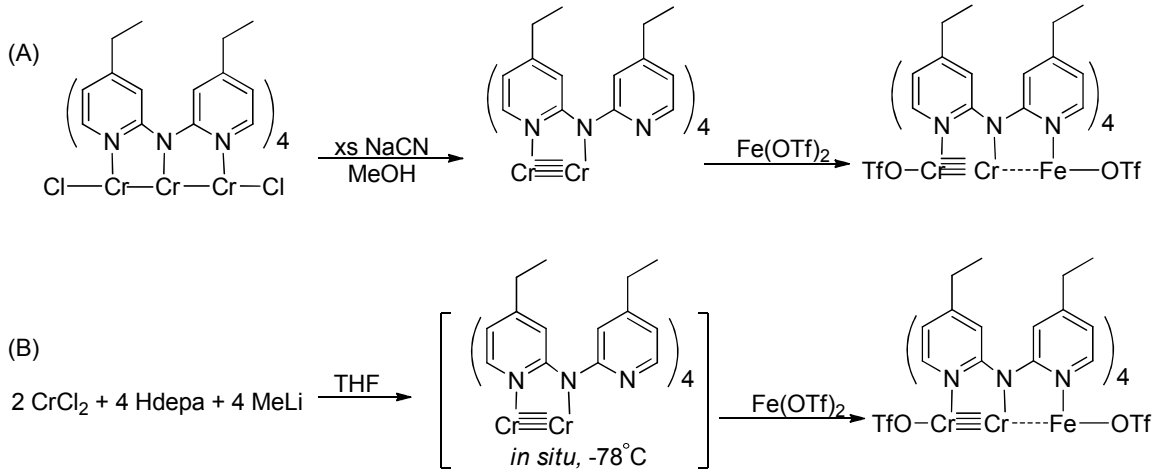

Scheme 6.2. Possible synthetic pathways for the formation of **4**.

Pathway B seemed like a promising synthetic route for the formation of **4** for our oxidation studies. Reaction of the orange-red $Cr_2(depa)_4$ solution with $Fe(OTf)_2$ in tetrahydrofuran overnight at room temperature leads to a color change to dark brown, similar in color to **1**. Recrystallization of the dark brown solid formed in this reaction from dichloromethane and hexanes afforded bright yellow blocks suitable for X-ray crystallography. Unfortunately, the X-ray data indicate the formation of $Fe(Hdepa)Cl_2$, although this product requires the presence of air or moisture, so more efforts toward the

synthesis of this compound are needed. Further investigation by reaction of **4** with oxidants will be of great interest to determine whether this ligand is able to better stabilize iron-oxo intermediates.

6.4.2 UV-Vis Spectroscopy

The absorption spectra of **1** and **2** are shown in Figure 6.3. Compound **1** in dichloromethane displays strong peaks at 490 nm and 690 nm, along with shoulder peaks at 445 nm and 550 nm. Compound **2** has an almost identical absorption spectrum, with features at 490 nm and 695 nm, but the peak at 695 nm is greater in intensity and the shoulder peak at 550 nm is absent.

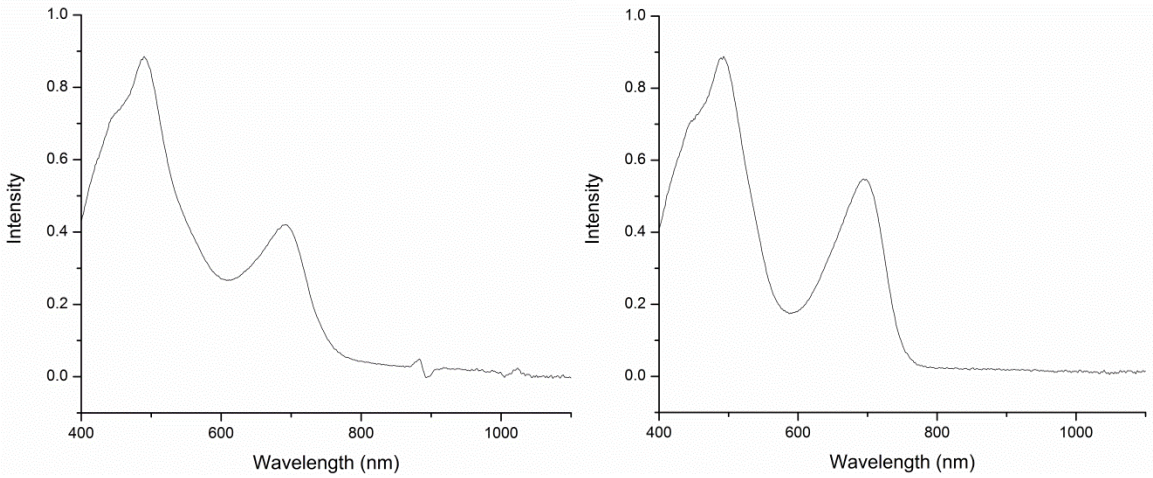

Figure 6.3. Absorption spectra of **1**(left) and **2** (right).

In this section, the oxidation chemistry will be discussed in three parts: 1) the reactions using *m*-CPBA or $PhI(OAc)_2$ as oxidants, 2) the reactions using HOO^tBu as oxidant, and 3) the oxidation of **3**.

1) Reactions of **1** with either *m*-CPBA or $PhI(OAc)_2$ have been examined. The former oxidant is an O-atom transfer reagent, while $PhI(OAc)_2$ is not. These two oxidants

were chosen so that we could distinguish differences in their reactivity. If both reagents react with **1** at similar rates to give similar products, then the possibility of O-atom transfer to form an iron-oxo intermediate would be rendered unlikely. However, this is not what happens. Reaction of **1** with *m*-CPBA is very fast, reaching completion in 5 minutes at 0°C, as shown in Figure 6.4 (note: below 500 nm, the oxidation spectra are not shown because the signals are saturated under the oxidation conditions).

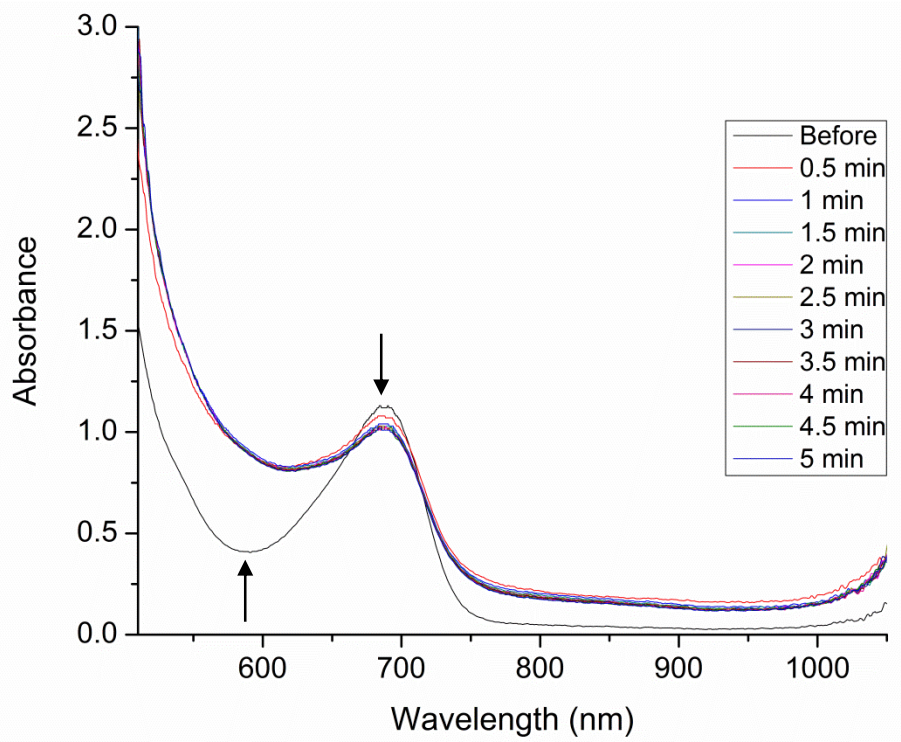

Figure 6.4. Oxidation of **1** by *m*-CPBA.

In contrast, reaction of **1** with $PhI(OAc)_2$ is much slower and is complete only after ~200 minutes (Figure 6.5). Moreover, a comparison of the UV-Vis features of the two products (Figure 6.6) shows marked differences.

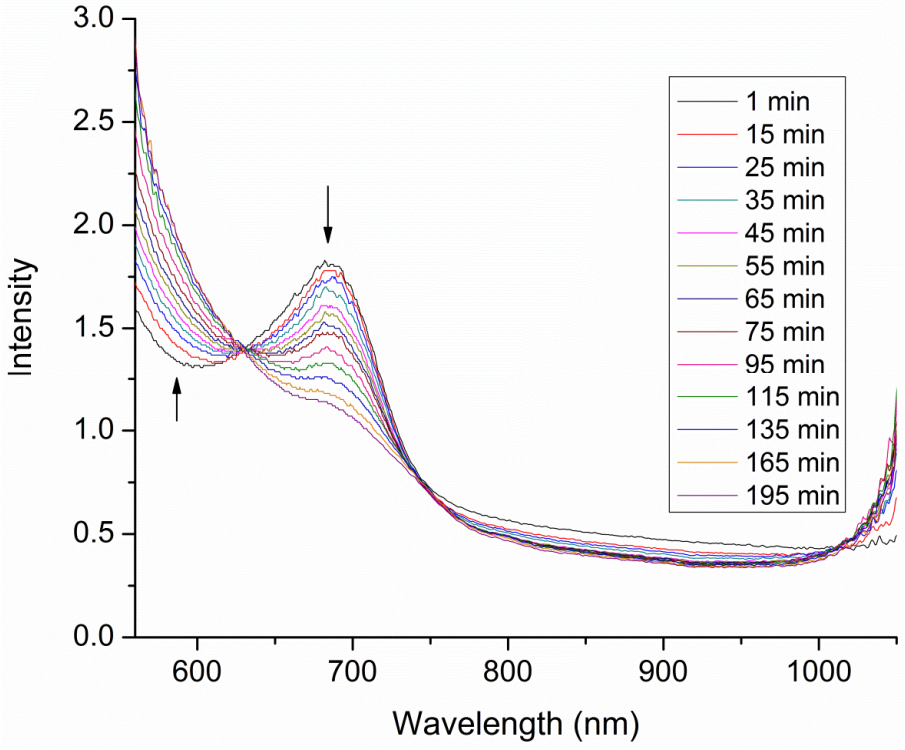

Figure 6.5. Oxidation of $Cr_2Fe(dpa)_4(OTf)_2$ by 1 equivalent of (diacetoxyiodo)benzene in DCM at 0°C.

Oxidation of **1** occurs with significant loss of the 690 nm MMCT band suggesting loss of the heterotrimetallic structure, perhaps by demetallation of the Fe. However, with *m*-CPBA, the 690 MMCT band is clearly retained. Though the *m*-CPBA product is indefinitely stable, it was not further characterized. Attempts to crystallize this product were unsuccessful.

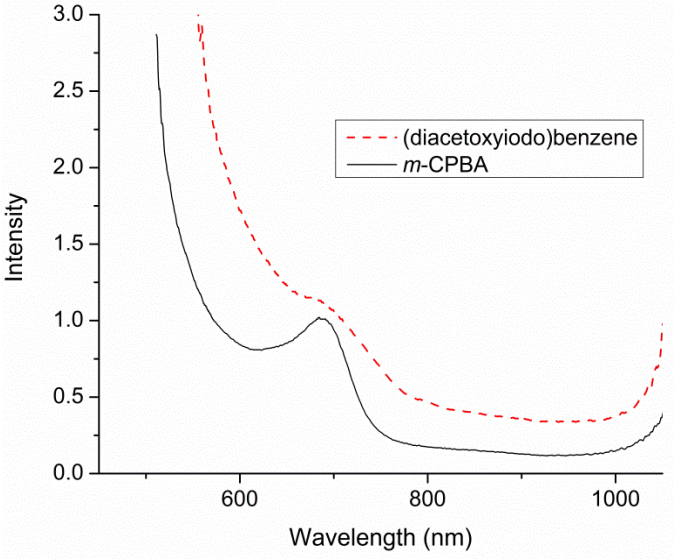

Figure 6.6. Comparison of products of reaction of **1** with m-CPBA and $PhI(OAc)_2$.

2) The reactions described in this section were all performed using *tert*-butyl hydroperoxide as the oxidant. Compound **1** in dichloromethane reacts with one equivalent of 0.055 M *tert*-butyl hydroperoxide in acetonitrile at 0°C. Monitoring the reaction by UV-Vis spectroscopy over the course of 8.5 hours results in a color change in the solution from yellow-brown to orange-brown, as shown in Figure 6.7.

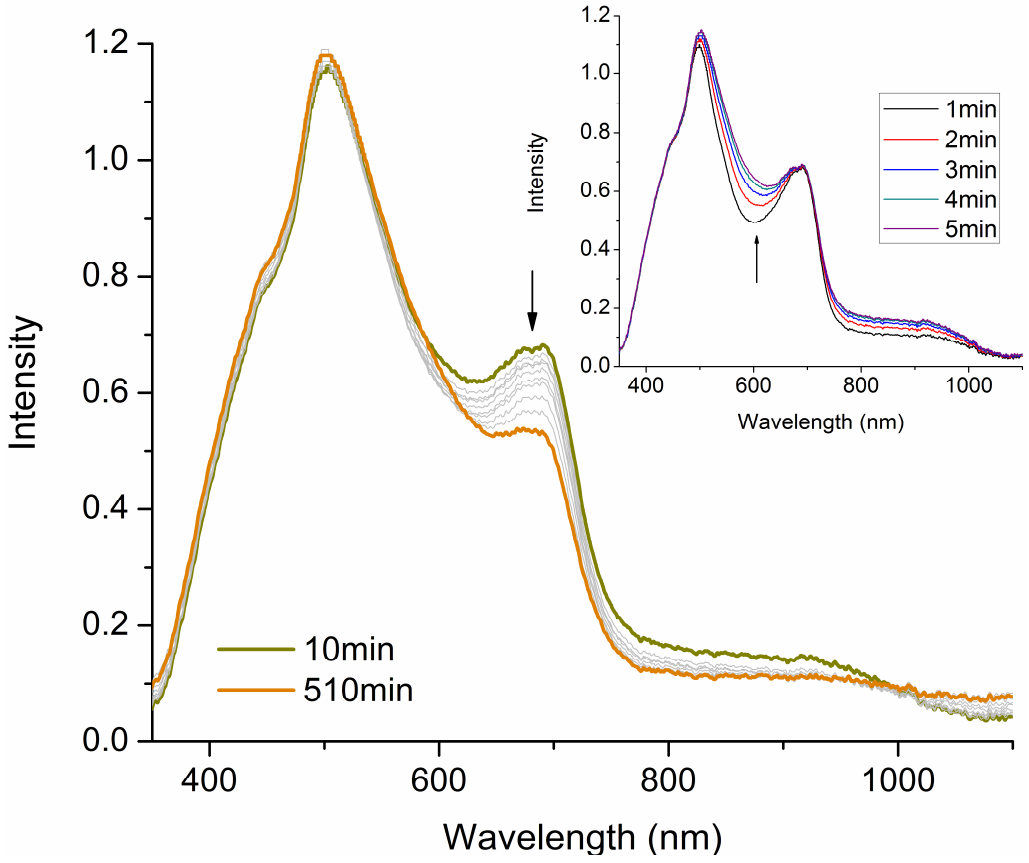

Figure 6.7. Oxidation of $Cr_2Fe(dpa)_4(OTf)_2$ by 1 equivalent of *tert*-butyl hydroperoxide in DCM at 0°C in two steps. Step one (inset) occurring over minutes 1-5 and step two occurring over minutes 10-510.

The first step, forming the intermediate, is a very fast reaction that is complete in less than 5 minutes, evidenced by the growth of the feature at 598 nm. The second part of the reaction occurs over about 8 hours, as seen by the disappearance of the intensity at 690 nm, forming product. Repeating this reaction with two equivalents of oxidant (Figure 6.8) results in the same first step, but the second step is a cleaner reaction (indicated by the presence of an isosbestic point at 624 nm) with the peak at 690 nm disappearing over the course of 7 hours. Because the main spectral features occur at the same wavelengths, it is likely that the same products are formed in both reactions.

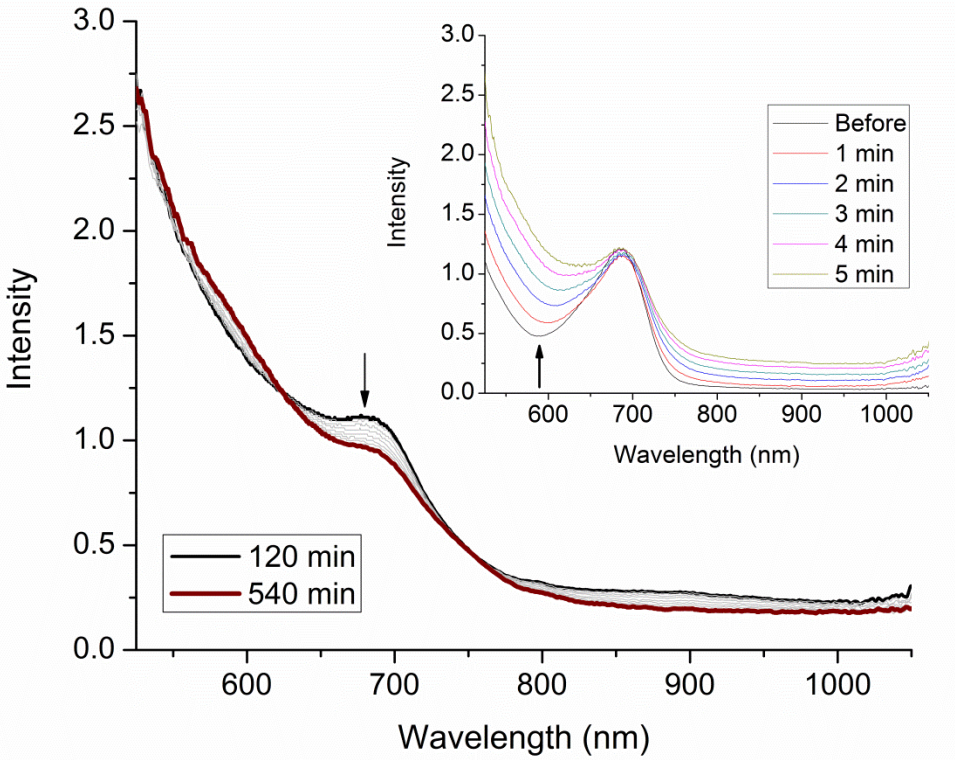

Figure 6.8. Oxidation of $Cr_2Fe(dpa)_4(OTf)_2$ by 2 equivalents of *tert*-butyl hydroperoxide in DCM at 0°C in two steps. Step one (inset) occurring over minutes 1-5 and step two occurring over minutes 120-540.

The reaction of the "blocked" trimetallic monotriflate compound $Cr_2Fe(dpa)_4(OTf)Cl$ (**2**) with *tert*-butyl hydroperoxide provides another example of starting material forming product without an observable intermediate (Figure 6.9).

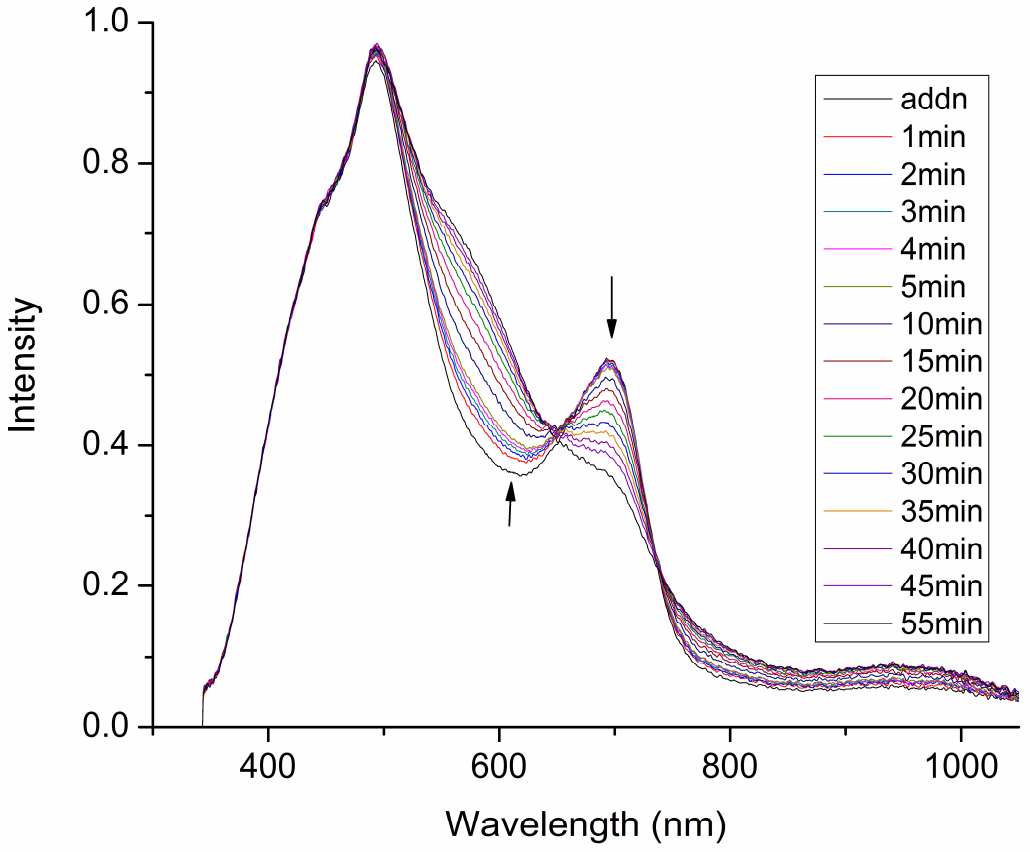

Figure 6.9. Oxidation of $Cr_2Fe(dpa)_4(OTf)Cl$ (**2**) by *tert*-butyl hydroperoxide in DCM at 0°C.

The reaction profile for the mono-triflate compound **2** with one equivalent of *tert*-butyl hydroperoxide displays two isosbestic points occurring at 650 nm and 740 nm and a peak at 696 nm that decreases in intensity during the conversion to product. Notably, the feature at 696 nm loses intensity but does not disappear, although it is not clear why this occurs.

To determine the nature of the products formed in the oxidations described above, numerous attempts were made to crystallize products out of the reaction solution, but this proved to be unfruitful. Though the oxidation products could not be isolated, we wanted

to gain some insight into their structure. Because of the orange tint of the solutions following oxidation we suspected that one possible product was $[Cr_2(dpa)_4]^{2+}$, which would form upon loss of iron from the trimetallic compound perhaps as Fe_2O_3 (heretofore known as demetallation). Comparison of the UV-Vis spectrum of $[Cr_2(dpa)_4]^{2+}$ (Figure 6.10) to the oxidation products indicates that this hypothesis is unlikely due to the absence of common absorption features.

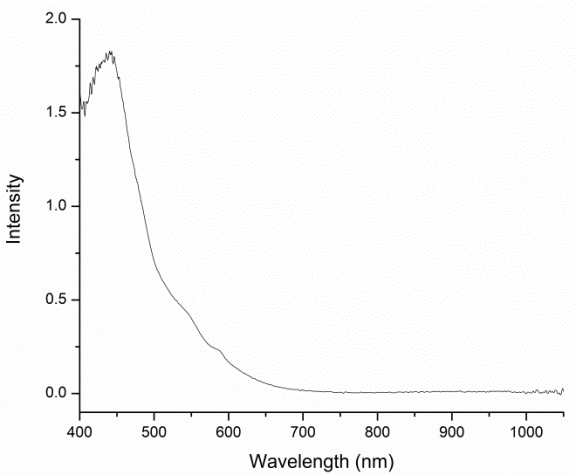

Figure 6.10. Absorption spectrum of $[Cr_2(dpa)_4]^{2+}$.

Upon examination of the spectra of the intermediates formed in these reactions, we noted similarities to the spectral features of $[Fe^{III}(L^8\text{-}py_2)(OO^tBu)(OTf)]$ (where $L^8\text{-}py_2$ = N,N'-bis(2-pyridylmethyl)-1,5-diazacyclooctane), which has a prominent feature at around 580 nm that is assigned as an LMCT band involving the $^tBuOO^-$ moiety .[14] The reactions presented here exhibit this feature growing in during the 5 minute conversion to the intermediate, but also have a peak around 690 nm, which we attribute to the Fe-Cr interaction since it appears to weaken in intensity as the reaction progresses and likely

forms new metal-axial ligand bonds. This nature of this intermediate is explored in more detail in section 6.4.2 using EPR spectroscopy.

3) The oxidation chemistry of $Mo_2Fe(dpa)_4(OTf)_2$ (**3**) was performed to investigate the effect of using dimolybdenum as an axial ligand in place of dichromium. Compound **3** reacts with two equivalents of *tert*-butyl hydroperoxide in dichloromethane at 0°C. Within one minute, all of the starting material was converted to an intermediate, as seen by the disappearance of the peak at 595 nm and the appearance of the broad feature centered at 820 nm (Figure 6.11).

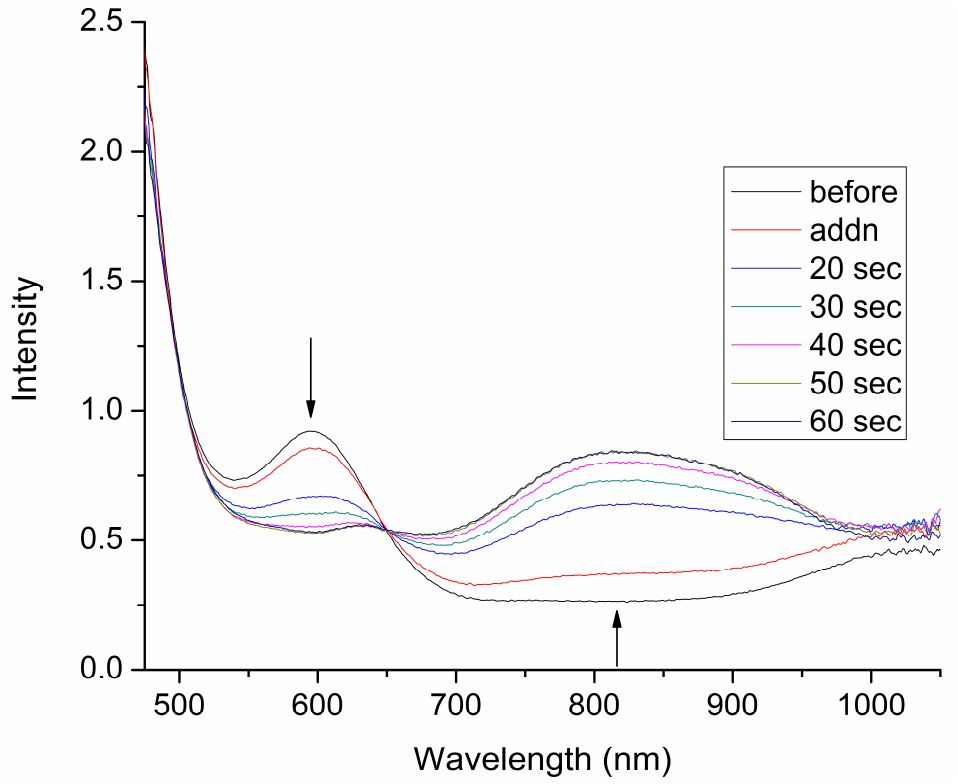

Figure 6.11. Reaction of **3** with tert-butyl hydroperoxide to form an intermediate.

The absorption spectrum of the intermediate is nearly identical to that of the one-electron oxidized dimolybdenum compound, $[Mo_2(dpa)_4]^+$,[15] indicating that the

intermediate either contains a $[Mo_2]^{5+}[Fe]^{2+}$ core or is demetallated. Further reaction of the intermediate with oxidant results in the formation of product as shown in Figure 6.12.

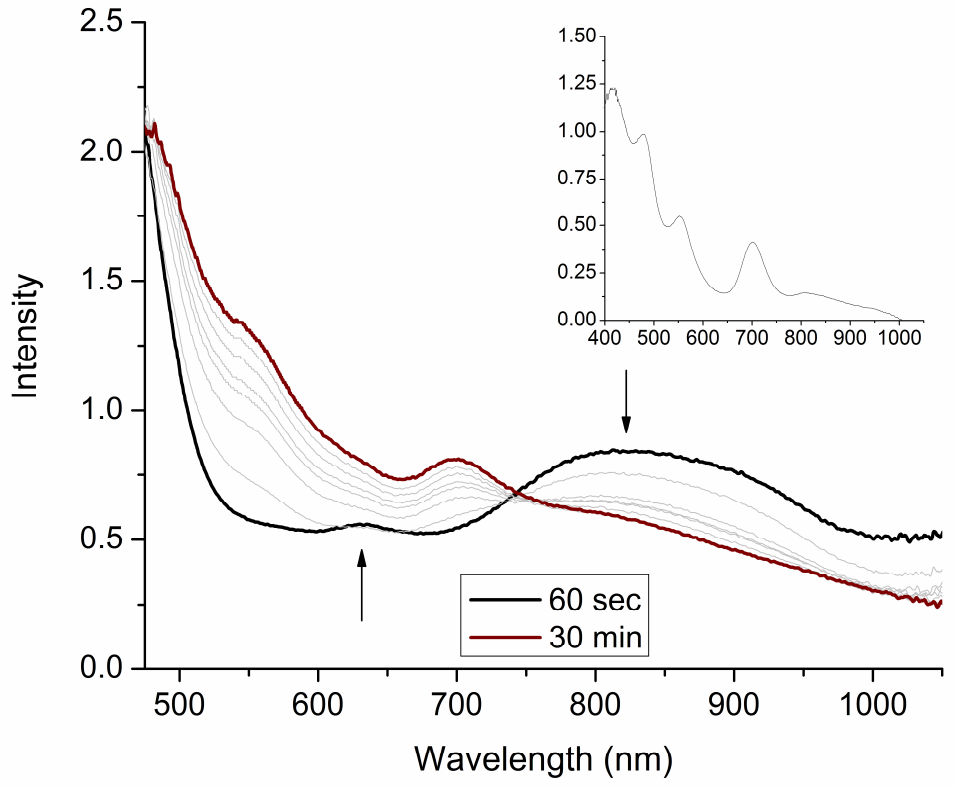

Figure 6.12. Intermediate forming product in the reaction of **3** with *tert*-butyl hydroperoxide. The absorption spectrum of $[Mo_2(dpa)_4]^{2+}$ is shown for comparison with the product (inset).

The oxidation product shows spectral features that are nearly identical to those of the $[Mo_2(dpa)_4]^{2+}$ dication. Thus, the oxidation appears to result in demetallation of the Fe, according to Scheme 6.3.

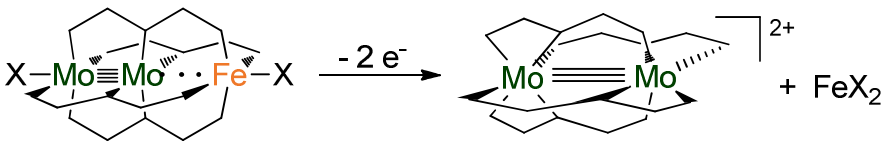

Scheme 6.3. Oxidation of **3** to yield the demetallation product $[Mo_2(dpa)_4]^{2+}$.

We hypothesize that the reason demetallation occurs when M = Mo, but not when M = Cr, is because of the increased Fe-N_{dpa} distances (by about 0.07 Å) in the former. The Mo-N_{dpa} distances (2.149[2] Å) are longer than Cr-N_{dpa} (2.069[3] Å) distances since Mo is larger and has more diffuse orbitals. As a result, the Fe-N distances are also elongated and in the presence of oxidant, Fe can more easily be pulled out of the trimetallic chain with a Mo_2 unit present.

6.4.3 EPR Spectroscopy

The 5 K X-band EPR spectrum of a frozen solution of **1** in CH_2Cl_2 (Figure 6.13) displays one sharp signal that grows in at g_{obs} = 1.99 and shifts to g_{obs} = 1.97 over the course of the 20 minute reaction with *tert*-butyl hydroperoxide. Given the established EPR silent S = 2 spin state of **1** and the sharpness of the g = 1.99 signal, the signal may be attributed to a minor Cr^{3+} impurity in the sample. There is another less intense signal at g_{obs} = 4.49 at the start of the reaction that shifts to g_{obs} = 4.18 after 20 minutes, which likely corresponds to Fe_2O_3, commonly seen as an artifact in EPR spectra. At 7 minutes, an intermediate is observed with large features at g_{obs} = 7.28, 6.52 and 5.24, which is consistent with an S = 5/2 system, similar to the Fe^{III} alkyperoxo features determined by Que and coworkers (g_{obs} = 8.8, 5.2, 3.2).[14]

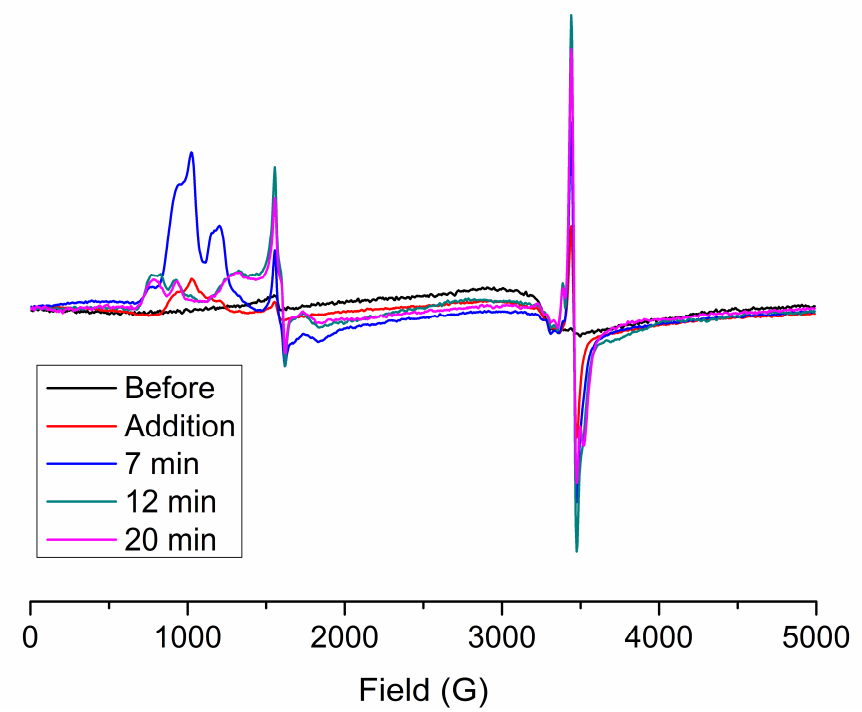

Figure 6.13. EPR spectrum of the reaction of **1** and *tert*-butyl hydroperoxide in CH_2Cl_2 at 5 K, at different intervals of the reaction.

Preliminary attempts to fit the EPR spectrum of the 7 minute intermediate using the Easyspin toolbox[16] for Matlab with the following parameters: g = 2.0, 2.0, 2.0; D = 0.83 cm^{-1}; E/D = 0.05; and S = 5/2, results in an axial signal in the expected region (Figure 6.14). As postulated from the UV-Vis experiments, this EPR simulation is consistent with a high-spin Fe^{III} system with axial symmetry, as would be expected for a Cr≡Cr···Fe^{III} *tert*-butylperoxo species forming as an intermediate. There appears to be another high-spin Fe^{III} species present in the EPR spectrum, perhaps a Cr≡Cr···Fe^{III}-OH species, but it was not simulated. The signal at g_{obs} = 4.49 can also be simulated as a rhombic S = 5/2 system with E/D = 0.33 and g = 2.0 and 2.0, consistent with a small amount of Fe_2O_3 present in the EPR sample or cavity. The signal at g_{obs} = 1.99 can be

modeled as a Cr^{3+} signal, with $S = 3/2$, $g = 1.94$, and D < hν and likely represents a small amount of Cr^{III} present in the sample.[17] It is important to note that the intensities shown in the simulation in Figure 6.13 are not comparable to the experimental data since this would require double integration of the spectrum, as well as Aasa Vangaard corrections.[18]

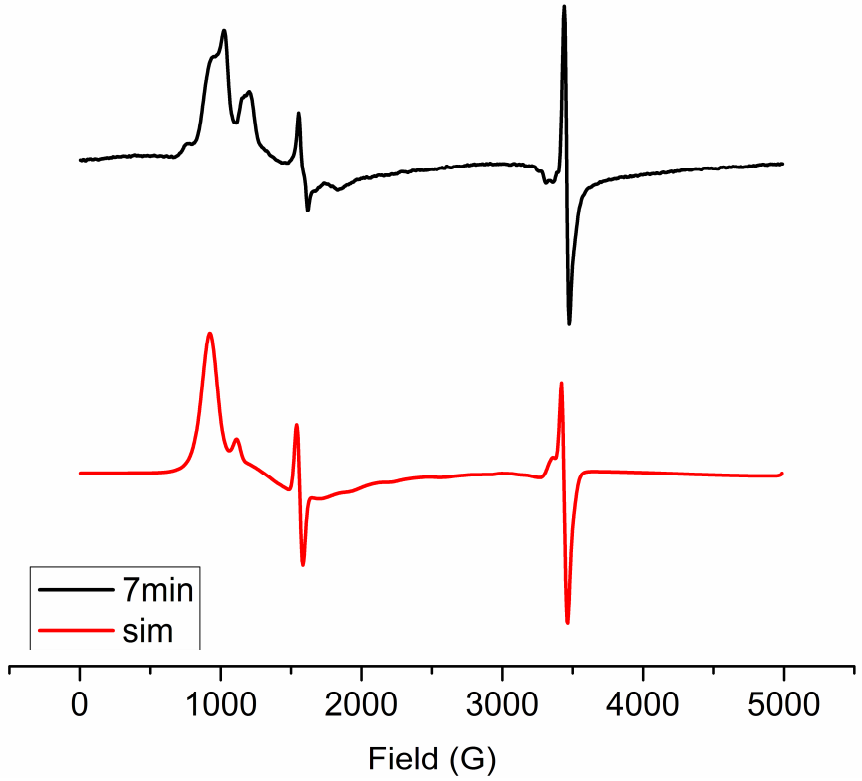

Figure 6.14. EPR spectrum of the 7 minute intermediate (top) and an additive simulation of the individual species present in solution (bottom).

The peak at $g_{obs} = 1.99$ is typical of Cr^{III} species and indicates some oxidation of a Cr atom in the compound, although this peak is quite sharp and therefore only constitutes a small portion of the sample. However, we should also consider the possibility of some oxidation chemistry occurring on the Cr side of the compound, forming a Cr^{III}- *tert*-butylperoxo species having an $S = ½$ spin state, as shown in Figure 6.15. Previous work

on other Cr_2^{5+} units shows that they have EPR signals with g_{obs} = 1.97, consistent with what is seen here. However, it the presence of an S = 2 Fe^{2+} center, the Cr_2^{5+} unit should be antiferromagnetically coupled to yield and S = 3/2 ground state with D > hν, which is contrary to what is observed. Notably, an S = 5/2 signal as observed can only arise from Fe-centered oxidation.

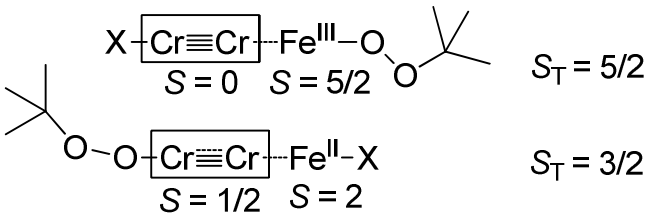

Figure 6.15. Possible oxidation products and their spin states.

Despite the possibility of the Cr^{III} *tert*-butylperoxo formation, the EPR spectrum of the intermediate species is more consistent with Fe oxidation and the formation of an Fe^{III} *tert*-butylhydroperoxo moiety. In this case, the sharp feature at g_{obs} = 1.99 is more likely "free" Cr^{3+} or "free" Cr_2^{5+}, which could result from partial demetallation of the starting material.

The 8 K X-band EPR spectrum of a frozen solution of **2** in CH_2Cl_2 shows a similar set of peaks over the course of the reaction with *tert*-butyl hydroperoxide (Figure 6.16). There is one sharp signal that starts at g_{obs} = 1.94 and shifts to g_{obs} = 1.97 over the course of the 20 minute reaction with *tert*-butyl hydroperoxide. There is a large feature at g_{obs} = 6.24 and 5.18, as described above for an Fe^{III} peroxo-*tert*-butyl moiety, as well as a feature at g_{obs} = 1.98, consistent with the Cr signal. Overall, the similarity of the main signals in the EPR spectra of **1** and **2** indicates that the oxidation products of both

reactions are similar and that the chloride ligand is likely more labile than we had expected under the oxidation conditions.

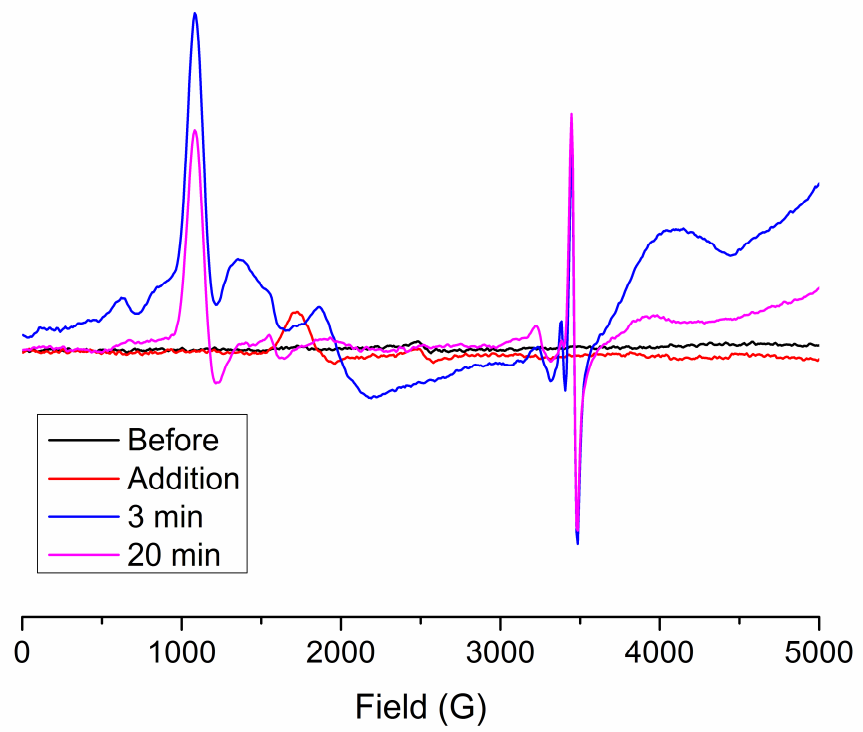

Figure 6.16. EPR spectrum of **2** and *tert*-butyl hydroperoxide in CH_2Cl_2 at 5 K, at different intervals of the reaction.

6.5 Conclusions

In summary, trimetallic $Cr_2Fe(dpa)_4(OTf)_2$ and $Cr_2Fe(dpa)_4(OTf)Cl$ react with oxidant *tert*-butyl hydroperoxide to form metal-*tert*-butyl peroxo intermediates. The analogous $Mo_2Fe(dpa)_4(OTf)_2$ compound loses iron in the presence of oxidant, although the dimolybdenum unit becomes oxidized in this reaction. This study also outlines attempts to prepare a trimetallic starting material with enhanced stability toward oxidation, and highlights important synthetic challenges associated with these trimetallic compounds.

References

(1) Krebs, C.; Galonić Fujimori, D.; Walsh, C. T.; Bollinger, J. M., *Acc. Chem. Res.* **2007,** *40*, 484.

(2) Que, L., *Acc. Chem. Res.* **2007,** *40*, 493.

(3) (a) Lim, M. H.; Rohde, J.-U.; Stubna, A.; Bukowski, M. R.; Costas, M.; Ho, R. Y. N.; Münck, E.; Nam, W.; Que, L., *Proc. Natl. Acad. Sci. USA* **2003,** *100*, 3665; (b) Rohde, J.-U.; In, J.-H.; Lim, M. H.; Brennessel, W. W.; Bukowski, M. R.; Stubna, A.; Münck, E.; Nam, W.; Que, L., *Science* **2003,** *299*, 1037.

(4) Kaizer, J.; Klinker, E. J.; Oh, N. Y.; Rohde, J.-U.; Song, W. J.; Stubna, A.; Kim, J.; Münck, E.; Nam, W.; Que, L., *J. Am. Chem. Soc.* **2004,** *126*, 472.

(5) (a) Lehnert, N.; Ho, R. Y. N.; Que, L.; Solomon, E. I., *J. Am. Chem. Soc.* **2001,** *123*, 12802; (b) Zang, Y.; Kim, J.; Dong, Y.; Wilkinson, E. C.; Appelman, E. H.; Que, L., *J. Am. Chem. Soc.* **1997,** *119*, 4197.

(6) Namuswe, F.; Kasper, G. D.; Sarjeant, A. A. N.; Hayashi, T.; Krest, C. M.; Green, M. T.; Moënne-Loccoz, P.; Goldberg, D. P., *J. Am. Chem. Soc.* **2008,** *130*, 14189.

(7) (a) Lubben, M.; Meetsma, A.; Wilkinson, E. C.; Feringa, B.; Que, L., *Angew. Chem. Int. Ed.* **1995,** *34*, 1512; (b) Roelfes, G.; Lubben, M.; Chen, K.; Ho, R. Y. N.; Meetsma, A.; Genseberger, S.; Hermant, R. M.; Hage, R.; Mandal, S. K.; Young, V. G.; Zang, Y.; Kooijman, H.; Spek, A. L.; Que, L.; Feringa, B. L., *Inorg. Chem.* **1999,** *38*, 1929; (c) Martinho, M.; Banse, F.; Sainton, J.; Philouze, C.; Guillot, R.; Blain, G.; Dorlet, P.; Lecomte, S.; Girerd, J.-J., *Inorg. Chem.* **2007,** *46*, 1709.

(8) Nippe, M.; Berry, J. F., *J. Am. Chem. Soc.* **2007,** *129*, 12684.

(9) Nippe, M.; Turov, Y.; Berry, J. F., *Inorg. Chem.* **2011,** *50*, 10592.

(10) (a) Berry, J. F.; Cotton, F. A.; Lei, P.; Lu, T.; Murillo, C. A., *Inorg. Chem.* **2003,** *42*, 3534; (b) Berry, J. F.; Cotton, F. A.; Lu, T.; Murillo, C. A.; Wang, X., *Inorg. Chem.* **2003,** *42*, 3595; (c) Berry, J. F.; Cotton, F. A.; Lu, T.; Murillo, C. A., *Inorg. Chem.* **2003,** *42*, 4425.

(11) Berry, J. F.; Cotton, F. A.; Lu, T.; Murillo, C. A.; Roberts, B. K.; Wang, X., *J. Am. Chem. Soc.* **2004,** *126*, 7082.

(12) Nippe, M.; Victor, E.; Berry, J. F., *Eur. J. Inorg. Chem.* **2008,** *2008*, 5569.

(13) Nippe, M.; Goodman, S. M.; Fry, C. G.; Berry, J. F., *J. Am. Chem. Soc.* **2011,** *133*, 2856.

(14) Bukowski, M. R.; Halfen, H. L.; van den Berg, T. A.; Halfen, J. A.; Que, L., *Angew. Chem. Int. Ed.* **2005,** *44*, 584.

(15) Nippe, M.; Victor, E.; Berry, J. F., *Inorg. Chem.* **2009,** *48*, 11889.

(16) Stoll, S.; Schweiger, A., *J. Magn. Reson.* **2006,** *178*, 42.

(17) The intensities of the peaks in the simulation are not comparable to the experimental data. The data were multiplied by a random correction factor to be on the same scale as the experimental data, then added together to make one simulation.

(18) Aasa, R.; Vanngard, T., *Z. Naturforsch.* **1964,** *19a*, 1425.

Appendix 1

Synthesis of a New Class of Ligands and Efforts toward the Preparation of M-M Bonded Complexes in Trigonal Symmetry

A1.1 Introduction

Complexes involving metal-metal interactions are of great general interest because of the broad range of electronic, bonding, reactivity, and even magnetic properties they exhibit. Though the chemistry of metal-metal bonded compounds has been well explored in the past several decades,[1] the understanding of metal-metal and metal-ligand interactions, especially for first row transition metals, remains an active area of study. This study aimed to study the chemical reactivity of metal-metal bonded complexes of first row transition metals in a relatively rare geometry to delve deeper into the variety of properties attainable by tuning the environment around a metal-metal bond.

While great efforts have been made in the discovery and understanding of metal-metal bonded systems, most studies have focused on complexes in tetragonal symmetry with bridging ligands.[2,3,4] For example, one of the most well-known of these tetragonal systems is $Rh_2(OAc)_4$, which is most commonly used as a catalyst for a variety of processes, including C-H functionalization,[5,6] enantioselective transformations[7] and many others.[8] Our goal is to enforce trigonal symmetry to exploit differently available bonding orbitals to probe the metal-metal interactions and allow for multiple bonds to ligands. Tetragonal systems are useful because they maintain a rigid structure (for example, $Cr_2(OAc)_4$ and other metal acetates), but still have open axial coordination sites for binding substrates. When we switch to the trigonal system, however, there are both axial

and equatorial sites for binding, which provides more access for substrates to bind to our metal-metal bonded complex.

For a mononuclear square planar complex (Figure A1.1, top left), the $d_{x^2-y^2}$ orbital lies very high in energy due to strong anti-bonding interactions with the ligands; as a result, when we invoke a metal-metal manifold, the $d_{x^2-y^2}$ orbitals do not participate in metal-metal bonding and are not shown in the binuclear molecular orbital diagram. In this scenario, the maximum metal-metal bond order is four. When moving to a trigonal system, the $d_{x^2-y^2}$ orbital is degenerate with the d_{xy} orbital, and is more available for bonding. In a bimetallic trigonal system, there are five bonding orbitals, with 2 sets of δ orbitals. Consequently, this presents the opportunity for the formation of quintuple bonds, as was shown by Tsai and coworkers,[9] as well as Manke and coworkers.[10]

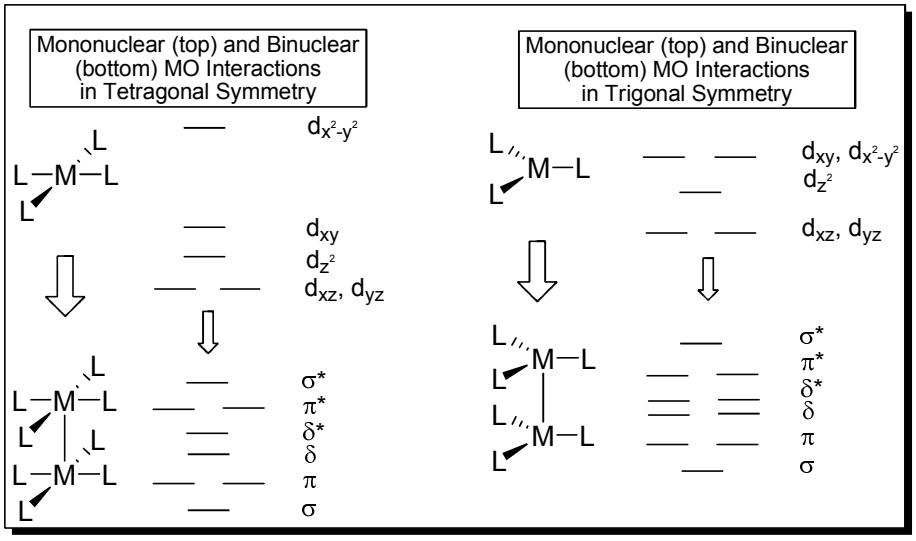

Figure A1.1. Comparison of MO interactions in both tetragonal and trigonal symmetry.

Some of the inspiration for using a trigonal system comes from the use of modified tripodal triamidoamine ligands for the preparation of, and reactivity studies on,

new coordination complexes that keep a fairly rigid 3-fold geometry, as demonstrated by Schrock and coworkers.[11] The 3-fold geometry maintained by these ligands provides three empty orbitals in early transition metals, the d_{xz} and d_{yz} for π bonding and the d_z^2 for σ bonding, which can bind axial ligands.[12] These ligands are used for myriad purposes, although most notably for mimicking biological systems that are thought to have metal-nitride or metal-oxo intermediates. This is because the empty orbitals can stabilize metal-ligand multiple bonds, even with the metal in a high oxidation state. Specifically, in the Schrock group, these tren-type ligands have been used with molybdenum centers to isolate possible intermediates in the catalytic turnover of dinitrogen to ammonia.[13,14] Similarly, a recent work by Que and coworkers[15] presents another example of using a tren-based ligand (tris-(tetramethylguanidine) tren) to form biologically relevant intermediates. The steric bulk of this ligand and its geometry allow for the formation of the Fe=O bond in a trigonal bipyramidal arrangement, which causes the d_{xy} and the $d_{x^2-y^2}$ orbitals to become degenerate. As a result, addition of oxygen to the iron(II) metal center furnishes the formation of a rare example of a high-spin ($S = 2$) iron(IV)-oxo complex.

Expanding upon the mononuclear systems, there are a few examples in the literature that feature a bimetallic core with three-fold symmetry. Much of Chisholm's work has centered on ethane-type M_2X_6 complexes in a staggered configuration, where the ligands typically have steric bulk and are monoanionic (Figure A1.2).[16] These types of complexes are well-studied and provide much of the groundwork for studies of metal-metal bonded systems with 3-fold axes of symmetry. When the complexes have an

eclipsed geometry, the trigonal geometry opens up orbitals for short metal-metal bonds, as well as interesting reactivity of the compounds.

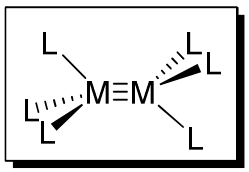

Figure A1.2. General structure of $L_3M{\equiv}ML_3$ ethane-like complexes.

A family of complexes with 3-fold symmetry and a metal-metal bond was prepared in the Cotton laboratory and involves three substituted formamidinato ligands (Figure A1.3).[17,18,19,20] These bridging ligands, as well as the identity and oxidation state of the metal, stabilize the unusual geometry of the compound.

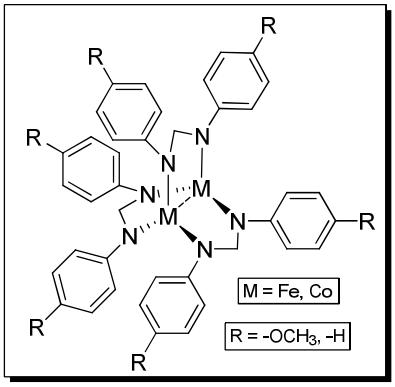

Figure A1.3. Trigonal dicobalt compounds, confirmed by X-ray crystallography.

Although these complexes were characterized by X-ray crystallography, their chemistry was not explored further, although it is clear that they are paramagnetic. The cobalt centers in the dicobalt molecule are coordinatively unsaturated and would provide several binding sites for substrates. The Cotton group showed, through these complexes, that the

trigonal geometry could be attained by simple reduction and deprotonation of the ligand, [17,18,19,20] which is promising for the preparation of similar complexes.

Although there are only several examples of trigonal metal-metal bonded complexes in the literature,[9-10] it is evident that there is some success in this area, yet also a need for systematic exploration. Our goal is to prepare a class of tripodal ligands with an extra tier to support a bimetallic system in a trigonal array (Figure A1.4).

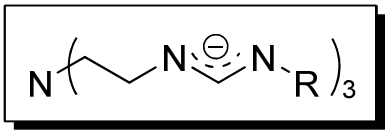

Figure A1.4. The general family of ligands used in the project with two metal binding sites.

While Schrock's system supports metal-ligand multiple bonds at an axial site, we hope that the extra tier will provide two additional access points for incoming substrates (Figure A1.5).

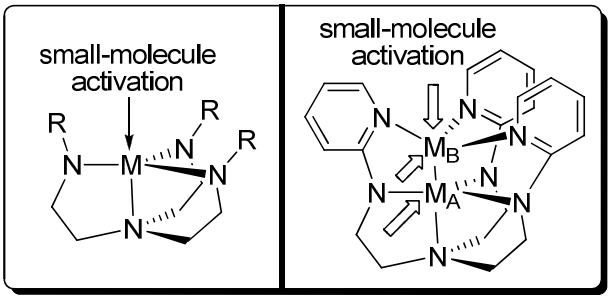

Figure A1.5. Schrock's tripodal ligand complex with one binding site (left). Proposed bimetallic motif with three available binding sites (right).

A comparison of the two systems shows that the extra tier provided by our proposed ligand provides extra binding sites for substrates, which could enable enhanced catalytic

properties and new studies on metal-metal and metal-ligand multiple bonding and reactivity.

Although expanded tren-type ligands are not well-developed, one example is the tripodal urea-type tren ligand used in the Borovik group. In this chemistry, the extra tier is used to support hydrogen bonding to a substrate such as water,[21] whereas we will use the extra bonding sites to facilitate metal coordination (Figure A1.6). Future work would explore the effects of adding a second metal to the system and probe the reactivity of the complexes toward small molecule activation.

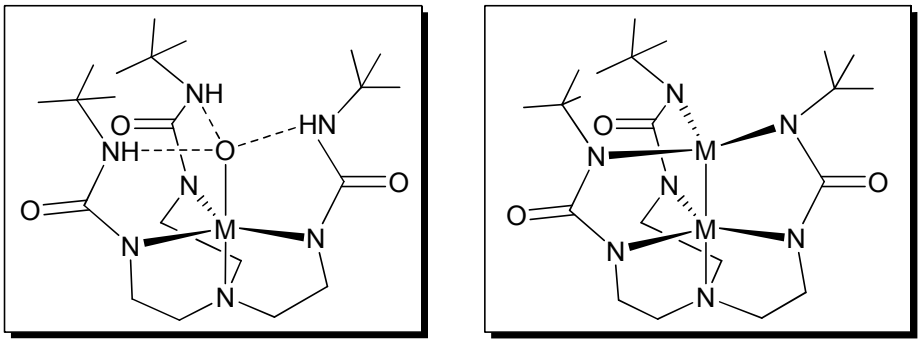

Figure A1.6. Borovik's hydrogen bonding network (left).[22,23] Bimetallic system with open coordination sites (right).

The coordination environment shown above is only one option, as the ligand could coordinate either through both nitrogen atoms, or through a nitrogen and oxygen atom.

Described herein are our efforts focusing both on ligand design and on metal complexation. We began with homometallic systems not only because these would use starting materials that are easy to prepare, but also because there is literature precedent for the formation of high order metal-metal bonds in these systems. To prepare metal

complexes in trigonal symmetry, we prepared three classes of tren-based ligands (Figure A1.7).

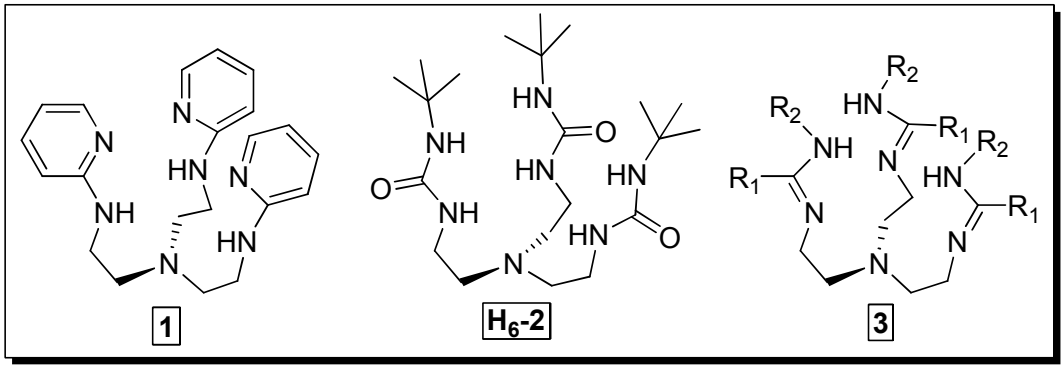

Figure A1.7. Three main types of ligands used to create a trigonal coordination geometry: pyridyl-amines (left, **1**), urea (center, **2**), and amidine (right, **3**).

A1.2 Experimental

A1.2.1 Materials and Methods

All reactions were conducted under nitrogen atmosphere in a Vacuum Atmospheres dry box or using Schlenk techniques. Dichloromethane was dried over CaH_2 and distilled before use. Tetrahydrofuran, acetonitrile, ether, hexanes, and toluene were obtained from a Vacuum Atmospheres Solvent System. All starting materials were commercially available and used as received, unless otherwise noted.

^1H NMR spectra were recorded at an operating frequency of 300 MHz on Bruker spectrometers in $CDCl_3$ at room temperature. The spectra were referenced to solvent residual peaks or to TMS at 0 ppm. Chemical shifts are reported in parts per million. Mass spectrometry was obtained by electrospray ionization (from diluted NMR solutions) or MALDI (in an anthracene matrix using a Bruker Reflex II instrument).

Pyridyl-amino Analog of Tren. The synthetic procedure for this ligand was adapted from a procedure initially detailed by Schrock and Greco.[11] To form Pd(BINAP), the catalyst for the reaction, racemic BINAP (2,2′-Bis(diphenylphosphino)-1,1′-binaphthalene) (0.18 g, 0.29 mmol) was dissolved in 15 mL of dry toluene with heating and stirring at 80°C and then added to solid $Pd_2(dba)_3$ (dba=dibenzylideneacetone) (0.12 g, 0.13 mmol). This deep red-purple solution was stirred for 10 minutes and then filtered over Celite under inert atmosphere to remove excess Pd metal, leaving a bright red-orange solution. The solution was filtered into a 100 mL Schlenk flask containing sodium *tert*-butoxide (2.28 g, 23.7 mmol), 2-bromopyridine (2.10 mL, 22.0 mmol), tren (tris(2-aminoethyl)amine) (1.10 mL, 7.34 mmol), and 40 mL dry toluene. The solution was then

heated to 80°C for 20 hours. After ten minutes of stirring, the solution was clear and deep red-orange. After two hours, the solution was dark orange and cloudy. After 20 hours, the solution was clear and deep red. The reaction mixture was filtered over a medium frit under inert atmosphere to remove sodium bromide and any insoluble palladium compounds. The resulting red-orange solution was concentrated under reduced pressure and the red-brown oil was applied to a silica gel column prepared with a 3:1 ratio of hexanes:ethyl acetate and 3% triethylamine to basify the column. The product was eluted last, with a 1:1 ratio of hexanes:ethyl acetate, as a yellow-brown oil in very low yield. **1**: MW = 377.49 g/mol; ^{1}H NMR ($CDCl_3$): δ 2.78 (t, $6H_{CH2}$), 3.35 (t, $6H_{CH2}$), 6.30 (d, $3H_{pyr}$), 6.53 (td, $3H_{pyr}$), 7.32 (m, $3H_{pyr}$), 8.08 (d, $3H_{pyr}$); ESI-MS: *m/z* = 378.3. Optimization of this procedure to increase yield is described later.

H_6-2: N,N',N''-(nitrilo-2,1,-ethanediyl)tris[N'-tertbutyl urea]. The synthetic procedure for the ligand most often seen in Borovik's work[21a,21b] was described in a paper by Bell and coworkers.[22] A 500 mL Schlenk flask was charged with 250 mL dry tetrahydrofuran. Sparged tris(2-aminoethyl)amine (5.50 mL, 32.5 mmol) was added to the tetrahydrofuran and the solution was stirred. Under inert atmosphere, *tert*-butylisocyanate (10.0 mL, 98.5 mmol) was added drop-wise with stirring at room temperature. The clear, colorless mixture was stirred for 20 hours at room temperature. The solvent was removed *in vacuo* to yield a white solid. The solid was dried under reduced pressure for 2 days with gentle heating. Yield: 11.56 g (80%).
H_6-**2**: MW = 443.63 g/mol. ^{1}H NMR ($CDCl_3$): δ 1.33 (s, $27H_{CH2}$), 2.49 (m, $6H_{CH2}$), 3.14 (m, $6H_{CH2}$), 4.89 (d, $3H_{NH}$), 5.47 (br, $3H_{NH}$); ESI-MS: *m/z* = 444.2.

Metal Insertion into 2, Mo_2buea^{2-}. **H_6-2** (0.61 g, 1.4 mmol) was dissolved in 30 mL dry tetrahydrofuran. The solution was cooled to -78°C and 1.6 M CH_3Li (in ether) (5.7 mL, 9.1 mmol) was added slowly to the **H_6-2** solution under inert atmosphere. The solution was warmed to room temperature and stirred for ten minutes, forming a white precipitate. The reaction mixture was cooled to -78°C once again, and added to a cooled solution of $Mo_2(OAc)_4$ in 30 mL tetrahydrofuran. The color changed immediately from yellow to orange-red to dark red to wine red and cloudy. The reaction mixture was stirred at -78°C for ten minutes, then at room temperature for 3 hours, and then heated to reflux overnight, yielding a dark red-brown precipitate. The solution was filtered on a medium frit under inert atmosphere. The precipitate was washed with 3 portions of 25 mL of dry tetrahydrofuran, followed by 25 mL of dry diethyl ether. The precipitate was then dried under reduced pressure, yielding a pale brown powder. Yield: 1.54 g (170%). This procedure likely also yields some insoluble lithium salts or decomposes the ligand. ^{1}H NMR spectra revealed signals at δ = 0.610 (s, 0.2H), 1.700 (br, m, 1.2H), 2.500 (s, 0.6H), 2.596 (m, 1.1H), 3.341 (d, 0.8H), and 4.438 (t, 1.0H), none of which are expected, although it is possible that these peaks indicate some ligand decomposition without metal insertion. MALDI mass spectrometry gives rise to peaks at m/z: 217.0, 345.0, 530.1, 695.1, 871.0, and 1060.1, along with much smaller peaks near the indicated m/z values, although none of these are close to either the starting ligand or the desired metal compound.

Acetanilide-Tren (3). This procedure was adapted from a published preparation by Grenon and Charette[23] and the ligand described in this procedure has R_1=CH_3 and R_2=Ph (Figure A1.8).

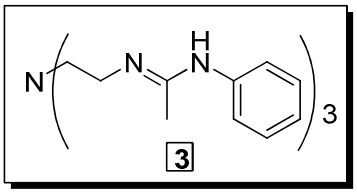

Figure A1.8. Acetanilide-tren.

Acetanilide (3.64 g, 26.9 mmol) was added to a 3-neck flask. Pyridine (6.6 mL, 81.6 mmol) was added to the flask under nitrogen flow, followed by 120 mL dry dichloromethane. The colorless reaction mixture was cooled to -40°C and Tf_2O (triflic anhydride) (10.0 g, 35.4 mmol) was added dropwise via addition funnel to the reaction mixture over 10 minutes, which caused an immediate color change to bright yellow. The reaction mixture was then warmed to 0°C and stirred for 2.5 hours. After 1 hour of stirring, the reaction mixture was bright orange and clear. After 2.5 hours of stirring, the mixture was cooled to -40°C and tren (4.0 mL, 26.7 mmol) was added in one portion, causing a color change to orange-yellow. After the addition, the reaction mixture was warmed to room temperature and stirred for 20 hours, at which point the solution was bright orange with bright orange precipitate. The reaction mixture was diluted with 50 mL dichloromethane and 100 mL of a saturated solution of sodium bicarbonate ($NaHCO_3$). The aqueous layer was washed six times with 125 mL portions of dichloromethane, yielding a bright orange organic layer and bright orange solid in the aqueous layer. The organic layer was dried over magnesium sulfate, filtered, and the

solvent removed under reduced pressure to yield a dark orange oil. The oil was washed with hexanes (3 x 5 mL) to remove excess pyridine, followed by diethyl ether (3 x 10 mL), deionized water (3 x 10 mL), and then a saturated solution of sodium bicarbonate (3 x 10 mL). The oil was dried under vacuum and then dissolved in hot hexanes to crystallize. ^{1}H NMR (300 MHz, $CDCl_3$) δ = 1.963 (t, 3H, CH_3), 2.815 (m, 2H, CH_2), 3.504 (m, 2H, CH_2), 5.282 (s, 0.3H, N*H*), 6.718 (m, 2H, C_6H_6), 7.015 (m, 2H, C_6H_6), 7.145 (m, 2H, C_6H_6). ESI-MS: *m/z* = 498.1 $(M+H)^+$, 648.0 (M+HOTf).

A1.2.2 Experimental Optimization

Boc-Protection. To prevent the recurring problem of over-substitution of the product, we decided to functionalize one site of tris(2-aminoethyl)amine with tert-butyloxycarbonyl (Boc) as a protecting group.

Boc-Tren.[24] Tris(2-aminoethyl)amine (tren) (6.0 mL, 40 mmol) was dissolved in 90 mL of dioxane. A solution of NaOH (14.54 g, 364 mmol) in 50 mL of water was added to the tren solution. The mixture was cooled in an ice bath and solid di-tert-butyl dicarbonate (50.23 g, 230 mmol) was added quickly in portions. A white solid formed immediately and was stirred for 30 minutes at 0°C, warmed to room temperature and then stirred overnight. After stirring, 200 mL of water were added to the reaction mixture and the aqueous layer was extracted with ethyl acetate. The ethyl acetate layer was dried over magnesium sulfate, filtered and dried under reduced pressure on a rotary evaporator to give a white solid. Yield: 15.79 g (88.3%). ^{1}H NMR (300 MHz, $CDCl_3$): 1.453 (9H, s), 2.520 (2H, t), 3.141 (2H, q), 5.133 (1H, s).

Boc-pyr-tren (1). BINAP (2,2′-Bis(diphenylphosphino)-1,1′-binaphthalene) (0.31 g, 0.50 mmol) was dissolved in 20 mL of dry toluene with heating and stirring at 80°C and then added to solid $Pd_2(dba)_3$ (dba=dibenzylideneacetone) (0.15 g, 0.16 mmol). The solution was stirred for 10 minutes and then filtered twice over celite. The dark orange solution was then added to a flask containing sodium *tert*-butoxide (3.73 g, 38.8 mmol), **1** (4.96 g, 11.1 mmol), and bromopyridine (3.0 mL, 31.5 mmol) in 150 mL of dry toluene. The reaction mixture was heated to 80°C and stirred for 20 hours, resulting in a cloudy, orange-red mixture. The reaction mixture was filtered over celite and the solvent was removed *in vacuo*, leaving a dark red-orange solid. The solid was dissolved in 10 mL of toluene and loaded onto a silica gel column packed with 1:1 ethyl acetate:hexanes and 3% triethylamine. The column was eluted with 1:1 ethyl actetate:methanol with 3% triethylamine and fractions monitored by TLC. White needle crystals formed in the collection tubes, which were collected and washed with methanol. Yield: 1.51 g (20.0%). ^{1}H NMR (300 MHz, CD_2Cl_2): δ = 8.284 (m, 1H), 7.599 (m, 2H), 6.959 (m, 1H), 3.892 (m, 2H), 2.769 (m, 2H), 1.463 (s, 9H).

A1.3 Results and Discussion

All of the ligands shown in Figure A1.7 (*vide supra*) are tripodal and would maintain a trigonal geometry upon addition of various metal centers. These are specific targets because they have literature precedents,[11,22,23] and because they have an uncommon structure capable of achieving our desired molecular geometry. We expect that these ligands will also be able to accommodate structural changes, including addition of steric bulk or electron-withdrawing and –donating groups.

*Pyridyl-Amine, **1**:* The pyridyl-amine ligand class is formed by the Pd-catalyzed coupling of tren with aryl bromides, as developed by Schrock and Greco.[11] Using this method, Schrock and coworkers prepared a large number of complexes, all by varying the choice of substituted aryl bromide. Although myriad functionalized aryl bromides were used, including bromoaniline, pyridines were excluded from the study. As a result, we hoped to expand upon the work described above and use a similar palladium catalyzed C-N bond forming reaction to prepare ligands such as **1** (Figure A1.9).

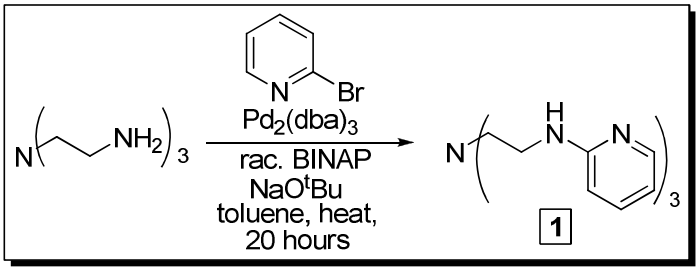

Figure A1.9. Preparation of **1**, following method by Schrock and Greco.[11]

The method modified from Greco's work yielded a pure sample of ligand **1**, which was analyzed by mass spectrometry and ^{1}H NMR. However, the yield of the reaction was very low (less than 10%) because of the formation of a side-product, an

"over-substituted" amine, **1a** (Figure A1.10). Though Greco and Schrock report this type of side product in their work,[25] they indicate that column chromatography is used to separate it from the desired product. We made multiple efforts in this direction and used eluents of increasing polarity in the column (up to ammonia solution in methanol), but these trials did not prove fruitful in separating the two products. Further, based on ESI mass spectrometry and proton NMR studies, it appears that the "over-substituted" product (**1a**) is formed in much higher yields than the desired product (**1**), and is likely more difficult to remove as a result of this.

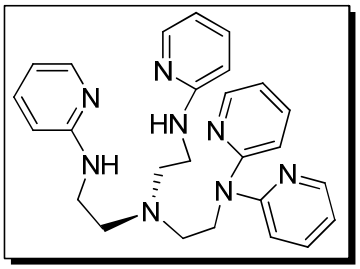

Figure A1.10. Complex **1a** with over-substitution at one "arm" of the pyridyl-amine ligand.

Clearly, the best method for improving the yield of **1** is to boc-protect the arms of the pendant amine, which leads to formation of the mono-substituted product in improved yield. Upon deprotection, the desired product **1** should be formed in near quantitative yield.

The synthesis of this ligand has proved to be a much more difficult task than originally expected. However, with further optimization, the ligand will be useful for stabilizing bimetallic compounds. The pyridine rings will provide some rigidity as well as steric bulk to a metal compound, which will both support coordinatively unsaturated

metal centers and provide a small binding pocket for an incoming molecule such as O_2, N_2 or CO.

*Urea-Tren, **H_6-2**:* The synthesis of this tripodal urea-based ligand proceeds via a nucleophilic addition reaction of an isocyanate with tren (Figure A1.11).[22] The reaction occurs in one step and leads to a high yield of the desired product; however, metal insertion reactions need further optimization to provide pure, isolable product.

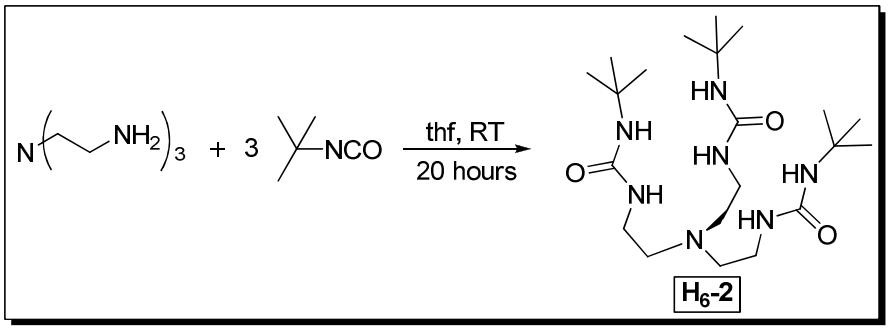

Figure A1.11. Synthesis of **H_6-2** via addition reaction.

In preliminary work, we attempted to remove all six protons of **H_6-2** at once using six equivalents of methyl lithium, followed by insertion of two metal centers both with (using such starting material as $Cr_2(OAc)_4$ and $Mo_2(OAc)_4$) and without (using two equivalents of $CrCl_2$) a pre-existing metal-metal bond. These reaction conditions typically yielded some brown or gray-brown precipitate, and characterization by MALDI-MS and NMR spectroscopy did not yield any insight into the identity of the product. However, since Borovik and coworkers typically use late transition metals such as iron or cobalt in their work,[21a] it is possible that our reaction conditions have not been suitable for our studies. With some manipulation of the reaction conditions and choice of metal, the project should yield a trigonal bimetallic complex.

Borovik and coworkers reported several mononuclear complexes with **H_6-2** to explore hydrogen bonding to a substrate.[21b] In order to achieve a binuclear complex, we plan to first prepare a mononuclear complex as described by Borovik by using three equivalents of potassium hydride to deprotonate the ligand just three times and then insert first one, and then a second, metal center, as shown in Figure A1.12. Though this procedure is published, we have had some difficulty replicating the results.

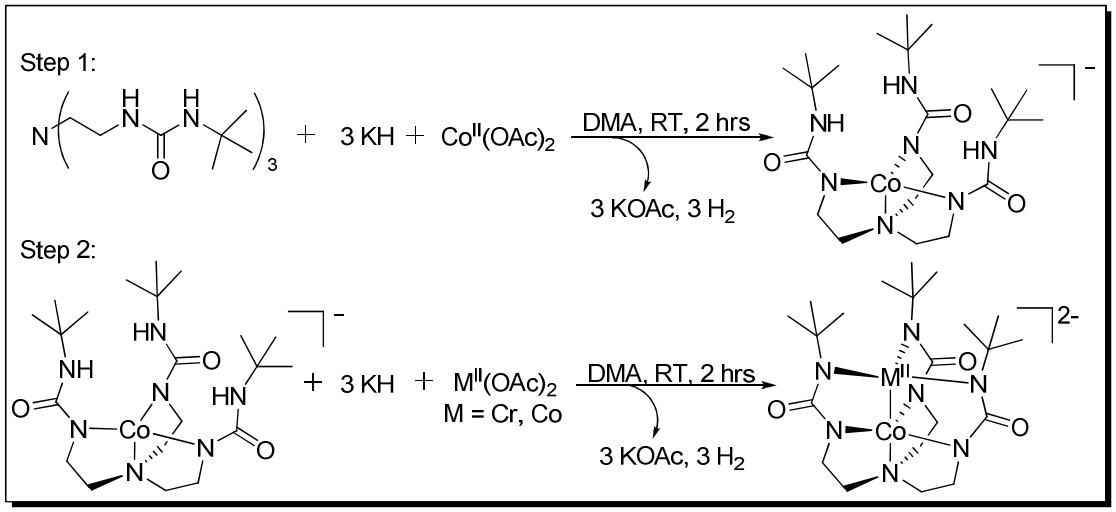

Figure A1.12. Preparation of [M_2-**2**]$^{2-}$ using Borovik's published method,[21b] in two steps.

*Amidine, **3**:* Ligand **3** is the class of ligands that will likely be easiest to modify, and it is clear that there are a multitude of substitutions that can happen at both R_1 and R_2, so it is of special interest to determine a straightforward route for its synthesis, and for the formation of substituted analogs. We went about the preparation of the amidine ligand **3** using two steps: activation of the amide, followed by reaction with the primary amine. Though there are several methods for activating amides, work by Charette[23] outlines a fairly straightforward preparation using triflic anhydride (Figure A1.13). The amide then

reacts with an amine, in our case, tren, to form the tripodal amidine ligand, all in a two-step reaction, followed by purification by crystallization.

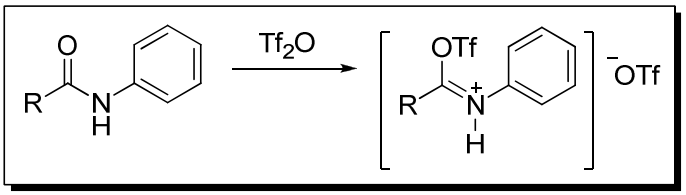

Figure A1.13. Activated triflate-amide species that reacts with amines via condensation.

At first, this reaction proved elusive because triflic anhydride is very moisture sensitive (and much to our surprise, reactive to Teflon tubing), and also quite corrosive, so cannulation techniques were ineffective, but this was quickly fixed by use of an addition funnel under nitrogen flow. Tren was added as a liquid and the reaction formed a fairly pure product, as evidenced by NMR spectroscopy.

A1.4 Outlook

The clear next step in this multi-faceted project is to optimize metal insertion reactions. Though several methods have been explored, it is clear that further work is necessary to pinpoint the correct avenue for directing two metal centers into the tripodal ligands shown above. One promising option is to use Borovik's method[21b] (Figure A1.12), and to experiment with various metal centers to achieve high yields of crystalline material.

Another interesting option is to follow the methods of metal insertion proposed by Cotton[26] and Manke,[10] (Figure A1.14) who have both achieved trigonal complexes featuring short M-M multiple bonds. From their work, we believe that it is likely that different metal precursors from the ones we have experimented with will be better for the preparation of these rare trigonal complexes. Cotton and coworkers[26] prepared a chloride-

bridged dichromium bis(amidinate) complex; however, in our system, there is much more steric bulk because the ligand is tripodal, so it is unlikely that a chloride-bridged complex would be an ideal precursor. Still, the general method of deprotonation of the ligand (the amidine ligand **3**, for example) by methyllithium in THF, followed by addition of a metal salt without a pre-existing metal-metal bond (such as $CrCl_2$) could be useful. We could add other metal salts, including salts of late transition metals such as iron, cobalt or copper, to see the effect on both bond length and bond order in this trigonal array.

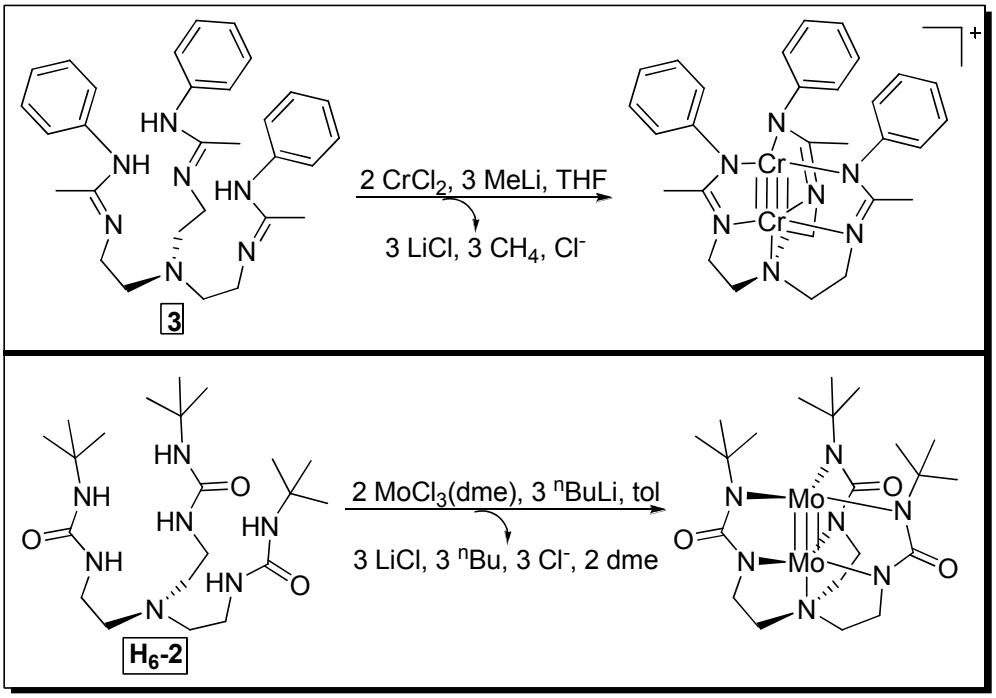

Figure A1.14. Preparation of bimetallic acetanilide-tren via Cotton's method[26] (top arrow) and Manke's method[10] (bottom arrow).

Manke and coworkers[10] achieve their Mo-Mo multiple bond by a similar synthetic method to that proposed by Cotton, although with a different metal salt. In this case, the starting material is trichloro(dimethoxyethane)molybdenum(III), but the procedure calls

for the addition of lithiated ligand at low temperature, followed by stirring overnight at room temperature, as in Cotton's procedure.

There are two overriding themes to the project described in this paper. The first is to determine the best method of preparing metal-metal bonded complexes in trigonal symmetry to study the metal-metal and metal-ligand interactions that result from this rare geometry, which has been described in detail above. The second centers on the idea that the project is important from both fundamental and practical perspectives. The practical side explores how this geometry affects the addition and activation of substrates such as dinitrogen.

Dinitrogen activation has been the target of many studies in recent years[13,14a,14b,27,28] because its conversion to ammonia is a process that humans depend on for food supplies, but the mechanism that bacteria use to perform this process in nature is not well understood. Nitrogenase enzymes have cofactors with multiple metal centers, including vanadium, molybdenum, and iron and are difficult to crystallize; as a result, researchers look to small molecule analogues to study the intermediates of this conversion and potentially mimic this catalytic process in the laboratory. Even though nitrogenase systems include multiple metal centers, most studies focus on a single metal center to convert dinitrogen to ammonia.[13,29] The FeMo cofactor, which is the most well characterized system, is thought to have most of its activity at low-coordinate iron centers.[30] We propose that our bimetallic system will be able to efficiently bind dinitrogen, and potentially reduce it with the addition of proton and electron sources, because each metal atom has a coordination number of 3 or 4, which mimics the cofactor.

Low coordination number is not the only factor that determines whether a complex will bind N_2; low oxidation states on the metal center also contribute greatly to this ability. Using our tren-based ligands, we should be able to prepare a variety of M_2tren complexes with metal centers in their +2 oxidation states, which would allow for small molecules such as N_2 (or CO_2, which exhibits very similar reactivity) to bind to the second metal center. These complexes would then be crystallized to examine the N-N and M-N bond distances to determine whether any activation is taking place. In addition, we can measure cyclic voltammetry on these compounds both in the presence of our small molecule substrates, either N_2 or CO_2, and under an inert atmosphere of argon to determine the redox couples present in our M_2tren-N_2 complexes. Once we are able to conclusively prove that our complex binds dinitrogen, we will be able to commence reactivity studies of the M_2tren-N_2 complexes.

Dinitrogen activation at transition metal sites is relevant for a variety of other substrate conversions, including alkylation and hydrogenation. This chemistry has been exploited as early as 1981, when Bossard and coworkers showed that a molybdenum dinitrogen compound was able to enantioselectively form C-N bonds.[31] This could be extended to our bimetallic system because there are sites for both dinitrogen and substrate coordination (as shown in Figure 7), and these types of turnovers will be explored further. Another example of the utility of transition metal-dinitrogen compounds comes from Chirik and coworkers, who showed that an $Fe(N_2)_2$ complex reacts with a substrate to undergo intramolecular C-H activation.[32] Similarly, Kupfer and Schrock showed that a molybdenum complex with a tripodal ligand can prepare intermediates in the conversion

of dinitrogen to triethylamine.[33] These types of turnovers are relevant not only to determine the mechanism of the bond forming reactions, but also from a synthetic standpoint, to be able to obtain useful products efficiently. We propose to introduce various alkyl substrates to our system once we have prepared the M_2tren-N_2 complex. By using a trigonal ligand environment with added steric bulk and working at low temperatures, we should be able to crystallize and electrochemically and spectroscopically visualize the process by which N_2 complexes react with substrates.

References

(1) Cotton, A. F. W., Richard A., *Multiple Bonds Between Metal Atoms*. 2nd ed.; Oxford University Press: New York, 1993.

(2) Brown, D. J.; Chisholm, M. H.; Gallucci, J. C., *Dalton Trans.* **2008**, 1615.

(3) Hansen, J.; Davies, H. M. L., *Coord. Chem. Rev.* **2008,** *252*, 545.

(4) Gracia, R.; Adams, H.; Patmore, N. J., *Dalton Trans.* **2009**, 259.

(5) Wee, A. G. H.; Liu, B.; McLeod, D. D., *J. Org. Chem.* **1998,** *63*, 4218.

(6) Muthusamy, S.; Gunanathan, C., *Synlett* **2002,** *2002*, 1783.

(7) Hu, W.; Xu, X.; Zhou, J.; Liu, W.-J.; Huang, H.; Hu, J.; Yang, L.; Gong, L.-Z., *J. Am. Chem. Soc.* **2008,** *130*, 7782.

(8) Davies, H. M. L.; Manning, J. R., *Nature* **2008,** *451*, 417.

(9) Tsai, Y.-C.; Hsu, C.-W.; Yu, J.-S. K.; Lee, G.-H.; Wang, Y.; Kuo, T.-S., *Angew. Chem. Int. Ed.* **2008,** *47*, 7250.

(10) Manke, D. R.; Loh, Z.-H.; Nocera, D. G., *Inorg. Chem.* **2004,** *43*, 3618.

(11) Greco, G. E.; Schrock, R. R., *Inorg. Chem.* **2001,** *40*, 3850.

(12) Schrock, R. R., *Acc. Chem. Res.* **1997,** *30*, 9.

(13) Yandulov, D. V.; Schrock, R. R., *Science* **2003,** *301*, 76.

(14) (a) Schrock, R. R., *Acc. Chem. Res.* **2005,** *38*, 955; (b) Schrock, R. R., *Angew. Chem. Int. Ed.* **2008,** *47*, 5512.

(15) England, J.; Martinho, M.; Farquhar, E. R.; Frisch, Jonathan R.; Bominaar, Emile L.; Münck, E.; Que Jr., L., *Angew. Chem. Int. Ed.* **2009,** *48*, 3622.

(16) Chisholm, M. H., *Acc. Chem. Res.* **2002,** *23*, 419.

(17) Cotton, F. A.; Li, Z.; Murillo, C. A.; Poplaukhin, P. V.; Reibenspies, J. H., *J. Cluster Sci.* **2008,** *19*, 89.

(18) Cotton, F. A.; Daniels, L. M.; Maloney, D. J.; Matonic, J. H.; Murillo, C. A., *Inorg. Chim. Acta* **1997,** *256*, 283.

(19) Cotton, A. F.; Feng, X.; Murillo, C. A., *Inorg. Chim. Acta* **1997,** *256*, 303.

(20) Cotton, F. A.; Daniels, L. M.; Falvello, L. R.; Matonic, J. H.; Murillo, C. A., *Inorg. Chim. Acta* **1997,** *256*, 269.

(21) (a) Borovik, A. S., *Acc. Chem. Res.* **2005,** *38*, 54; (b) MacBeth, C. E.; Gupta, R.; Mitchell-Koch, K. R.; Young, V. G.; Lushington, G. H.; Thompson, W. H.; Hendrich, M. P.; Borovik, A. S., *J. Am. Chem. Soc.* **2004,** *126*, 2556.

(22) Bell, K. J.; Westra, A. N.; Warr, R. J.; Chartres, J.; Ellis, R.; Tong, C. C.; Blake, A. J.; Tasker, P. A.; Schroder, M., *Angew. Chem. Int. Ed.* **2008,** *47*, 1745.

(23) Charette, A. B.; Grenon, M., *Tetrahedron Lett.* **2000,** *41*, 1677.

(24) Ghanem, N.; Martinez, J.; Stien, D., *Tetrahedron Lett.* **2002,** *43*, 1693.

(25) Wolfe, J. P.; Buchwald, S. L., *J. Org. Chem.* **2000,** *65*, 1144.

(26) Cotton, F. A.; Daniels, L. M.; Murillo, C. A.; Schooler, P., *J. Chem. Soc., Dalton Trans.* **2000**, 2001.

(27) Greco, G. E.; Schrock, R. R., *Inorg. Chem.* **2001,** *40*, 3861.

(28) Weare, W. W.; Schrock, R. R.; Hock, A. S.; Muller, P., *Inorg. Chem.* **2006,** *45*, 9185.

(29) Hendrich, M. P.; Gunderson, W.; Behan, R. K.; Green, M. T.; Mehn, M. P.; Betley, T. A.; Lu, C. C.; Peters, J. C., *Proceedings of the National Academy of Sciences* **2006,** *103*, 17107.

(30) Smith, J. M.; Sadique, A. R.; Cundari, T. R.; Rodgers, K. R.; Lukat-Rodgers, G.; Lachicotte, R. J.; Flaschenriem, C. J.; Vela, J.; Holland, P. L., *J. Am. Chem. Soc.* **2005,** *128*, 756.

(31) Bossard, G. E.; George, T. A., *Inorg. Chim. Acta* **1981,** *54*, L241.

(32) Bart, S. C.; Bowman, A. C.; Lobkovsky, E.; Chirik, P. J., *J. Am. Chem. Soc.* **2007,** *129*, 7212.

(33) Kupfer, T.; Schrock, R. R., *J. Am. Chem. Soc.* **2009**.